AD_______________

Award Number: W81XWH-09-1-0543

TITLE: Role of Cathepsin C During Breast Cancer Metastasis

PRINCIPAL INVESTIGATOR: Brian Ruffell, Ph.D.

CONTRACTING ORGANIZATION: University of California
San Francisco, CA 94143-0962

REPORT DATE: September 2011

TYPE OF REPORT: Annual Summary

PREPARED FOR: U.S. Army Medical Research and Materiel Command
Fort Detrick, Maryland 21702-5012

REPORT DOCUMENTATION PAGE			*Form Approved OMB No. 0704-0188*
Public reporting burden for this collection of information is estimated to average 1 hour per response, including the time for reviewing instructions, searching existing data sources, gathering and maintaining the data needed, and completing and reviewing this collection of information. Send comments regarding this burden estimate or any other aspect of this collection of information, including suggestions for reducing this burden to Department of Defense, Washington Headquarters Services, Directorate for Information Operations and Reports (0704-0188), 1215 Jefferson Davis Highway, Suite 1204, Arlington, VA 22202-4302. Respondents should be aware that notwithstanding any other provision of law, no person shall be subject to any penalty for failing to comply with a collection of information if it does not display a currently valid OMB control number. **PLEASE DO NOT RETURN YOUR FORM TO THE ABOVE ADDRESS.**			
1. REPORT DATE September 2011	**2. REPORT TYPE** Annual Summary		**3. DATES COVERED** 1 September 2010 – 31 August 2011
4. TITLE AND SUBTITLE Role of Cathepsin C During Breast Cancer Metastasis			**5a. CONTRACT NUMBER**
			5b. GRANT NUMBER W81XWH-09-1-0543
			5c. PROGRAM ELEMENT NUMBER
6. AUTHOR(S) Brian Ruffell, Ph.D.			**5d. PROJECT NUMBER**
			5e. TASK NUMBER
E-Mail: brian.ruffell@ucsf.edu			**5f. WORK UNIT NUMBER**
7. PERFORMING ORGANIZATION NAME(S) AND ADDRESS(ES) University of California San Francisco, CA 94143-0962			**8. PERFORMING ORGANIZATION REPORT NUMBER**
9. SPONSORING / MONITORING AGENCY NAME(S) AND ADDRESS(ES) U.S. Army Medical Research and Materiel Command Fort Detrick, Maryland 21702-5012			**10. SPONSOR/MONITOR'S ACRONYM(S)**
			11. SPONSOR/MONITOR'S REPORT NUMBER(S)
12. DISTRIBUTION / AVAILABILITY STATEMENT Approved for Public Release; Distribution Unlimited			
13. SUPPLEMENTARY NOTES			

14. ABSTRACT

The presence of some innate immune cell types in developing neoplasms provides a significant pro-tumor advantage. Myeloidlineage immune cells, such as tumor-associated macrophages (TAMs) and immature myeloid-derived cells/monocytes, promote tumor development by exerting pro-tumor activities including activating angiogenic programs, suppressing anti-tumor immunity, and enhancing migratory and metastatic properties of malignant cells. We have now established in both murine models and human patients that exposure to neoadjuvant chemotherapy induces the recruitment of myeloid populations, including tumor-associated macrophage. Using the dependency of this population on the CSF1/CSF1R pathway for recruitment to the tumor microenvironment, we have demonstrated that preventing macrophage influx improves the response of transgenic mice to chemotherapy, resulting in lower primary tumor and pulmonary metastatic burden. Despite this success, human breast cancers are infiltrated by a wider variety of myeloid populations, for example mast cells, that may share overlapping functions with macrophages but that are not dependent on the CSF1/CSF1R pathway. Identifying common molecular pathways mediating chemoresistance may therefore improve the chance and/or efficacy of clinical translation. Along these lines, preliminary data suggests that CSF1/CSF1R blockage selectively reduces infiltration of an IL-10 producing subpopulation of macrophages, and that blockade of IL-10 signaling may be similarly efficacious to direct macrophage targeting. These studies therefore hold great potential for improving the rate of pathological complete response in patients and prolonging survival.

15. SUBJECT TERMS

breast cancer, mouse models, inflammation, proteases, cathepsin protease, immune cells, leukocytes

16. SECURITY CLASSIFICATION OF:			**17. LIMITATION OF ABSTRACT**	**18. NUMBER OF PAGES**	**19a. NAME OF RESPONSIBLE PERSON** USAMRMC
a. REPORT U	**b. ABSTRACT** U	**c. THIS PAGE** U	UU	65	**19b. TELEPHONE NUMBER** *(include area code)*

TABLE OF CONTENTS

I. INTRODUCTION:

In an original cohort of mice I described an reduction in the number of metastatic lesions in mice deficient for the cysteine protease cathepsin C. Extensive characterization of these mice revealed expression of cathepsin C in multiple cell types, but did not identify differences between cathepsin C proficient and deficient tumors in terms of leukocytic infiltrate, stromal composition, vasculature, proliferation, cell death, or hypoxia. Analysis of circulating carcinoma cells also found to be unchanged, all of which was detailed in the first annual report.

These findings lead me to both examine lung seeding as a potential mechanism and to enroll an additional cohort of animals into an end stage study of metastatic burden to confirm our original observation. I can now report that lung seeding was unaltered in cathepsin C deficient animals, and that no difference in spontaneous lung metastasis was observed in the second cohort of animals. Based upon these negative results, I have completed the study of cathepsin C in breast cancer metastasis and have submitted a manuscript for publication detailing these findings.

Utilizing the technical expertise gained for this extensive work, I initiated parallel studies to comprehensively profile the leukocytic infiltrate in human breast cancer. This analysis revealed higher proportions of lymphocytes within carcinomas compared to normal tissue, and surprisingly that these proportions were reversed in carcinomas exposed to neoadjuvant chemotherapy. This study is now listed as a new Aim 4 in the statement of work, and has been published in a special breast cancer issue of PNAS.

Based upon these findings in breast cancer, and our recent publication describing that removing macrophages from the microenvironment of mammary carcinomas through targeting of the CSF1-CSF1R pathway improves response to chemotherapy (1), I have detailed a new Aim 5 wherein I will determine the mechanism by which macrophages restrict this response. This may prove critical to understanding the results of future clinical trials involving macrophage-targeted agents, including an upcoming trial based upon our paper in Cancer Discovery. In addition, in an attempt to monitor the effectiveness of agents that reduce macrophage infiltration within tumors, I have collaborated with the laboratory of Dr. Heike Daldrup-Link at Stanford University to investigate whether iron oxide nanoparticles can be used to non-invasively measure macrophage density through MR imaging.

II. RESEARCH ACCOMPLISHMENTS BODY:

AIM 1: DETERMINE THE FUNCTIONAL ROLE OF CATHEPSIN C IN REGULATING LEUKOCYTE INFILTRATION AND BIOACTIVITY IN MAMMARY ADENOCARCINOMA DEVELOPMENT AND METASTASIS

Establish the profile of cells expressing CTSC during tumor development and metastasis:

Profile CTSC expression in mammary and lung tissue of MMTV-PyMT mice by flow cytometry. ***(months 1-6)***

Evaluate cathepsin C activity using a selective probe, FY01, in lysates of purified leukocytes isolated from mammary glands, peripheral blood and lung from MMTV-PyMT mice. ***(months 3-6)***

Quantitatively assess activity of cathepsin C enzymatic substrates in purified leukocytes from PyMT/CC$^{+/-}$ versus PyMT/CC$^{-/-}$ mice using selective protease activity assays ***(months 6-12)***

STATUS: COMPLETE

Assess functional significance of cathepsin C in regulating macrophage phenotype:

Analyze polarization state of tumor-associated macrophages by intracellular staining for cytokine expression. ***(months 1-6)***

Verify macrophage polarization by iNOS and arginase expression levels by real time PCR. ***(months 6-9)***

Compare the ability of PyMT/CC$^{+/-}$ and PyMT/CC$^{-/-}$ tumor-associated macrophages to influence invasive properties of malignant MECs grown as organoids using the 3D organotypic model. ***(months 6-12)***

STATUS: COMPLETE

Evaluate leukocyte infiltration regulated by cathepsin C in PyMT mice:

Analysis of leukocyte infiltration in mammary and lung tumors in PyMT/CC$^{+/-}$ and PyMT/CC$^{-/-}$ mice using multicolor flow cytometry. ***(months 1-6)***

Measure cytokine expression levels in mammary and lung tumors in PyMT/CC$^{+/-}$ and PyMT/CC$^{-/-}$ mice via ELISA. ***(months 3-9)***

Identify leukocyte populations with altered cytokine expression profiles in mammary and lung tumors in PyMT/CC$^{+/-}$ versus PyMT/CC$^{-/-}$ mice using intracellular cytokine staining and multicolor flow cytometry. ***(months 9-12)***

STATUS: COMPLETE

AIM 2: DETERMINE AT WHICH STAGE OF CANCER DEVELOPMENT CATHEPSIN C FUNCTIONALLY REGULATES PULMONARY METASTASIS OF MAMMARY CARCINOGENESIS

<u>Determine if cathepsin C regulates intravasation from primary mammary tumors into the circulation:</u>

Measure the number of circulating neoplastic cells in the blood of PyMT/CC$^{+/-}$ and PyMT/CC$^{-/-}$ mice at day 85 and 95 using either flow cytometry or PCR. ***(months 12-18)***

Examine directional growth of neoplastic cells in the 3D organotypic model during co-culture with the leukocyte populations identified in Aim 1. ***(months 12-18)***

Examine the ability of leukocyte populations to induce chemotaxis of neoplastic cells using a modified Boyden chamber ***(months 18-21)***

Adoptive transfer of CC$^{+/-}$ and CC$^{-/-}$ splenic T cells into PyMT/CC-/- mice and evaluation of lung metastasis and the number of circulating MECs. ***(months 18-24)***

STATUS: COMPLETE

<u>Determine of cathepsin C regulates MEC survival in blood, lung seeding, or outgrowth:</u>

Generate 4 neoplastic cell lines from PyMT/CC$^{+/-}$ and PyMT/CC$^{+/-}$ mice that are also transgenic for GFP (2 from early non-invasive mammary tumors and 2 from late, invasive tumors). ***(months 1-6)***

Intravenously inject neoplastic cell lines in wildtype and CC$^{-/-}$ mice and measure MEC survival in the blood, lung infiltration, and outgrowth/tumor progression. ***(months 12-18)***

If extravastion into the lung is affected by cathepsin C expression, then examine rolling, adhesion, and transmigration of neoplastic cell lines on immortalized mouse endothelial cells. ***(months 18-24)***

If tumor growth or development is altered, inject neoplastic cells subcutaneously in a xenograft model along with purified tumor-associated leukocytes and measure early growth. ***(months 18-24)***

STATUS: COMPLETE

<u>Determine if metastasis of mammary tumors is regulated by leukocyte-derived cathepsin C:</u>

Generate bone marrow chimeric mice by using irradiated PyMT/CC$^{+/-}$ and PyMT/CC$^{+/-}$ mice and the bone marrow from GFP^{+} and GFP^{+}/CC$^{-/-}$ mice. ***(months 12-24)***

Analyze tumor incidence, growth, progression and metastasis in the four combinations of chimeric mice. ***(months 18-36)***

If tissue cathepsin C expression appears to be important, generate chimeric mice that do not express PyMT and measure tumor growth in a xenograft model and lung metastasis following intravenous injection. ***(months 18-36)***

STATUS: COMPLETE

AIM 3: DEVELOP DIAGNOSTIC AND THERAPEUTIC APPROACHES BASED ON CATHEPSIN C BIOACTIVITY TO IMPROVE BREAST CANCER PATIENT SURVIVAL

<u>Develop a probe to measure cathepsin C activity in live mice:</u>

Generate FY01-GdDTPA and FY01-FITC. ***(months 12-18)***

Adjust animal protocol to include use of FY01-GdDTPA and JCP410. ***(months 12-18)***

Evaluate entrance of labeled FY01 into purified TAMs ***(months 18-21)***

Evaluate entrance of labeled FY01 into TAMs in vivo ***(months 18-21)***

Analyze entrance of FY01-GdDTPA into tumors using MRI. ***(months 21-24)***

STATUS: NOT INITIATED*

<u>Evaluate efficacy of a selective cathepsin C inhibitor in reducing pulmonary metastasis:</u>

Examine the effect of the selective cathepsin C inhibitor JCP410 in the 3D organotypic co-culture model. ***(months 24-30)***

Evaluate the ability of JCP410 to inhibit cathepsin C activity in mammary and lung tumors by analyzing post-injection activity by MRI or staining unfixed tissue sections. ***(months 24-36)***

Evaluate the efficacy of JCP410 in inhibiting pulmonary metastasis through bi-weekly i.p injection in mice of age 60 and 80 days. ***(months 24-36)***

STATUS: NOT INITIATED*

<u>Evaluate cathepsin C activity during human breast cancer progression:</u>

Submit proposal for use of human tissue ***(months 12-24)***

Analyze expression of cathepsin C in fixed sections of human mammary tumors by double staining for cathepsin C and leukocyte markers followed by confocal microscopy. ***(months 24-36)***

If cathepsin C expression is observed, measure activity in unfixed tissue sections using FY01-FITC. ***(months 24-36)***

Correlate cathepsin C expression and activity with information available about the clinical stage of the cancer and/or the outcome. ***(months 30-36)***

Analyze breast cancer tissue microarray data with 10 year follow up data for a correlation between cathpesin C expression and clinical stage and/or outcome. ***(months 30-36)***

Evaluate role of human leukocytes to promote invasive growth in the 3D organotypic co-culture model using human breast cancer cell lines ***(months 24-30)***

Evaluate ability of JCP410 to inhibit the promotion of invasive growth by leukocytes **(months 30-36)**

STATUS: WILL NOT BE INITIATED*

***Based on results from Aims 1 and 2, we have revised our hypothesis as it is now clear that cathepsin C is not a significant regulator of mammary carcinogenesis; thus, evaluating cathepsin C in human samples is without merit. Based on this, we have added a new Aim 4 and Aim 5.**

#NEW AIM 4: EXAMINE THE COMPOSITION OF LEUKOCYTES WITHIN HUMAN BREAST CARCINOMAS AND NORMAL TISSUE IN THE PRESENCE OR ABSENCE OF NEOADJUVANT THERAPY

Determine leukocyte composition within normal and tumor tissue:

Utilize polychromatic flow cytometry to generate leukocyte profiles. ***(months 12-24)***

To evaluate the composition of tumor-infiltrating leukocytes in human BC, tumors from 20 patients were evaluated by polychromatic flow cytometry and IHC detection of leukocyte lineages in tissue sections as described in Materials and Methods. Nine invasive ductal carcinomas (IDC) and five invasive lobular carcinomas (ILC) – mostly histological grade two or three – were obtained from patients with no prior exposure to CTX (CTX-naïve) at the time of primary surgery for early stage BC, although one patient had received neoadjuvant tamoxifen. Six tumor samples were obtained from patients previously treated with neoadjuvant CTX prior to resection (CTX-treated), consisting entirely of grade two or three IDC. Notably, three of six CTX-treated tumors were HER2/neu-positive, compared to only one of fourteen CTX-naïve tumors, whereas both groups contained roughly equivalent percentages of tumors negative for estrogen, progesterone and HER2 receptors (triple negative). Ipsilateral nonadjacent tissue was also obtained from seven CTX-naïve and four CTX-treated patients for use as “normal” tissue, in

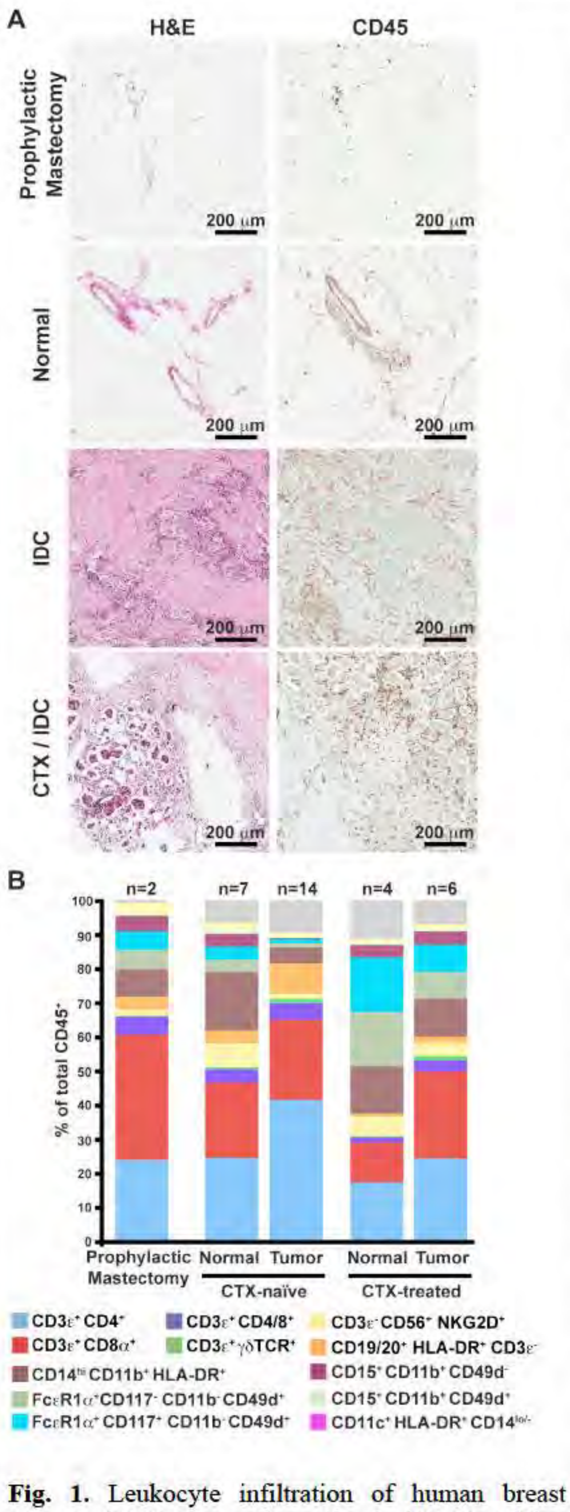

Fig. 1. Leukocyte infiltration of human breast tumors. (A) Hematoxylin and eosin (H&E) staining of tissue sections (left panels) with representative immunohistochemistry for CD45 shown for each (right panels). (B) Flow cytometric analysis of leukocyte populations within human breast tumors. Results are shown as a percent of total $CD45^+$ cells with markers used to define specific lineages shown below.

addition to tissues from two contralateral prophylactic mastectomies from patients with ipsilateral ductal carcinoma in situ (DCIS).

Immune infiltrates detected with the pan-leukocyte marker CD45 were present in both normal and tumor tissue, but with substantially increased density in BC (**Fig. 1A**). Leukocyte subsets were evaluated using a combination of lineage markers to identify specific subpopulations, with the complexity of these populations shown in **Fig. 1B** as a percentage of the total number of $CD45^+$ cells in each sample. BC tissues from CTX-naïve patients contained infiltrates dominated by T lymphocytes ($CD3\varepsilon^+$), with minor populations of natural killer cells ($CD3\varepsilon^-CD56^+NKG2D^+$) and B lymphocytes ($CD19/20^+HLA\text{-}DR^+CD3^-$). In comparison, myeloid-lineage cells including macrophages ($CD14^{hi}CD11b^+HLA\text{-}DR^+$), mast cells ($Fc\varepsilon R1\alpha^+CD117^+CD11b^-CD49d^+$) and neutrophils ($CD15^+CD11b^+CD49d^-$) were more evident in the normal tissue from these patients. A similar immune profile was observed in breast tissues obtained from the two prophylactic mastectomies (**Fig 1B**).

Evaluate presence of tumor-associated macrophages with CD68, CD163 and/or colony-stimulating factor 1 receptor (CSF1R). ***(months 18-24)***

Macrophages are well established as regulators of murine mammary tumorigenesis (2), where they can represent up to 80% of leukocytes present within late stage mammary carcinomas (3). In human BC, immunoreactivity for CD68 has been used extensively for identification of macrophages, with $CD68^+$ cell density associated with reduced overall survival (1, 4-6).

The high number of $CD68^+$ cells reported in the literature, and shown in **Fig. 3A**, was in contrast to the limited number of $CD14^{hi}CD11b^+HLA\text{-}DR^+$ macrophages observed by flow cytometry in the BC suspensions examined. To understand this discrepancy, we first evaluated CD68 expression in BC tissue sections, as compared to CD163 (a hemoglobin scavenger

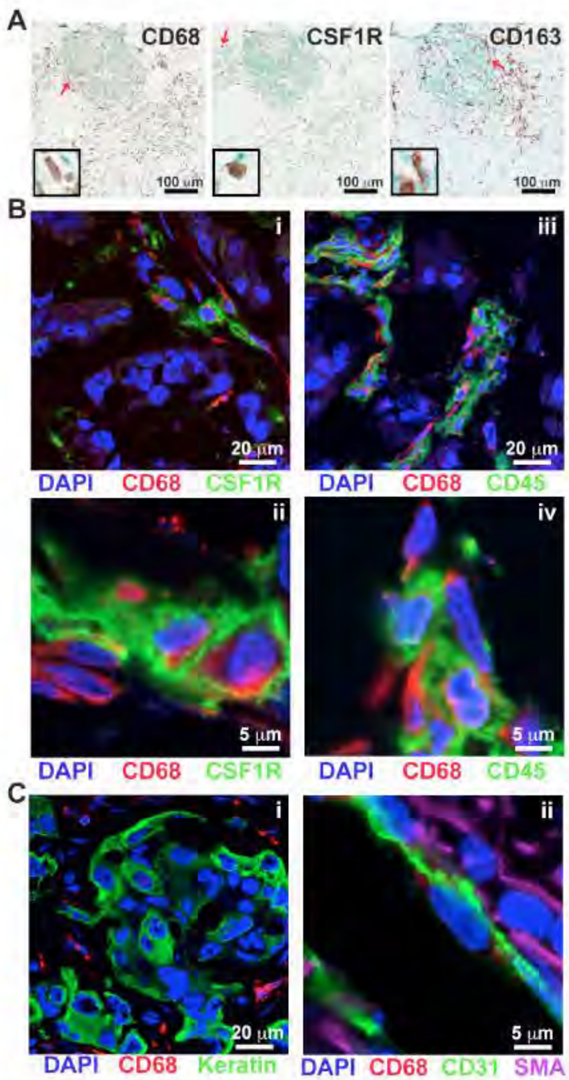

Fig. 2. CD68 is not a specific macrophage marker in human breast tumor tissue. (A) Representative immunohistochemistry within tumors for CD68 (left), CSF1R (middle), and CD163 (right) in serial sections from a CTX-treated patient. Red arrows indicate cells displayed in enlarged insets. (B) Immunofluorescent staining of human breast tumors for CD68 (red) in conjunction with CSF1R (i-ii) or CD45 (iii-iv). (C) Immunofluorescent staining for CD68 (red) in conjunction with pan-keratin (green; i), or CD31 (green) and smooth muscle actin-α (SMA; purple; ii).

receptor also commonly used as a marker for macrophages) and CSF1R (**Fig 2A**). This comparative analysis revealed a lack of correlation in cell density between the three markers. We next evaluated frozen BC tissue sections by confocal microscopy following immunofluorescent detection of CD68 in combination with CSF1R or CD45 (**Fig. 2B**). While all cells expressing high levels of the CSF1R also expressed CD68, there was a distinct population of $CD68^+$ cells that expressed neither CSF1R, nor CD45. CD68 did not significantly co-localize with $keratin^+$ epithelial cells, $CD31^+$ endothelial cells or smooth muscle actin α-expressing mural cells surrounding vasculature (Fig. 3C). This contrasted with murine mammary tumors isolated from MMTV-PyMT transgenic mice (7), where $CD68^+$ cells co-expressed both CSF1R and the murine macrophage marker F4/80 (**data not shown**). In agreement with historic literature (8, 9), these results thus indicate that CD68 is not a macrophage-specific marker in human BC.

STATUS: COMPLETE

<u>Evaluate the phenotype of lymphocyte populations:</u>

Examine expression of activation markers and chemokine receptor expression on lymphocyte populations by flow cytometry. ***(months 12-24).***

To reveal the phenotype of T cells infiltrating BCs, we examined surface marker and chemokine receptor expression of tissue-infiltrating $CD4^+$ and $CD8^+$ T cells (**Fig. 3A, B**). Specifically, both $CD4^+$ and $CD8^+$ T cells displayed increased expression of activation markers CD69 and HLA-DR compared to peripheral blood T cells, with a corresponding loss of markers for naïve T cells, CD45RA and CCR7. Furthermore, while all T cells constitutively expressed the co-stimulatory receptor CD28 (**data not shown**), expression of CD27, another co-stimulatory receptor, was reduced in a large proportion of tissue-infiltrating cells, indicative of shedding following interaction with its ligand CD70

(10) and potential acquisition of effector functions (11, 12). CD4^{+} and CD8^{+} T cells also displayed substantially upregulated expression of chemokine receptors CCR4 and CCR5 (**Fig. 3B**), and while CD8^{+} T cells constitutively expressed CXCR3, tissue-infiltrating CD4^{+} T cells exhibited higher CXCR3 expression than their counterparts in peripheral blood. Surface marker expression by tissue-infiltrating CD4^{+} and CD8^{+} T cells was subtly different between tumor and benign tissue in some samples; however, these changes were not consistent across patients, or between CTX-naïve and CTX-treated groups (**data not shown**).

Examine the presence of regulatory T cells through flow cytometry of CD25^{hi} cells and FoxP3 immunohistochemistry. ***(months 12-24).***

Despite the apparent reduction in the percentage of CD4^{+} T cells in tumors from CTX-treated patients, the density of IHC detected regulatory T cells expressing FoxP3 (**Fig. 4A**), specifically expressed by CD3^{+}CD4^{+} cells in the tumor (**Fig. 4B**), was not altered. Gating on CD25^{hi} cells, consisting of greater than 80% of FoxP3^{+} cells in all samples tested, also revealed

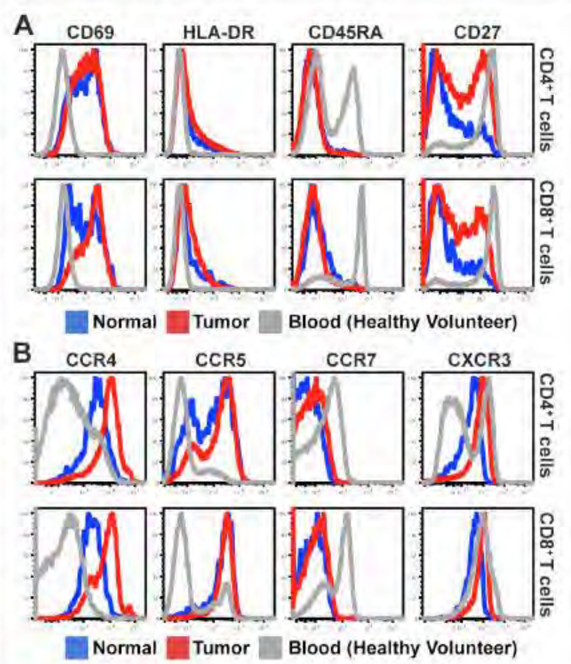

Fig. 3. Tissue-infiltrating T cells display an activated phenotype. (A-B) Representative histograms of CD3^{+}CD4^{+} (top) or CD3^{+}CD8^{+} (bottom) T cells isolated from a single CTX-treated patient with both normal (blue) and tumor (red) tissue. Expression of activation markers CD69 (left), HLA-DR (middle left), CD45RA (middle right) and CD27 (right) are shown in (A), and expression of chemokine receptors CCR4 (left), CCR5 (middle left), CCR7 (middle right) and CXCR3 (right) are shown in (B).

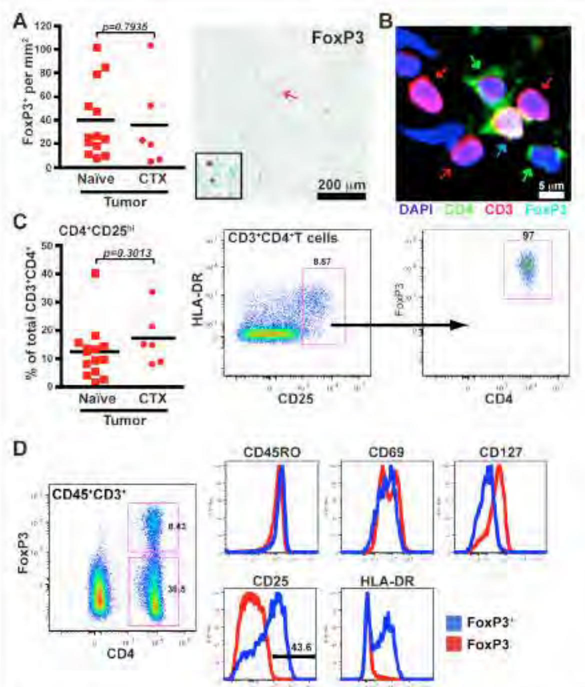

Fig. 4. Presence of CD4^{+}FoxP3^{+} regulatory T cells within tumors. (A) Number of FoxP3 positive cells per area as determined by automated counting (left) with a representative stained section shown (right). (B) Immunofluorescent staining of tumors for CD4 (green), CD3 (red) and FoxP3 (teal). Arrows indicate CD3^{+}CD4^{-}FoxP3^{-} (red), CD3^{+}CD4^{+}FoxP3^{-} (green) and CD3^{+}CD4^{+}FoxP3^{+} (teal) cells. (C) Percent of CD25^{hi} cells within the CD3^{+}CD4^{+} T cell population (left panel) with a representative polychromatic dot plot demonstrating FoxP3 staining within this population (right panels). (D) Representative histograms of CD3^{+}CD4^{+}FoxP3^{-} (red) and CD3^{+}CD4^{+}FoxP3^{+} cells (blue) showing expression of CD45RO, CD69, CD25, CD127 and HLA-DR.

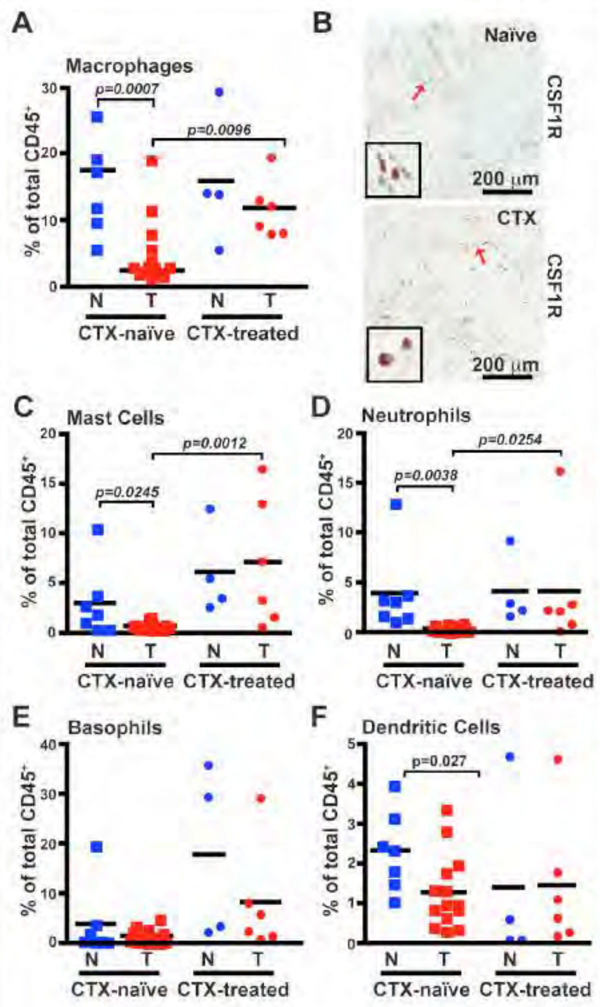

Fig. 5. Increased myeloid-lineage leukocyte infiltration within CTX-treated patients (A) $CD14^{hi}CD11b^{+}HLA\text{-}DR^{+}$ macrophages shown as a percent of total $CD45^{+}$ cells as determined by flow cytometry. (B) Representative immunohistochemistry for CSF1R in tumors from either untreated (top) or CTX-treated (bottom) patients. (C) $Fc\varepsilon R1\alpha^{+}CD117^{+}CD11b^{-}CD49d^{+}$ mast cells, (D) $CD15^{+}CD11b^{+}CD49d^{-}$ neutrophils, (E) $Fc\varepsilon R1\alpha^{+}CD117^{-}CD11b^{-}CD49d^{+}$ basophils, and (F) $CD11c^{+}HLA\text{-}DR^{+}CD14^{lo/-}$ DCs shown as a percent of total $CD45^{+}$ cells. N, nonadjacent normal; T, tumor.

that the relative percentage of these cells was invariant between groups (**Fig. 4C**). Phenotypically, $CD4^{+}FoxP3^{+}$ cells displayed an activated phenotype with equivalent surface levels of CD45RO and CD69 to $CD4^{+}FoxP3^{-}$ cells, and as has been reported for cells in peripheral blood (13), expressed lower levels of CD127 (**Fig. 4D**). Interestingly, while not all $FoxP3^{+}$ cells expressed HLA-DR, they did comprise the majority of HLA-DR-expressing $CD4^{+}$ T cells, in addition to coexpressing high levels of CD25.

STATUS: COMPLETE

<u>Compare leukocyte infiltration in patients treated with neoadjuvant chemotherapy:</u>

Utilize polychromatic flow cytometry to compare relative frequency of myeloid populations, including macrophages, mast cells, neutrophils, basophils, dendritic cells, and eosinophils. ***(months 12-24)***

Comparative analysis of residual BC tissue removed from patients following neoadjuvant CTX revealed an obvious difference in the percentages of myeloid-lineage cells compared to the CTX-naïve group. With some exceptions, this included an increased presence of macrophages as a percent of total leukocytes (**Fig. 5A**), as well as by density evaluation of CSF1 receptor (CSF1R)-positive cells in tissue by IHC (**Fig. 5B**). Increased percentages of mast cells (**Fig. 5C**) and neutrophils (**Fig. 5D**) were also evident in most CTX-treated patients, with an approximate 14-fold increase in CTX-treated versus CTX-naïve groups. Basophils ($Fc\varepsilon R1\alpha^{+}CD117^{-}CD11b^{-}CD49d^{+}$; **Fig. 5E**) were highly increased in only one of six CTX-treated samples, while the percentage of myeloid dendritic cells ($CD11c^{+}HLA\text{-}DR^{+}CD14^{lo/-}$; **Fig. 5F**) was unchanged. Evaluation of plasmacytoid dendritic cells expressing CD85g/ILT7 detected an insufficient number of events for analysis. Thus, with the exception of basophils, dendritic cells and $CD15^{+}CD11b^{+}CD49d^{+}$ eosinophils – which were present just at a detectable level in the tissues examined – increased presence of myeloid-lineage cells typified residual tumors of women treated with neoadjuvant CTX.

Utilize polychromatic flow cytometry to compare relative frequency of lymphocyte populations, including NK cells, B cells, $CD4^+$ T cells, $CD8^+$ T cells, and γδ T cells. ***(months 12-24)***

While we observed no difference in the percent of $CD3e^-CD56^+NKG2D^+$ natural killer (NK) cells (**Fig. 6A**), higher levels of $CD19/CD20^+HLA\text{-}DR^+$ B cells were evident in several CTX-naïve tumors as compared to both normal tissue and CTX-treated tumors (**Fig. 6B**). As has been previously reported (14), B cells were clustered together in association with T cells (**Fig. 6C**). Notably, $CD4^+$ T cells as a percent of the total $CD45^+$ population were also increased in CTX-naïve tumors as compared to both normal tissue and residual post-neoadjuvant tumors (**Fig. 6D**). As the percent of $CD8^+$ T cells was unchanged within the CTX-treated group (**Fig. 5E**), this

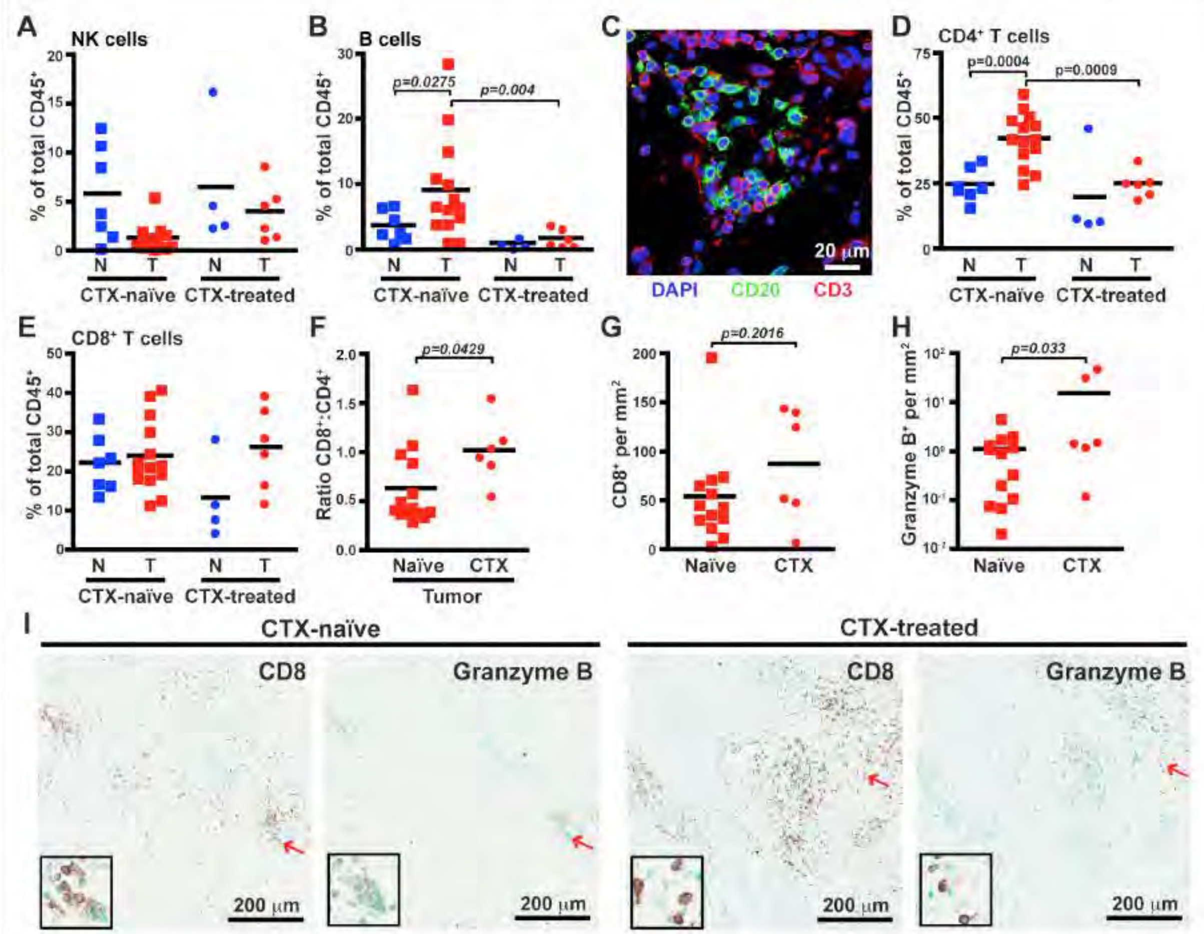

Fig. 6. Improved cytotoxic T cell response in CTX-treated tumors. (A) $CD3\varepsilon^-CD56^+NKG2D^+$ natural killer cells and (B) $CD3\varepsilon^-CD19/20^+HLA\text{-}DR^+$ B cells shown as a percent of total $CD45^+$ cells as determined by flow cytometry. (C) Immunofluorescent staining of tumors for CD20 (green) and CD3 (red). (D) $CD3\varepsilon^+CD4^+$ T cells and (E) $CD3\varepsilon^+CD8^+$ T cells shown as a percent of total $CD45^+$ cells. (F) Ratio of $CD8^+$ to $CD4^+$ T cells within CTX-naive versus CTX-treated tumors. Number of CD8-positive (G) and granzyme B-positive (H) cells per area as determined by automated counting. (I) Representative sections stained with CD8 or granzyme B from CTX-naive (left panels) or CTX-treated (right panels) tumors. Red arrows indicate cells displayed in enlarged insets. N, nonadjacent normal; T, tumor.

resulted in an altered ratio of $CD8^+$ to $CD4^+$ T cells (**Fig. 6F**). Although it was unclear whether the density of $CD8^+$ cells in CTX-treated residual tumors was increased (**Fig. 6G**), the number of cells expressing granzyme B was strikingly evident in two of six CTX-treated tumors (**Fig. 6H**), while minimal granzyme B staining was observed in CTX-naïve tumors, even in areas with high numbers of $CD8^+$ T cells (**Fig. 6I**).

STATUS: COMPLETE

#NEW AIM 4 was initiated in the last 12 months and has resulted in a PNAS manuscript (Ruffell et al., 2011). Please see appendix for attached manuscript.

##NEW AIM 5: EVALUATE DIAGNOSTIC AND THERAPEUTIC APPROACHES TARGETING MACROPHAGES IN MAMMARY ADENOCARCINOMA

Examine effects of tumor-associated macrophage depletion, via CSF1-CSF1R pathway blockade, on characteristics of tumor progression and/or response to chemotherapy:

Examine effects of chemotherapy (paclitaxel) on the presence of distinct macrophage populations within mammary tumors. ***(months 18-30)***

We have already established that the number of TAMs is increased in both human patients that have undergoing neoadjuvant chemotherapy (15), and tumor bearing MMTV-PyMT mice treated with paclitaxel (1). While we have not yet evaluated TAM subsets in chemotherapy treated animals, we have found two distinct subsets of TAMs in normal mammary glands and mammary tumors, distinguishable largely on the basis of MHCII expression (**Fig. 7A and 7B**). These subpopulations differentially express a variety of other markers (**Fig. 7C**), but are morphologically similar (**Fig. 7D**).

Examine effects of CSF1R kinase blockade on distinct macrophage populations, and other leukocyte subtypes in mammary tumors and their pulmonary metastases. ***(months 18-30)***

Preliminary analysis of TAM populations following treatment with the CSF1R kinase inhibitor PLX3397 has revealed that $MHCII^{LO}$ TAMs are preferentially lost during treatment (**Fig. 8**). Intriguingly, a similar phenomenon has recently been reported in mice during gestation, wherein although CSF1R blockade reduces macrophage accumulation in the myometrium during pregnancy, there is a preferential loss of the $MHCII^{LO}$ population (16).

Examine effects of CSF1R small molecule kinase inhibitor in combination with chemotherapy on mammary tumor growth and metastasis. ***(months 24-36)***

These studies have not yet initiated.

STATUS: ONGOING

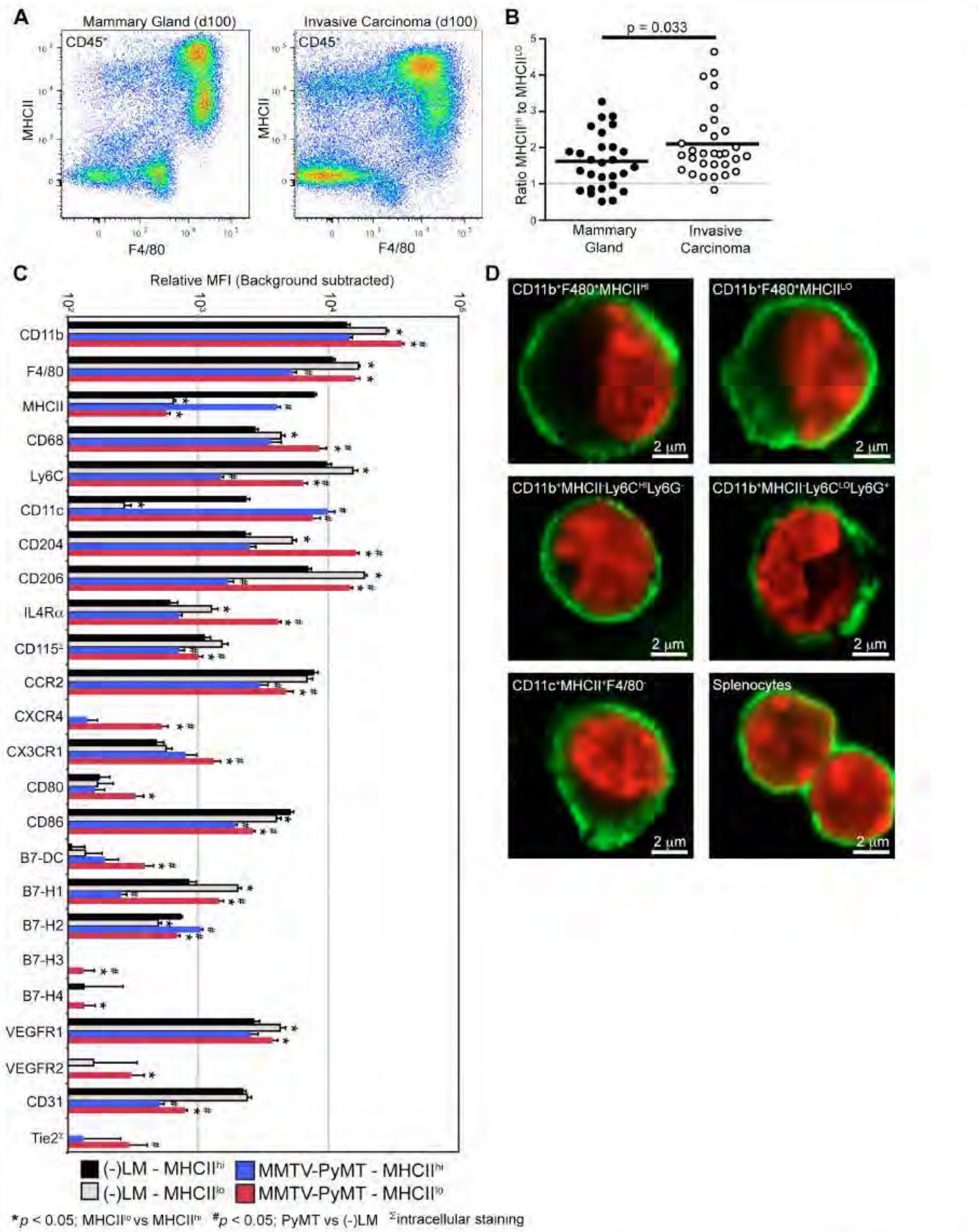

Fig. 7. Distinct macrophage subsets in mammary glands and tumors defined by MHCII expression. (A) Flow cytometric profiles of $CD45^+$ cells displaying MHCII and F4/80 expression. (B) Ratio of $MHCII^{HI}$ to $MHCII^{LO}$ macrophages in mammary glands versus tumors. (C) Expression of various markers as determined through fluorescence measurement via flow cytometry. (D) Cytospins of purified populations stained with β-actin (green) and DAPI (red).

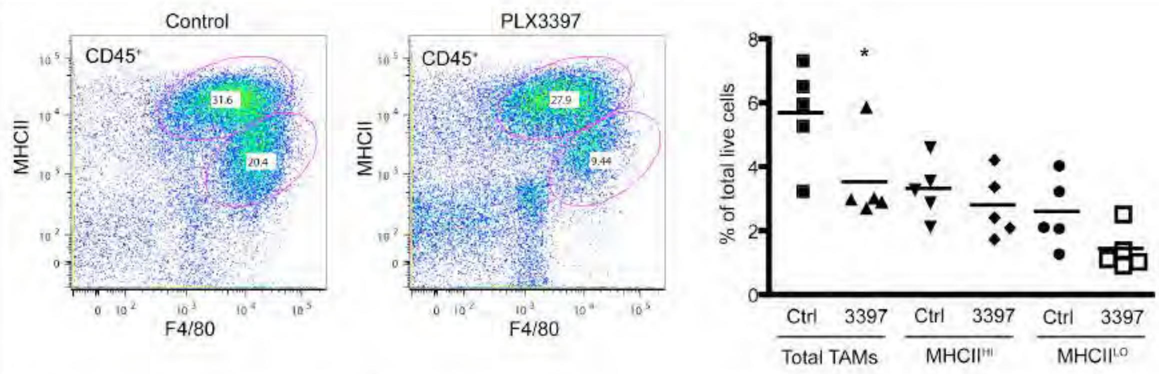

Fig. 8. Selective loss of MHCII^{LO} TAMs following treatment with CSF1R kinase inhibitor PLX3397.

<u>Determine the mechanism by which a reduction in tumor-associated macrophages improves response to chemotherapy:</u>

Examine whether cytotoxic activity of CD8^{+} T cells is necessary for enhancement of chemotherapy with CSF1-CSF1R targeting. ***(months 18-30)***

Examine whether CSF1-CSF1R targeting alters the vasculature to enhance penetration of chemotherapeutic agents. ***(months 24-30)***

These studies have not yet initiated.

Examine whether CSF1-CSF1R targeting selectively affects different functional subsets of tumor-associated macrophages: ie T_H1/T_H2, Tie2^{+}, or FoxP3^{+}. ***(months 30-36)***

These studies have not yet initiated.

Identify molecular pathways by which macrophages alter the vasculature or restrict cytotoxic activity. Utilize neutralizing/blocking antibodies to confirm role of these molecules in limiting the response to chemotherapy. ***(months 30-36)***

Gene expression analysis of the individual TAM subsets revealed an array of differences between MHCII^{HI} and MHCII^{LO} TAMs, but most strikingly, found that MHCII^{LO} TAMs expressed higher levels of IL-10 and arginase-1, both of which are established immunosuppressive molecules (**Fig. 9**). As we have already established that CD8^{+} T cells are critical for the enhanced response to chemotherapy following blockade of the CSF1-CSF1R pathway, these findings suggest that direct suppression of the T cell response by MHCII^{LO} TAMs may be a critical mediator of the chemoresponse.

STATUS: ONGOING

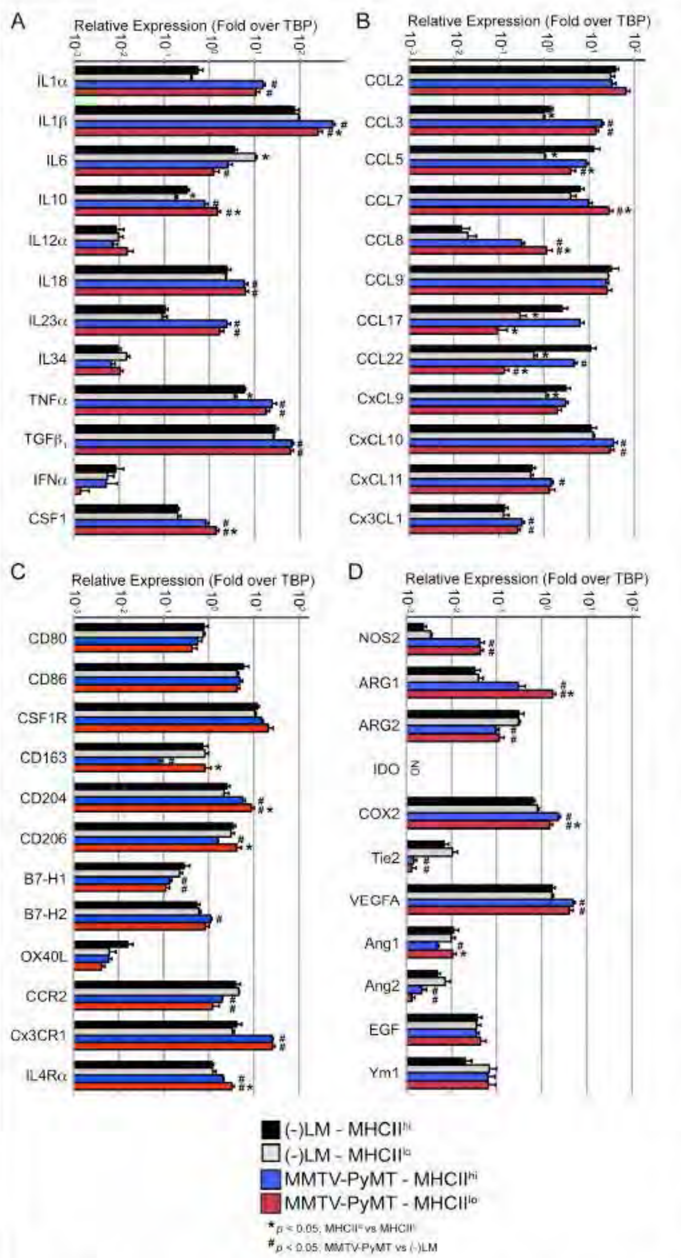

Fig. 9. Macrophage subsets display unique gene expression profiles. (A) Cytokine gene expression. (B) Chemokine gene expression. (C) Surface marker expression. (D) Immunosuppressive and angiogenesis related gene expression.

<u>Evaluate ultrasmall super paramagnetic iron oxide nanoparticles (USPIO) for detection of macrophages within mammary carcinomas by magnetic resonance (MR) imaging:</u>

Examine in vitro uptake of USPIOs by tumor-associated macrophages. ***(months 18-24)***

Following incubation with the iron oxide nanoparticle ferumoxytol, F4/80$^+$ TAMs demonstrated a markedly decreased signal on T2-weighted MR images, while F4/80$^-$ cells demonstrated minimal signal changes compared to untreated controls (**Fig. 10A**). Calculation of changes in relaxation rates (DR) as quantitative measures of the MR signal enhancement corroborated the qualitative findings with significantly higher DR2 data for ferumoxytol-exposed F4/80$^+$ TAMs compared to ferumoxytol-exposed F4/80$^-$ cells consisting primarily of carcinoma cells ($p>0.05$). Determination of iron content in the samples revealed that increased iron uptake was responsible for the observed relaxation rate changes (**Fig. 10B**).

Since both TAMs and malignant epithelial cells highly express the folate receptor, folate-linked USPIO have been recently developed for "tumor-targeted imaging" (17-19). F4/80$^+$ TAMs incubated with folate-engrafted P1133 nanoparticles demonstrated significantly stronger visual and quantitative MR signal enhancement as compared to ferumoxytol and P904 (**Fig. 10**). However, folate-engraftment also lead to significantly increased nanoparticle uptake and MR enhancement of F4/80$^-$ populations. The P1133-induced signal effect was inhibited by co-incubation with free folic acid to P904 levels, thus indicating that folate-targeting mediates increased USPIO uptake into mammary carcinomas.

Evaluate USPIOs for contrast enhancement within mammary carcinomas. ***(months 18-30)***

We investigated 90-day-old MMTV-PyMT mice (n=16) bearing late-stage mammary adenocarcinomas before and after intravenous injection of ferumoxytol, as well as syngeneic mice with PyMT-derived orthotopic mammary tumors (n=8) (**Fig. 11**). All tumors demonstrated an initial negative (dark) enhancement on immediate postcontrast T2-weighted MR images, that was most pronounced in the tumor periphery and which increased slowly and gradually up to 1.0-hour (h) post injection (p.i.). This corresponds to an initial blood pool perfusion of USPIO with slow, gradual transendothelial leakage of the nanoparticles into the tumor interstitium (20-23). At 24 h p.i. of ferumoxytol, all tumors demonstrated a persistent signal decline, which was most pronounced in tumor centers (**Fig. 11**).

Determine whether USPIOs are selectively labeling tumor-associated macrophages and can be used to quantify the level of macrophages within tumors. ***(months 24-30)***

Detection of iron using DAB-enhanced Prussian Blue staining, and immunodetection of $CD68^+$ TAMs in tissue sections of mammary tumors localized ferumoxytol to $CD68^+$ TAMs (**Fig 12A**). As it was difficult to show selective uptake using DAB-generated contrast due to high background, we also generated ferumoxytol-FITC to show colocalization by immunofluorescence using an Alexa 488 conjugated anti-FITC antibody. As shown in **Fig. 12B**, ferumoxytol was specifically found within $CD68^+$ TAMs, but not keratin 18-expressing malignant epithelial cells. While ferumoxytol was not found within all TAMs, these results indicate that the MR signal effects on delayed MR images were largely due to TAM-mediated uptake of contrast agent.

STATUS: COMPLETE

[##]NEW AIM 5 was initiated in the last 6 months based upon our recent publication in Cancer Discovery (DeNardo et al. 2011). The final subaim involving MRI has also been completed and is now published as the cover article in Clinical Cancer Research (Daldrup-Link et al. 2011). Please see appendix for attached papers.

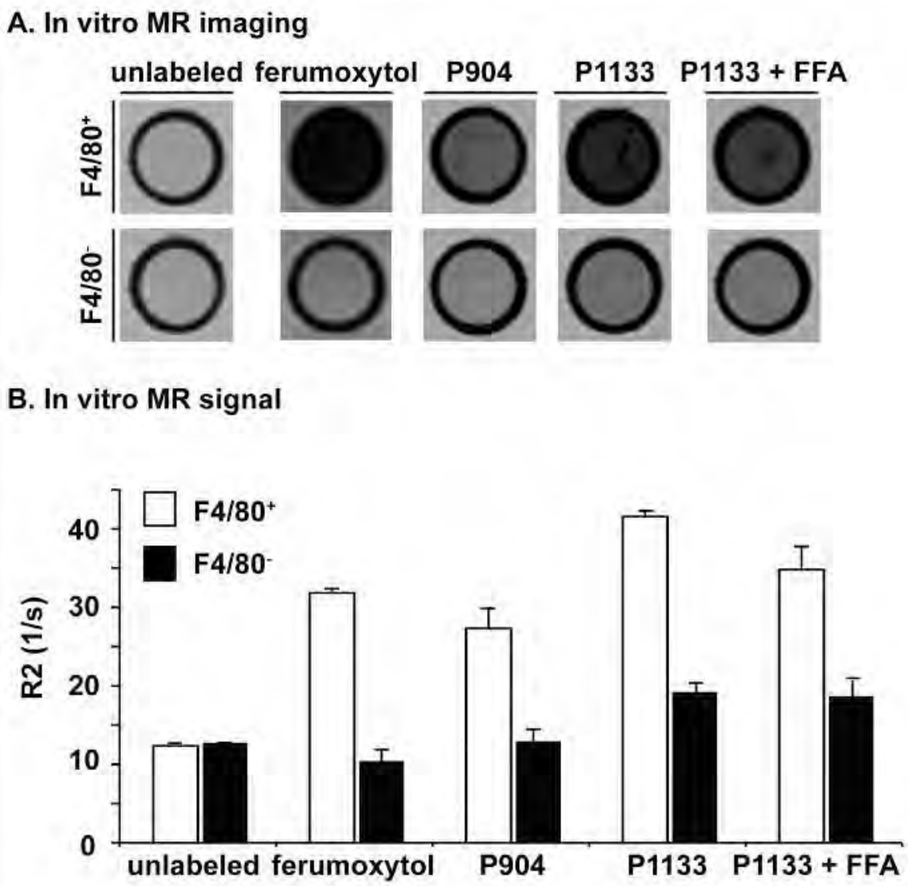

Fig. 10. In vitro MR scans of iron oxide nanoparticle-labeled cells with corresponding quantitative MR signal enhancement and spectrometry data. (A) Axial T2-weighted MR images through test tubes containing F4/80$^+$ versus F4/80$^-$ cells labeled overnight with Ferumoxytol, P904, P1133 alone or P1133 with free folic acid (FFA). Cells were kept in suspension in ficoll solution and test tubes were placed in a water bath to avoid artifacts by surrounding air (which would cause a dark MR signal). Image parameters: 3 Tesla, SE 2000/60 (TR/TE in ms). (B) Corresponding R2 relaxation rates, i.e. quantitative measures of the MR signal effect, of iron oxide nanoparticle labeled and unlabeled F4 F4/80$^+$ versus F4/80$^-$ cells, displayed as mean +/- standard deviation from duplicate experiments.

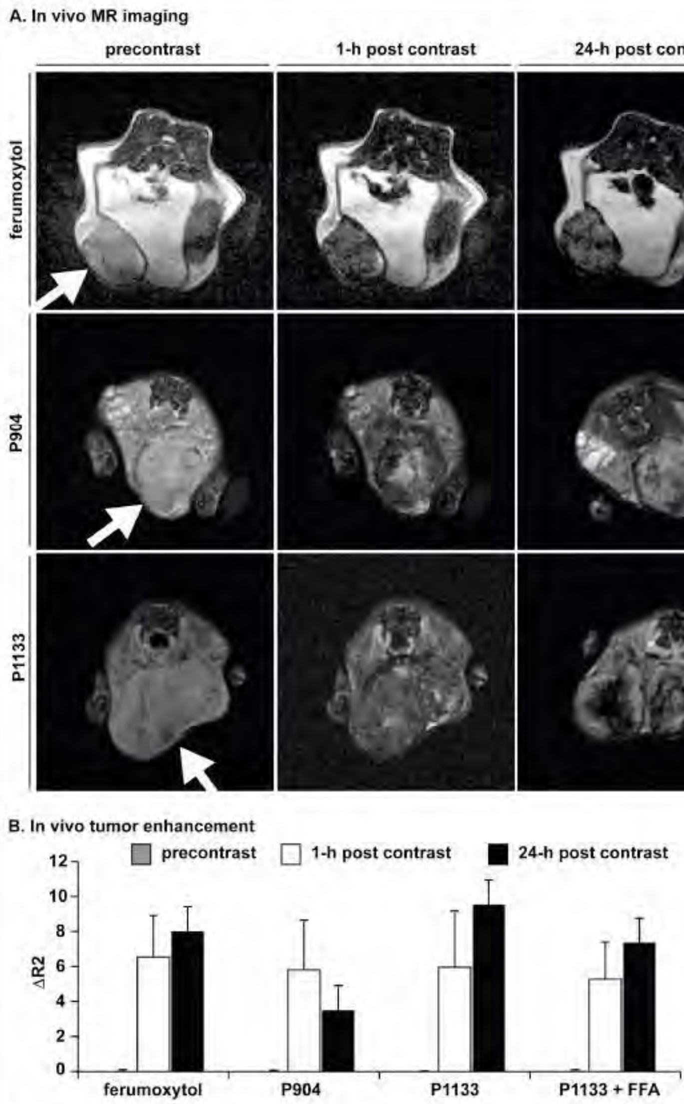

Fig. 11. In vivo MR imaging of iron oxide nanoparticles. **(A)** T2-weighted SE images of representative mammary tumors in MMTV-PyMT mice prior to (precontrast), 1 hour (h) and 24 h after administration of 0.5 mmol [Fe]/kg of ferumoxytol, P904 or P1133. The iron oxide nanoparticle-based contrast agents cause a negative (dark) signal effect in the tumor tissue on these scans (arrows point to tumors). **(B)** Quantitation of MR signal enhancement (delta R2 measurement),of mammary tumors in MMTV-PyMT mice before and after iron oxide-nanoparticle administration, displayed as means +/- standard deviation (n=7 mice/group, except P1133+FFA which contained 3 mice). Note that all tumors show a nanoparticle retention at 24 hours, which is most pronounced for the folate-linked nanoparticle P1133.

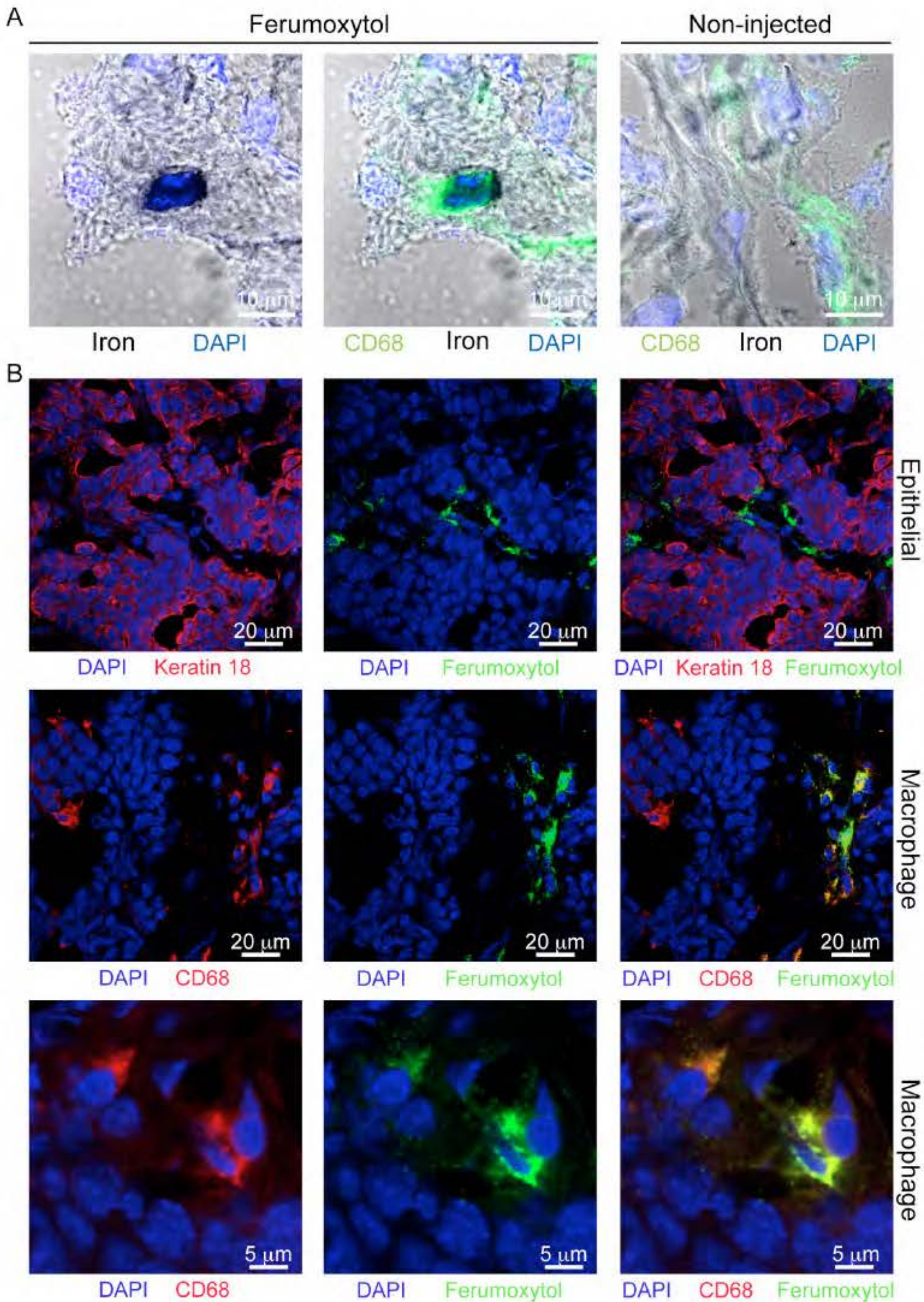

Fig. 12. Uptake of ferumoxytol by TAMs in vivo. (A) Localization within OCT-embedded mammary tumors of ferumoxytol (iron; black contrast) to $CD68^+$ macrophages (green) using phase contrast of DAB staining and confocal microscopy. (B) Localization of ferumoxytol-FITC (green) to $CD68^+$ macrophages (red) but not Keratin 18^+ carcinoma cells (red) within mammary tumors. Scale bars are shown in images.

III. KEY RESEARCH ACCOMPLISHMENTS:

Aim 4: Completed a comprehensive analysis of leukocytic infiltrate in human breast carcinomas, revealing a unique infiltrate compared to murine tumors, and pronounced influx of myeloid cells in tumors exposed to neoadjuvant chemotherapy.

Aim 5: Identified two distinct populations of tumor-associated macrophages in murine mammary tumors that appear to be preferentially affected by the CSF1/CSF1R pathway. Have identified a way to use MR imaging to monitor TAM infiltration, which may prove critical for the proper evaluation of therapies designed to reduce the presence of TAMs within breast tumors.

IV. REPORTABLE OUTCOMES:

Manuscripts:

Ruffell B, Au A, Rugo HS, Esserman LJ, Hwang ES, Coussens LM. (2011) Leukocyte composition of human breast cancer. Proc. Natl. Acad. Sci. (*Epub ahead of print*)

Daldrup-Link HE, Golovko D, **Ruffell B,** DeNardo DG Castaneda R, Ansari C, Rao J, Tikhomiron GA, Wendland M, Corot C, Coussens LM. (2011) MR Imaging of tumor associated macrophages with clinically-applicable iron oxide nanoparticles. Clin. Cancer Res. 17; 5695-5704.

DeNardo DG, Brennan DJ, Rexhepaj E, **Ruffell B**, Shiao SL, Madden SF, Gallagher WM, Wadhwani N, Keil SD, Junaid SA, Rugo HS, Hwang ES, Jirstrom K, West BL, Coussens LM. (2011) Leukocyte complexity predicts breast cancer survival and functionally regulates response to chemotherapy. Cancer Discov. 1(1): 54-67.

Abstracts/Posters:

- DOD Era of Hope Meeting. Orlando, FL. August 2-5, 2011.
- AACR 102nd Annual Meeting 2011. Orlando, FL. April 2-6, 2011.
- Breast Oncology Program Retreat. San Francisco, CA. January 27-28, 2011.

Presentations:

- Life Sciences Institute, Vancouver, BC (July, 2011)
- 7th Internation Symposium on the Intraductal Approach to Breast Cancer (Feb, 2011)

V. CONCLUSION:

It is now clear that infiltrating immune cells profoundly regulate solid tumor development. Diverse populations of cells infiltrate tumor microenvironments and are altered by cancer cells and surrounding stroma in such a way that many of their bioactivities are co-opted to aid growth and/or metastasis of tumors. Out of this realization emerges novel targets for therapy that may impact patient survival, i.e., immune targets regulating primary tumor development, and those regulating metastatic dissemination and growth. It is thus hypothesized that manipulating the immune response and neutralizing its effect on neoplastic cells represents an efficacious alternative approach to current disease management.

We have now established in both murine models and human patients that exposure to neoadjuvant chemotherapy induces the recruitment of myeloid populations, including tumor-associated macrophages (1, 15). Using the dependency of this population on the CSF1/CSF1R pathway for recruitment to the tumor microenvironment, we have demonstrated that preventing macrophage influx improves the response of transgenic mice to chemotherapy, resulting in lower primary tumor and pulmonary metastatic burden (1). Despite this success, human breast cancers are infiltrated by a wider variety of myeloid populations, for example mast cells, that may share overlapping functions with macrophages but that are not dependent on the CSF1/CSF1R pathway. Identifying common molecular pathways mediating chemoresistance may therefore improve the chance and/or efficacy of clinical translation. Along these lines, preliminary data suggests that CSF1/CSF1R blockage selectively reduces infiltration of a subpopulation of macrophages with enhanced immunosuppressive properties. Identifying the immunosuppressive pathways involved in restricting the response to chemotherapy therefore hold great potential for improving the rate of pathological complete response in patients and prolonging survival.

VI. BIBLIOGRAPHY:

1. DeNardo, D. G., D. Brennan, E. Rexhapaj, B. Ruffell, S. Shiao, W. M. Gallagher, N. Wadhani, S. D. Kial, S. A. Junaid, H. S. Rugo, E. S. Hwang, K. Jirstrom, B. West, and L. M. Coussens. 2011. Leukocyte complexity in breast cancer predicts overall survival and functionally regulates response to chemotherapy. *Cancer Discovery* 1:54-67.
2. Qian, B. Z., and J. W. Pollard. 2010. Macrophage diversity enhances tumor progression and metastasis. *Cell* 141:39-51.
3. DeNardo, D. G., J. B. Barreto, P. Andreu, L. Vasquez, D. Tawfik, N. Kolhatkar, and L. M. Coussens. 2009. CD4(+) T cells regulate pulmonary metastasis of mammary carcinomas by enhancing protumor properties of macrophages. *Cancer Cell* 16:91-102.
4. Leek, R. D., C. E. Lewis, R. Whitehouse, M. Greenall, J. Clarke, and A. L. Harris. 1996. Association of macrophage infiltration with angiogenesis and prognosis in invasive breast carcinoma. *Cancer Res* 56:4625-4629.
5. Campbell, M. J., N. Y. Tonlaar, E. R. Garwood, D. Huo, D. H. Moore, A. I. Khramtsov, A. Au, F. Baehner, Y. Chen, D. O. Malaka, A. Lin, O. O. Adeyanju, S. Li, C. Gong, M. McGrath, O. I. Olopade, and L. J. Esserman. 2010. Proliferating macrophages associated with high grade, hormone receptor negative breast cancer and poor clinical outcome. *Breast Cancer Res Treat* [Epub ahead of print].
6. Tsutsui, S., K. Yasuda, K. Suzuki, K. Tahara, H. Higashi, and S. Era. 2005. Macrophage infiltration and its prognostic implications in breast cancer: the relationship with VEGF expression and microvessel density. *Oncol Rep* 14:425-431.
7. Guy, C. T., R. D. Cardiff, and W. J. Muller. 1992. Induction of mammary tumors by expression of polyomavirus middle T oncogene: a transgenic mouse model for metastatic disease. *Mol Cell Biol* 12:954-961.
8. Pulford, K. A., A. Sipos, J. L. Cordell, W. P. Stross, and D. Y. Mason. 1990. Distribution of the CD68 macrophage/myeloid associated antigen. *Int Immunol* 2:973-980.
9. Kunz-Schughart, L. A., A. Weber, M. Rehli, E. Gottfried, G. Brockhoff, S. W. Krause, R. Andreesen, and M. Kreutz. 2003. [The "classical" macrophage marker CD68 is strongly expressed in primary human fibroblasts]. *Verh Dtsch Ges Pathol* 87:215-223.
10. Hintzen, R. Q., S. M. Lens, M. P. Beckmann, R. G. Goodwin, D. Lynch, and R. A. van Lier. 1994. Characterization of the human CD27 ligand, a novel member of the TNF gene family. *J Immunol* 152:1762-1773.
11. Hamann, D., P. A. Baars, M. H. Rep, B. Hooibrink, S. R. Kerkhof-Garde, M. R. Klein, and R. A. van Lier. 1997. Phenotypic and functional separation of memory and effector human CD8+ T cells. *J Exp Med* 186:1407-1418.

12. Okada, R., T. Kondo, F. Matsuki, H. Takata, and M. Takiguchi. 2008. Phenotypic classification of human CD4+ T cell subsets and their differentiation. *Int Immunol* 20:1189-1199.
13. Liu, W., A. L. Putnam, Z. Xu-Yu, G. L. Szot, M. R. Lee, S. Zhu, P. A. Gottlieb, P. Kapranov, T. R. Gingeras, B. Fazekas de St Groth, C. Clayberger, D. M. Soper, S. F. Ziegler, and J. A. Bluestone. 2006. CD127 expression inversely correlates with FoxP3 and suppressive function of human CD4+ T reg cells. *J Exp Med* 203:1701-1711.
14. Nelson, B. H. 2010. CD20+ B cells: the other tumor-infiltrating lymphocytes. *J Immunol* 185:4977-4982.
15. Ruffell, B., A. Au, H. S. Rugo, L. J. Esserman, E. S. Hwang, and L. M. Coussens. 2011. Leukocyte composition in human breast cancer. *Proc Natl Acad Sci U S A* in press.
16. Tagliani, E., C. Shi, P. Nancy, C. S. Tay, E. G. Pamer, and A. Erlebacher. 2011. Coordinate regulation of tissue macrophage and dendritic cell population dynamics by CSF-1. *J Exp Med* 208:1901-1916.
17. Kim, S., and J. Lee. 2010. Folate-targeted drug-delivery systems prepared by nano-comminution. *Drug Dev Ind Pharm*.
18. Meier, R., T. D. Henning, S. Boddington, S. Tavri, S. Arora, G. Piontek, M. Rudelius, C. Corot, and H. E. Daldrup-Link. 2010. Breast cancers: MR imaging of folate-receptor expression with the folate-specific nanoparticle P1133. *Radiology* 255:527-535.
19. Puig-Kroger, A., E. Sierra-Filardi, A. Dominguez-Soto, R. Samaniego, M. T. Corcuera, F. Gomez-Aguado, M. Ratnam, P. Sanchez-Mateos, and A. L. Corbi. 2009. Folate receptor beta is expressed by tumor-associated macrophages and constitutes a marker for M2 anti-inflammatory/regulatory macrophages. *Cancer Res* 69:9395-9403.
20. Daldrup-Link, H. E., J. Rydland, T. H. Helbich, A. Bjornerud, K. Turetschek, K. A. Kvistad, E. Kaindl, T. M. Link, K. Staudacher, D. Shames, R. C. Brasch, O. Haraldseth, and E. J. Rummeny. 2003. Quantification of breast tumor microvascular permeability with feruglose-enhanced MR imaging: initial phase II multicenter trial. *Radiology* 229:885-892.
21. Daldrup-Link, H. E., G. H. Simon, and R. C. Brasch. 2006. Imaging of tumor angiogenesis: current approaches and future prospects. *Curr Pharm Des* 12:2661-2672.
22. Turetschek, K., S. Huber, E. Floyd, T. Helbich, T. P. Roberts, D. M. Shames, K. S. Tarlo, M. F. Wendland, and R. C. Brasch. 2001. MR imaging characterization of microvessels in experimental breast tumors by using a particulate contrast agent with histopathologic correlation. *Radiology* 218:562-569.
23. Turetschek, K., T. P. Roberts, E. Floyd, A. Preda, V. Novikov, D. M. Shames, W. O. Carter, and R. C. Brasch. 2001. Tumor microvascular characterization using ultrasmall superparamagnetic iron oxide particles (USPIO) in an experimental breast cancer model. *J Magn Reson Imaging* 13:882-888.

VII. APPENDICES:

A. Complete academic Curriculum vitae for Dr. Brian Ruffell
B. Collected publications from months 13-24

- Leukocyte composition of human breast cancer. Proc. Natl. Acad. Sci. (*Epub ahead of print*)
- MR Imaging of tumor associated macrophages with clinically-applicable iron oxide nanoparticles. Clin. Cancer Res. 17; 5695-5704.
- Leukocyte complexity predicts breast cancer survival and functionally regulates response to chemotherapy. Cancer Discov. 1(1): 54-67.

BIOGRAPHICAL SKETCH

NAME	POSITION TITLE
Brian Ruffell	Postdoctoral Scholar University of California, San Francisco

EDUCATION/TRAINING *(Begin with baccalaureate or other initial professional education, such as nursing, and include postdoctoral)*

INSTITUTION AND LOCATION	DEGREE *(if applicable)*	YEAR(s)	FIELD OF STUDY
University of California, San Francisco, CA	n/a	Current	Cancer Immunology
University of British Columbia, Vancouver, BC	PhD	2008	Immunology
University of British Columbia, Vancouver, BC	BSc	2001	Cell Biology/Genetics

POSITIONS AND HONORS:

2008 – pres. Postdoctoral Scholar: Department of Pathology, University of California, San Francisco, San Francisco, CA.

2002 - 2008 Graduate Student: Department of Microbiology and Immunology. University of British Columbia, Vancouver, BC, Canada

1997 - 2001 Undergraduate Student: Department of Science. University of British Columbia, Vancouver, BC, Canada

FELLOWSHIPS AND AWARDS:

2009 DOD Breast Cancer Research Program Postdoctoral Award
2006 Heart and Stroke Foundation of Canada Doctoral Research Award
2006 Robert Emmanuel and Mary Day Endowment Award
2005 John Richard Turner Fellowship in Microbiology
2005 Armauer-Hansen Memorial Scholarship

PUBLICATIONS:

1. **Ruffell B**, Au A, Rugo HS, Esserman LJ, Hwang ES, Coussens LM. (2011) Leukocyte composition of human breast cancer. Proc. Natl. Acad. Sci. (*Epub ahead of print*)
2. Daldrup-Link HE, Golovko D, **Ruffell B,** DeNardo DG Castaneda R, Ansari C, Rao J, Tikhomiron GA, Wendland M, Corot C, Coussens LM. (2011) MR Imaging of tumor associated macrophages with clinically-applicable iron oxide nanoparticles. Clin. Cancer Res. 17; 5695-5704.
3. DeNardo DG, Brennan DJ, Rexhepaj E, **Ruffell B**, Shiao SL, Madden SF, Gallagher WM, Wadhwani N, Keil SD, Junaid SA, Rugo HS, Hwang ES, Jirstrom K, West BL, Coussens LM. (2011) Leukocyte complexity predicts breast cancer survival and functionally regulates response to chemotherapy. Cancer Discov. 1(1): 54-67.
4. **Ruffell B**, Poon GFT, Lee S, Brown KL, Tjew SL, Cooper J, Johnson P. (2011) Differential use of chondroitin sulfate to regulate hyaluronan binding by receptor CD44 in inflammatory and interleukin 4-activated macrophages. J. Biol. Chem. 286(22): 19179-19190.
5. **Ruffell B**, Coussens LM. (2011) Histamine restricts cancer: nothing to sneeze at. Nat. Med. 17: 43-44.
6. **Ruffell B**, DeNardo DG, Affara, NI, Coussens LM. (2010) Lymphocytes in cancer development: polarization towards pro-tumor immunity. Cytokine Growth Factor Rev. 21(1): 3-10.
7. Johnson P, **Ruffell B**. (2009) CD44 and its role in inflammation and inflammatory diseases. Inflamm. Allergy Drug Targets. 8(3): 208-220.
8. **Ruffell B**, Johnson P. (2009) The regulation and function of hyaluronan binding by CD44 in the immune system. Glycoforum: Science of Hyaluronan Today 33: 1-20.
9. **Ruffell B**, Johnson P. (2008) Hyaluronan induces cell death in activated T cells through CD44. J. Immunol. 181: 7044-7054.

10. **Ruffell B**, Johnson P. (2005) Chondroitin sulfate addition to CD44H negatively regulates hyaluronan binding. Biochem. Biophys. Res. Commun. 334(2): 306-312.
11. Khan AI, Kerfoot SM, Heit B, Liu L, Andonegui G, **Ruffell B**, Johnson P, Kubes P. (2004) Role of CD44 and hyaluronan in neutrophil recruitment. J. Immunol. 173(12): 7594-7601.

ABSTRACTS:

1. **Ruffell B,** DeNardo DG, Au A, Rugo HS, Hwang ES, Coussens LM. (2011). Leukocyte complexity in human breast cancer and response to chemotherapy. AACR Proceedings 52: 647.
2. **Ruffell B**, Johnson P. (2006) Hyaluronan induces apoptosis through CD44 in activated lymphoma cells. EJC Supplements 4(12): 147.
3. **Ruffell B**, Johnson P. (2004) Chondroitin sulfate chains on CD44 negatively regulate its ability to bind hyaluronan. Glycobiology 14(11): 1108.

POSTERS:

1. DOD Era of Hope Meeting. Orlando, FL. August 2-5, 2011.
2. AACR 102nd Annual Meeting 2011. Orlando, FL. April 2-6, 2011.
3. Breast Oncology Program Retreat. San Francisco, CA. January 27-28, 2011.
4. Diller Building Scientific Symposium. San Francisco, CA. August 27-28, 2009.
5. Breast Oncology Program Retreat. San Francisco, CA. January 29-30, 2009.
6. 18th EORTC-NCI-AACR: Symposium on Molecular Targets and Cancer Therapeutics. Prague, Czech Republic. November 7-10, 2006
7. US/Japan Glycobiology 2004. Honolulu, HI. November 17-20, 2004

CONFERENCES:

1. DOD Era of Hope Meeting. Orlando, FL. August 2-5, 2011.
2. AAI 98th Annual Meeting 2011. San Francisco, CA. May 13-17, 2011.
3. AACR 102nd Annual Meeting 2011. Orlando, FL. April 2-6, 2011.
4. 7th International Symposium on the Intraductal Approach to Breast Cancer. Santa Monica, CA. February 23-26, 2011.
5. Breast Oncology Program Retreat. San Francisco, CA. January 27-28, 2011.
6. Molecular and Cellular Biology of Immune Escape in Cancer. Keystone, CO. February 7-12, 2010
7. Diller Building Scientific Symposium. San Francisco, CA. August 27-28, 2009.
8. 6th International Symposium on the Intraductal Approach to Breast Cancer. Santa Monica, CA. February 19-21, 2009.
9. Breast Oncology Program Retreat. San Francisco, CA. January 29-30, 2009.
10. 18th EORTC-NCI-AACR: Symposium on Molecular Targets and Cancer Therapeutics. Prague, Czech Republic. November 7-10, 2006
11. US/Japan Glycobiology 2004. Honolulu, HI. November 17-20, 2004

ORAL PRESENTATIONS:

1. Life Sciences Institute, Vancouver, BC (July, 2011)
2. 7th Internation Symposium on the Intraductal Approach to Breast Cancer (Feb, 2011)
3. Pacific Coast Protease Meeting, Borrego Springs, CA (April, 2010)
4. Stanford University School of Medicine, Stanford, CA (Aug, 2009)
5. Dr. Susan Love Research Foundation, Los Angeles, CA (Jan, 2009)
6. Helen Diller Family Comprehensive Cancer Center, San Francisco, CA (June 2008)
7. Deeley Research Centre, Victoria, BC (May, 2008)
8. BC Cancer Research Centre, Vancouver, BC (May, 2008)
9. Life Sciences Institute, Vancouver, BC (Jan, 2008)

Leukocyte composition of human breast cancer

Brian Ruffell[a], Alfred Au[a,b], Hope S. Rugo[b,c], Laura J. Esserman[b,d], E. Shelley Hwang[b,d], and Lisa M. Coussens[a,b,1]

[a]Department of Pathology and [b]Helen Diller Family Comprehensive Cancer Center, University of California, San Francisco, CA 94143; and Departments of [c]Medicine and [d]Surgery, University of California, San Francisco, CA 94115

Edited by Kornelia Polyak, Dana Farber Cancer Institute, Boston, MA, and accepted by the Editorial Board July 13, 2011 (received for review March 17, 2011)

Retrospective clinical studies have used immune-based biomarkers, alone or in combination, to predict survival outcomes for women with breast cancer (BC); however, the limitations inherent to immunohistochemical analyses prevent comprehensive descriptions of leukocytic infiltrates, as well as evaluation of the functional state of leukocytes in BC stroma. To more fully evaluate this complexity, and to gain insight into immune responses after chemotherapy (CTX), we prospectively evaluated tumor and nonadjacent normal breast tissue from women with BC, who either had or had not received neoadjuvant CTX before surgery. Tissues were evaluated by polychromatic flow cytometry in combination with confocal immunofluorescence and immunohistochemical analysis of tissue sections. These studies revealed that activated T lymphocytes predominate in tumor tissue, whereas myeloid lineage cells are more prominant in "normal" breast tissue. Notably, residual tumors from an unselected group of BC patients treated with neoadjuvant CTX contained increased percentages of infiltrating myeloid cells, accompanied by an increased CD8/CD4 T-cell ratio and higher numbers of granzyme B-expressing cells, compared with tumors removed from patients treated primarily by surgery alone. These data provide an initial evaluation of differences in the immune microenvironment of BC compared with nonadjacent normal tissue and reveal the degree to which CTX may alter the complexity and presence of selective subsets of immune cells in tumors previously treated in the neoadjuvant setting.

inflammation | macrophage

Several subtypes of CD45 expressing leukocytes infiltrate breast cancer (BC), including $CD4^+$ and $CD8^+$ T cells, $CD20^+$ B cells, and multiple myeloid lineage cells including tumor associated macrophages (TAMs) that are often identified by immunohistochemical (IHC) detection of CD68 (1). High lymphocyte infiltration is associated with increased survival in patients <40 y of age (2) and with a favorable prognosis in subsets of patients whose tumors are also heavily infiltrated by TAMs (3). More specifically, large cohort studies of patients with BC have revealed that the presence of $CD68^+$ cells in tumor tissue correlates with poor prognostic features (4 6), higher tu mor grade (7 9), increased angiogenesis (10 13), decreased disease free survival (6, 11, 14, 15), and increased risk for sys temic metastasis when assessed in conjunction with endothelial and carcinoma cell markers (16).

The functional significance of specific leukocytes in BC de velopment has been implied based on experimental studies using murine models of mammary carcinogenesis where mice harboring homozygous null mutations in genes specifying leukocyte de velopment or recruitment have been evaluated. In transgenic mice expressing the polyoma virus middle T antigen regulated by the mouse mammary tumor virus promoter (MMTV PyMT mice), progression of mammary carcinomas and metastases to lungs are reduced in mice lacking the *colony stimulating factor 1* (*csf1*) gene, a cytokine critical for macrophage maturation and recruitment (17, 18). TAMs in mammary tumor tissue are often associated with vasculature (19), where their production of VEGFA fosters an giogenic programming of tissue (20, 21), and their production of EGF promotes invasive tumor growth and subsequent metastases (22, 23). Moreover, TAMs regulated by epithelial CSF1 express higher levels of several hypoxia induced genes (*iNOS* and *arginase 1*) that, in turn, mediate suppression of anti tumor immunity by blocking cytotoxic T cell proliferation and activation (6, 24). Thus, TAM presence and bioactivity within mammary tumors corre spond to their clinical activity, further indicating the importance of TAMs, not only in promoting tumor development, but also in suppression of anti tumor immunity.

$CD4^+$ T cells isolated from human BC produce high levels of type II helper (T_H2) cytokines including IL 4 and IL 13 (25, 26), which are significant in light of studies demonstrating that several protumor activities of TAMs are regulated by IL 4 derived from $CD4^+$ T cells (1, 27). Based on these findings, we recently reported that infiltration by $CD68^+$, $CD4^+$, and $CD8^+$ immune cells in human BC is predictive of overall survival, and that the ratio of *CD68* to *CD8a* mRNA in tumor tissue correlates with complete pathologic response (pCR) in patients undergoing neoadjuvant chemotherapy (CTX) for early stage BC (6). Despite the clear correlation between these specific immune cell types and BC clinical outcome, leukocyte complexity within tumor tissue remains poorly described, with most studies relying on single marker IHC detection. Furthermore, although some studies have examined the effects of CTX on the presence and function of circulating peripheral blood leukocytes (28), data regarding the effect of CTX on tumor infiltrating immune cells are limited (29).

Herein, we evaluated leukocytic infiltrates in breast tissue from predominantly hormone receptor positive patients who had, or had not, received CTX before definitive surgery. In CTX naïve patients, we found that activated T lymphocytes comprised the majority of immune cells within tumors, whereas myeloid lineage cells predominate in nonadjacent normal breast tissue. In contrast, tumors from patients with residual disease after neo adjuvant CTX contained higher levels of infiltrating myeloid cells, with a simultaneous shift away from a T_H2 dominated lymphocyte response.

Results

Increased Presence of T Cells in Tumor Tissue. To evaluate the composition of tumor infiltrating leukocytes in human BC, tumors from 20 patients were evaluated by polychromatic flow cytometry and IHC detection of leukocyte lineages in tissue sections as described in *Materials and Methods*. Nine invasive ductal carcinomas (IDC) and five invasive lobular carcinomas (ILC) mostly histological grade two or three were obtained from patients with no prior exposure to CTX (CTX naïve) at the time of primary surgery for early stage BC, although one patient had received neoadjuvant tamoxifen. Six tumor samples were obtained from patients previously treated with neoadjuvant CTX before resection (CTX treated), consisting entirely of grade two or three IDC. Notably, three of six CTX treated tumors were HER2/neu positive, compared with only 1 of 14 CTX naïve tumors, whereas both groups contained roughly equivalent per centages of tumors negative for estrogen, progesterone, and HER2 receptors (triple negative). Details of tumor pathology are outlined in Table S1. Ipsilateral nonadjacent tissue was also obtained from seven CTX naïve and four CTX treated patients

Author contributions: B.R. and L.M.C. designed research; B.R. performed research; A.A., H.S.R., L.J.E., and E.S.H. contributed new reagents/analytic tools; B.R. and L.M.C. analyzed data; and B.R. and L.M.C. wrote the paper.

The authors declare no conflict of interest.

This article is a PNAS Direct Submission. K.P. is a guest editor invited by the Editorial Board.

[1]To whom correspondence should be addressed. E-mail: lisa.coussens@ucsf.edu.

This article contains supporting information online at www.pnas.org/lookup/suppl/doi:10.1073/pnas.1104303108/-/DCSupplemental.

for use as "normal" tissue, in addition to tissues from two con tralateral prophylactic mastectomies from patients with ipsilat eral ductal carcinoma in situ (DCIS).

Immune infiltrates detected with the pan leukocyte marker CD45 were present in both normal and tumor tissue, but with substantially increased density in BC (Fig. 1*A*). Leukocyte subsets were evaluated by using a combination of lineage markers to identify specific sub populations (Figs. S1 and S2), with the complexity of these pop ulations shown in Fig. 1*B* as a percentage of the total number of $CD45^+$ cells in each sample. BC tissues from CTX naïve patients contained infiltrates dominated by T lymphocytes ($CD3\varepsilon^+$), with minor populations of natural killer cells ($CD3\varepsilon^-CD56^+NKG2D^+$) and B lymphocytes ($CD19/20^+HLA\ DR^+CD3^-$). In comparison, myeloid lineage cells including macrophages ($CD14^{hi}CD11b^+HLA\ DR^+$), mast cells ($Fc\varepsilon R1\alpha^+CD117^+CD11b^-CD49d^+$) and neu trophils ($CD15^+CD11b^+CD49d^-$) were more evident in the normal tissue from these patients. A similar immune profile was observed in breast tissues obtained from the two prophylactic mastectomies (Fig. 1*B*).

Increased Presence of Myeloid-Lineage Cells in Residual Tumors from Patients Exposed to Neoadjuvant CTX. Comparative analysis of residual BC tissue removed from patients after neoadjuvant CTX revealed an obvious difference in the percentages of myeloid lineage cells compared with the CTX naïve group. With some exceptions, this difference included an increased presence of mac rophages as a percent of total leukocytes (Fig. 2*A*), as well as by density evaluation of CSF1 receptor (CSF1R) positive cells in tissue by IHC (Fig. 2*B*). Increased percentages of mast cells (Fig. 2*C*) and neutrophils (Fig. 2*D*) were also evident in most CTX treated patients, with an ≈14 fold increase in CTX treated versus CTX naïve groups. Basophils ($Fc\varepsilon R1\alpha^+CD117^-CD11b^-CD49d^+$; Fig. 2*E*) were highly increased in only one of six CTX treated samples, whereas the percentage of myeloid dendritic cells ($CD11c^+HLA\ DR^+CD14^{lo/-}$; Fig. 2*F*) was unchanged. Evaluation of plasmacytoid dendritic cells expressing CD85g/ILT7 detected an insufficient number of events for analysis. Thus, with the exception of baso phils, dendritic cells, and $CD15^+CD11b^+CD49d^+$ eosinophils which were present just at a detectable level in the tissues ex amined increased presence of myeloid lineage cells typified residual tumors of women treated with neoadjuvant CTX.

CD68 Is Not a Macrophage-Specific Marker in Human BC. Macro phages are well established as regulators of murine mammary tumorigenesis (30), where they can represent up to 80% of leukocytes present within late stage mammary carcinomas (1). In human BC, immunoreactivity for CD68 has been used exten sively for identification of macrophages, with $CD68^+$ cell density associated with reduced overall survival (6, 11, 14, 15).

The high number of $CD68^+$ cells reported in the literature, and shown in Fig. 3*A*, was in contrast to the limited number of $CD14^{hi}CD11b^+HLA\ DR^+$ macrophages observed by flow cytometry in the BC suspensions examined (Figs. 1*B* and 2*A*). To understand this discrepancy, we first evaluated CD68 expression in BC tissue sections, compared with CD163 (a hemoglobin scav enger receptor also commonly used as a marker for macrophages) and CSF1R (Fig. 3*A*). This comparative analysis revealed a lack of correlation in cell density among the three markers. We next evaluated frozen BC tissue sections by confocal microscopy after immunofluorescent detection of CD68 in combination with CSF1R or CD45 (Fig. 3*B*). Although all cells expressing high lev els of the CSF1R also expressed CD68, there was a distinct pop ulation of $CD68^+$ cells that expressed neither CSF1R nor CD45. CD68 did not significantly colocalize with $keratin^+$ epithelial cells, $CD31^+$ endothelial cells, or smooth muscle actin α expressing mural cells surrounding vasculature (Fig. 3*C*). This expression contrasted with murine mammary tumors isolated from MMTV PyMT transgenic mice (17), where $CD68^+$ cells coexpressed both CSF1R and the murine macrophage marker F4/80 (Fig. S3). In agreement with historic literature (31, 32), these results thus indicate that CD68 is not a macrophage specific marker in human BC.

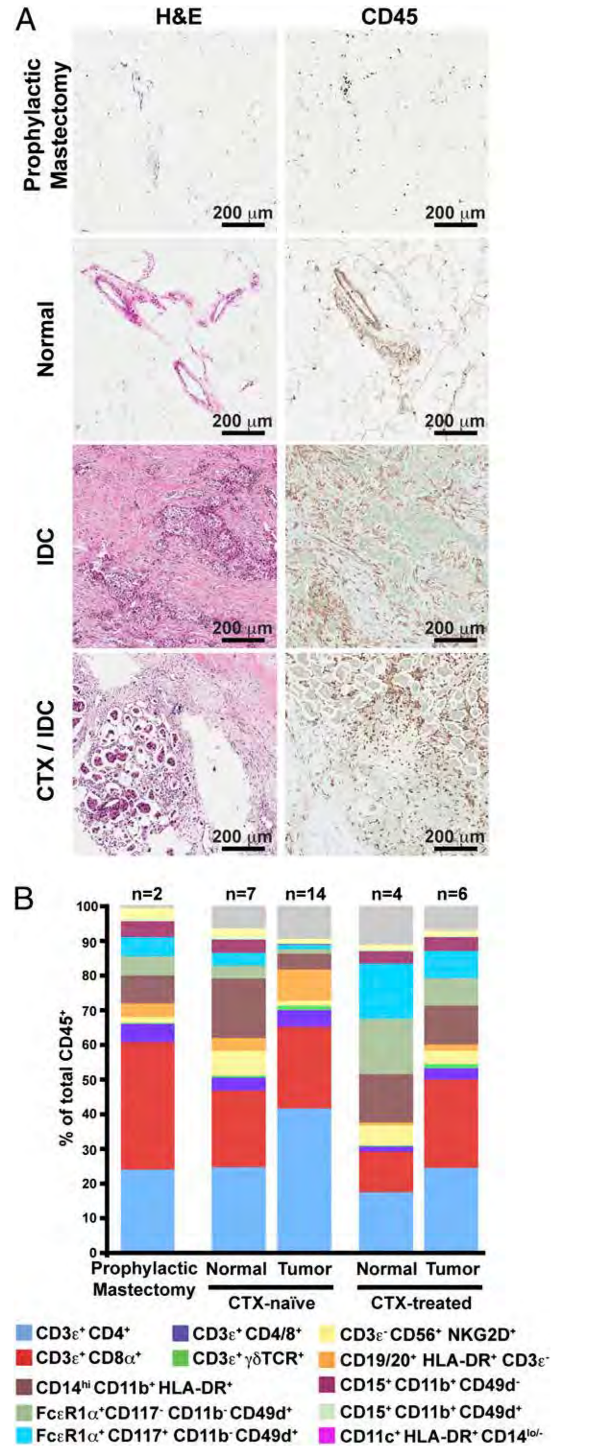

Fig. 1. Leukocyte infiltration of human breast tumors. (*A*) Hematoxylin and eosin (H&E) staining of tissue sections (*Left*) with representative immunohis tochemistry for CD45 (*Right*) shown for each. (*B*) Flow cytometric analysis of leukocyte populations within human breast tumors. Results are shown as a percent of total $CD45^+$ cells with markers used to define specific lineages shown below.

Tumor-Infiltrating T Cells Display an Activated Phenotype. To reveal the phenotype of T cells infiltrating BCs, we examined surface marker and chemokine receptor expression of tissue infiltrating $CD4^+$ and $CD8^+$ T cells (Fig. 4 *A* and *B*). Specifically, both $CD4^+$ and $CD8^+$ T cells displayed increased expression of ac tivation markers CD69 and HLA DR compared with peripheral

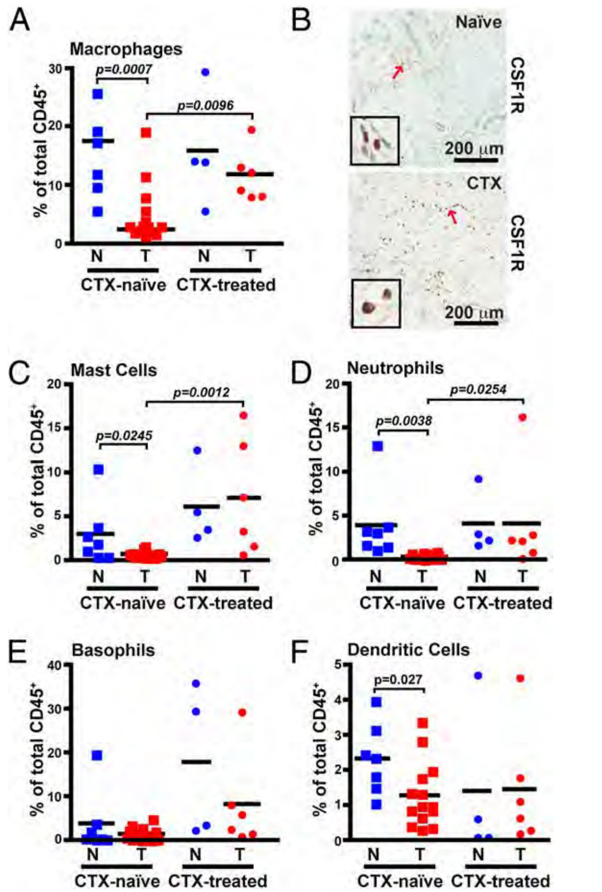

Fig. 2. Increased myeloid lineage leukocyte infiltration within CTX treated patients. (*A*) CD14^{hi}CD11b^{+}HLA DR^{+} macrophages shown as a percent of total CD45^{+} cells as determined by flow cytometry. (*B*) Representative im munohistochemistry for CSF1R in tumors from either CTX naïve (*Upper*) or CTX treated (*Lower*) patients. Red arrows indicate cells displayed in enlarged insets. FcεR1α^{+}CD117^{+}CD11b CD49d^{+} mast cells (*C*), CD15^{+}CD11b^{+}CD49d neutrophils (*D*), FcεR1α^{+}CD117 CD11b CD49d^{+} basophils (*E*), and CD11c^{+}HLA DR^{+}CD14$^{lo/}$ (*F*) DCs shown as a percent of total CD45^{+} cells. N, nonadjacent normal; T, tumor.

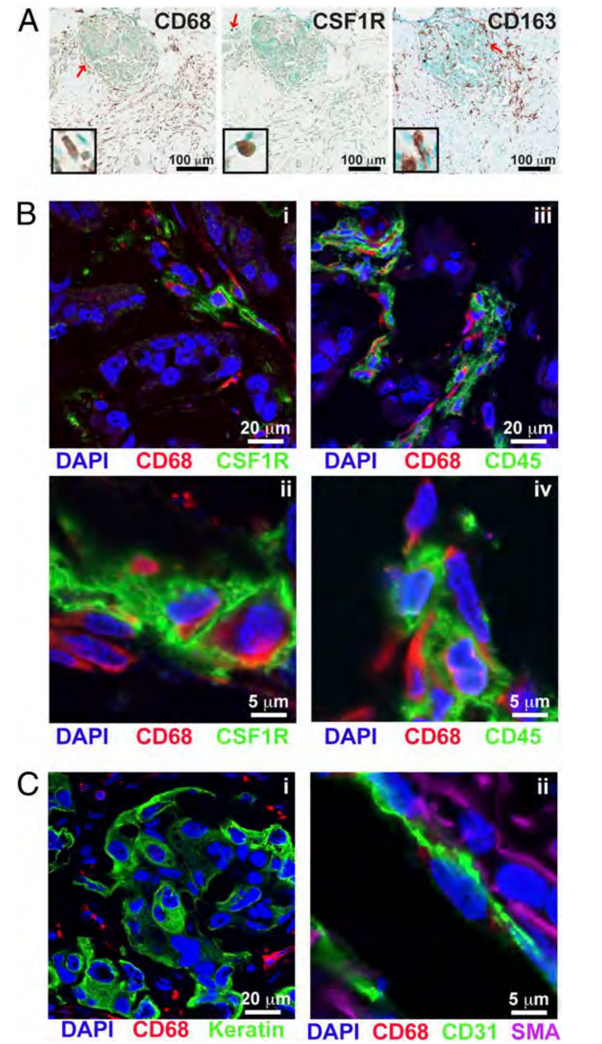

Fig. 3. CD68 is not a specific macrophage marker in human breast tumor tissue. (*A*) Representative immunohistochemistry within tumors for CD68 (*Left*), CSF1R (*Center*), and CD163 (*Right*) in serial sections from a CTX trea ted patient. Red arrows indicate cells displayed in enlarged insets. (*B*) Im munofluorescent staining of human breast tumors for CD68 (red) in conjunction with CSF1R (*i* and *ii*) or CD45 (*iii* and *iv*). (C) Immunofluorescent staining for CD68 (red) in conjunction with pan keratin (green; *i*), or CD31 (green) and smooth muscle actin α (SMA; purple; *ii*).

blood T cells, with a corresponding loss of markers for naïve T cells, CD45RA, and CCR7. Furthermore, although all T cells constitutively expressed the costimulatory receptor CD28 (Fig. S4*A*), expression of CD27, another costimulatory receptor, was reduced in a large proportion of tissue infiltrating cells, in dicative of shedding after interaction with its ligand CD70 (33) and potential acquisition of effector functions (34, 35). CD4^{+} and CD8^{+} T cells also displayed substantially up regulated ex pression of chemokine receptors CCR4 and CCR5 (Fig. 4*B*), and although CD8^{+} T cells constitutively expressed CXCR3, tissue infiltrating CD4^{+} T cells exhibited higher CXCR3 expression than their counterparts in peripheral blood. Surface marker ex pression by tissue infiltrating CD4^{+} and CD8^{+} T cells was subtly different between tumor and benign tissue in some samples; however, these changes were not consistent across patients, or between CTX naïve and CTX treated groups (Fig. S4*B*).

Altered Lymphocyte Balance in Residual Tumors After Neoadjuvant CTX. Although we observed no difference in the percent of CD3e^{-}CD56^{+}NKG2D^{+} natural killer (NK) cells (Fig. 5*A*), higher levels of CD19/CD20^{+}HLA DR^{+} B cells were evident in several CTX naïve tumors compared with both normal tissue and CTX treated tumors. As has been reported (36), B cells were clustered together in association with T cells (Fig. 5*C*). Notably, CD4^{+} T cells as a percent of the total CD45^{+} pop ulation were also increased in CTX naïve tumors compared with both normal tissue and residual postneoadjuvant tumors (Fig. 5*D*). As the percent of CD8^{+} T cells was unchanged (Fig. 5*E*), the lower percentage of CD4^{+} T cells within the CTX treated group resulted in an increased CD8 to CD4 ratio (Fig. 5*F*). Al though it was unclear whether the density of CD8^{+} cells in CTX treated residual tumors was increased (Fig. 5*G*), the number of cells expressing granzyme B was strikingly evident in two of six CTX treated tumors (Fig. 5*H*), whereas minimal granzyme B staining was observed in CTX naïve tumors, even in areas with high numbers of CD8^{+} T cells (Fig. 5*I*).

Despite the reduced percentage of CD4^{+} T cells in tumors from CTX treated patients, there was no change in the density of IHC detected regulatory T cells expressing FoxP3 (Fig. S5*A*), which was specifically expressed by CD3^{+}CD4^{+} cells in the tumor (Fig. S5*B*). Gating on CD25^{hi} cells, consisting of >80% FoxP3^{+} cells in all samples tested, also revealed that the relative percentage of these cells was invariant between groups (Fig. S5*C*). Phenotypically, CD4^{+}FoxP3^{+} cells displayed an activated phenotype with equivalent surface levels of CD45RO and CD69

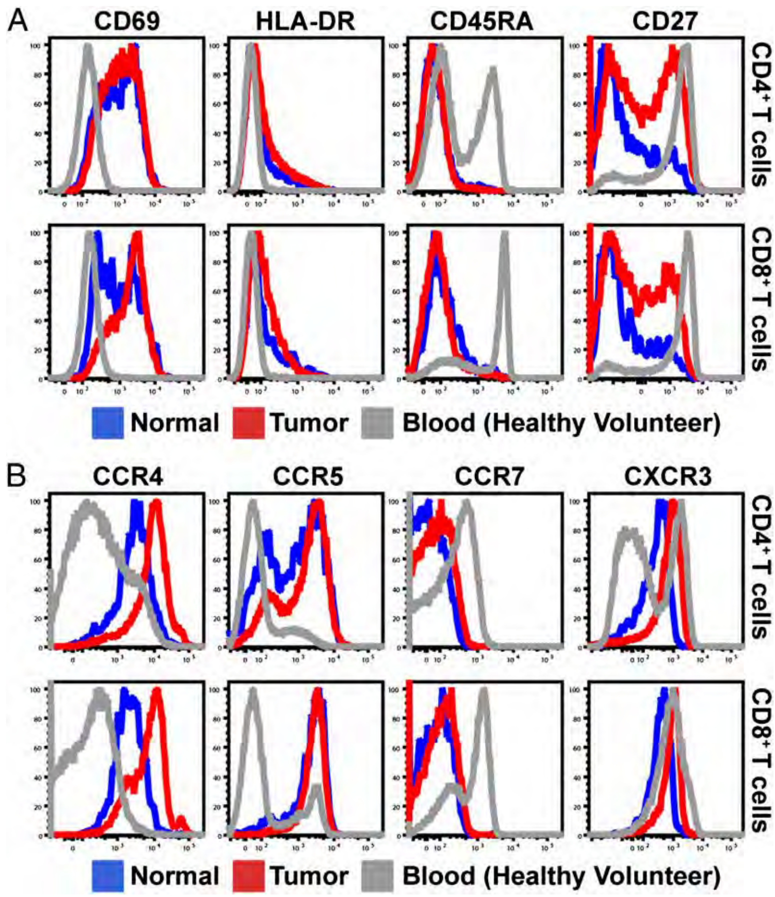

Fig. 4. Tissue infiltrating T cells display an activated phenotype. (*A* and *B*) Representative histograms of CD3$^+$CD4$^+$ (*Upper*) or CD3$^+$CD8$^+$ (*Lower*) T cells isolated from a single CTX treated patient with both normal (blue) and tumor (red) tissue. Expression of activation markers CD69 (*Left*), HLA DR (*Center Left*), CD45RA (*Center Right*), and CD27 (*Right*) are shown in *A*, and expression of chemokine receptors CCR4 (*Left*), CCR5 (*Center Left*), CCR7 (*Center Right*) and CXCR3 (*Right*) are shown in *B*.

to CD4$^+$FoxP3$^-$ cells and, as has been reported for cells in peripheral blood (37), expressed lower levels of CD127 (Fig. S5*D*). Interestingly, although not all FoxP3$^+$ cells expressed HLA DR, they did comprise the majority of HLA DR expressing CD4$^+$ T cells, in addition to coexpressing high levels of CD25.

These data collectively reveal a shift within tumors toward a T_H2 type response in BC characterized by increased presence of B cells and CD4$^+$ T cells, in comparison with nonadjacent normal breast tissue. This shift is reversed in tumors obtained from CTX treated patients, with additional evidence of a cytotoxic T cell response through a more favorable CD8/CD4 T cell ratio and increased presence of granyzme B expressing lymphocytes; thus, even residual tumors from patients with a poor response to CTX may contain immune microenvironments that are more favorably skewed towards an anti tumor, T_H1 type immune response.

Discussion

Herein, we present a detailed description of leukocyte complexity in BC as evaluated in a cohort of CTX naïve patients with stage 2/3 tumors, compared with patients with significant residual disease after neoadjuvant CTX. T lymphocytes were the major population within both CTX naïve and CTX treated tumors, found almost exclusively in an activated state as determined by increased expression of CD69 and chemokine receptors, with simultaneous loss of naïve markers CCR7 and CD45RA. The presence of activation markers, however, does not definitively demonstrate that intratumoral T cells are functionally active. In fact, granzyme B expression was minimal within tumors from CTX naïve patients, suggesting negligible cytotoxic activity by infiltrating CD8$^+$ T cells. In comparison, granzyme B was highly expressed in one third of the CTX treated tumors, suggestive of a more cytotoxic T cell response within some tumors after exposure to CTX.

Importantly, residual tumors from CTX treated patients also contained reduced percentages of B cells and CD4$^+$ T cells. Tumor infiltrating CD4$^+$ T cells in BC are known to express the T_H2 cytokines IL 4 and IL 13 concomitantly with the production of IFN γ (25, 26), consistent with coexpression of CXCR3 and CCR4 (38, 39) as we observed herein. It remains to be determined whether cytokine production by CD4$^+$ T cells is altered by neoadjuvant CTX; however, the combined reduction in both CD4$^+$ T cells and B cells is indicative of a favorable shift away from a T_H2 microenvironment. This shift could be relevant for TAM function, as has been described in the MMTV PyMT model where TAMs are programmed by IL 4 toward a T_H2 phenotype (1), and more recently in pancreatic ductal adenocarcinoma during treatment where an agonist CD40 monoclonal antibody fostered cytolytic macrophage activities (40).

Although the extent of lymphocyte infiltration has been associated with improved prognosis in subsets of patients (2, 3), and with pCR after CTX (41, 42), information regarding the relationship between individual lymphocyte subsets to survival is limited. High FoxP3 counts correlate with reduced overall and relapse free survival in estrogen receptor (ER) positive tumors (43), and pCR to neoadjuvant CTX is associated with reduced FoxP3 grading (44, 45). Although two studies examining T cell infiltration by flow cytometry found conflicting results regarding the CD8:CD4 ratio and lymph node metastasis (46, 47), the number of CD8$^+$ T cells within tissue has been associated with improved patient survival (48). We have also reported a CD68/CD4/CD8 immune signature predicting overall and relapse free survival, with inverse correlations evident for CD4 when used in conjunction with other markers (6). There is thus an urgent need for additional prospective investigations where multiple parameters of lymphocytic infiltration and functionality are evaluated to determine the most significant biomarker comparisons that predict outcome and guide specific therapy.

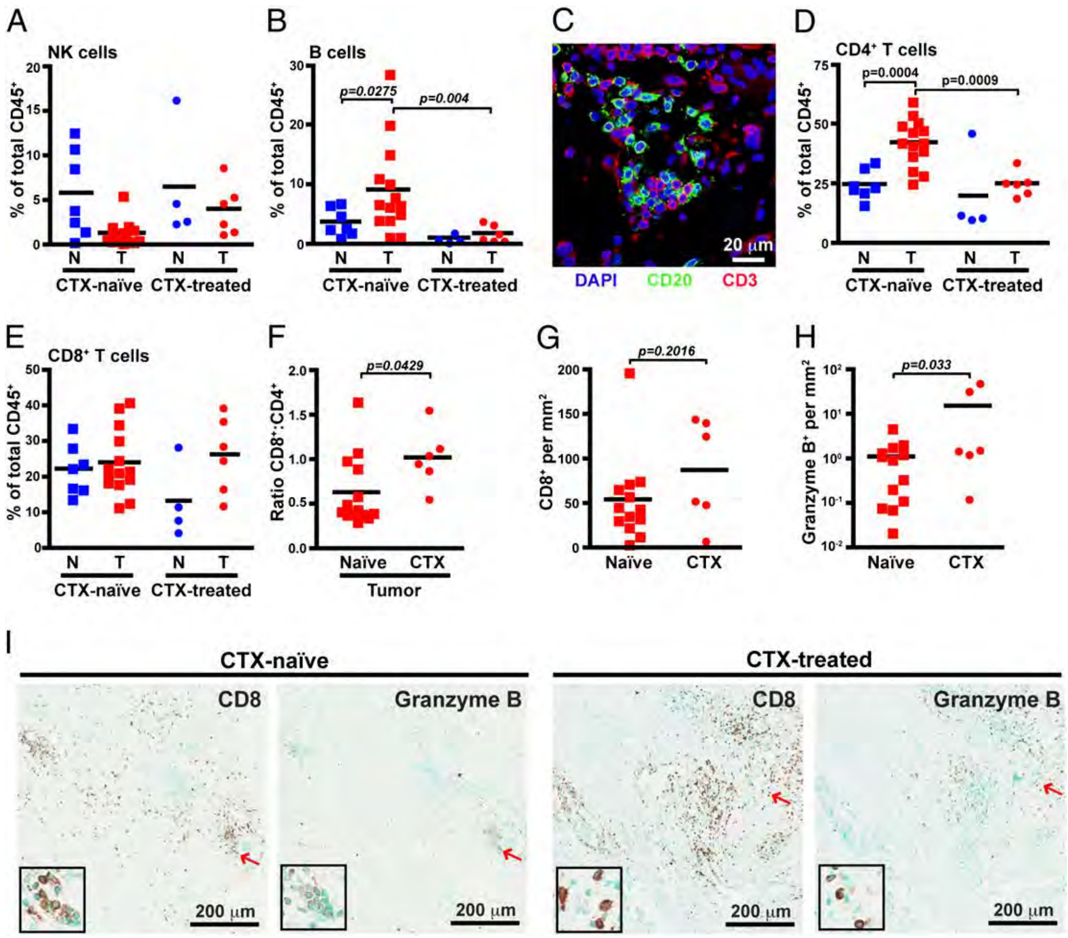

Fig. 5. Improved cytotoxic T cell response in CTX treated tumors. CD3ε CD56$^+$NKG2D$^+$ natural killer cells (*A*) and CD3ε CD19/20$^+$HLA DR$^+$ B cells (*B*) shown as a percent of total CD45$^+$ cells as determined by flow cytometry. (*C*) Immunofluorescent staining of tumors for CD20 (green) and CD3 (red). CD3ε$^+$CD4$^+$ T cells (*D*) and CD3ε$^+$CD8$^+$ T cells (*E*) are shown as a percent of total CD45$^+$ cells. (*F*) Ratio of CD8$^+$ to CD4$^+$ T cells within CTX naive versus CTX treated tumors. Number of CD8 positive (*G*) and granzyme B positive (*H*) cells per area as determined by automated counting. (*I*) Representative sections stained with CD8 or granzyme B from CTX naive (*Left*) or CTX treated (*Right*) tumors. Red arrows indicate cells displayed in enlarged insets. N, nonadjacent normal; T, tumor.

Although used successfully in multiple studies to relate TAM infiltration with clinically relevant outcomes, our results indicate that CD68 alone cannot accurately evaluate macrophage presence in human breast tissue given that multiple stromal cells express it and that a subset of these are CSF1R and CD45 negative. We observed that the nonleukocytic CD68$^+$ cells were predominantly located within tumor stroma and, thus, based on this localization and morphology, we speculate that CSF1R$^-$CD68$^+$ cells likely reflect tumor associated fibroblasts or monocyte derived fibro cytes in agreement with other reports (31, 32, 49 52). Our findings do not invalidate CD68 as a clinically relevant marker and, im portantly, CSF1 response gene signatures have been identified in breast adenocarcinomas that are predictive of recurrence risk and metastasis (53, 54). However, given the important role that fibroblasts (and perhaps fibrocytes) play in fostering aspects of tumorigenesis (55 57), differentiating among macrophages, fibroblasts, and other stromal populations within tumors has the potential to improve diagnostic information currently generated by immunodetection of CD68.

As we have reported for expression of *csf1* mRNA (6), mul tiple genes encoding myeloid cell chemoattractants are differ entially expressed by human BC cell lines, with variable induction of these genes in response to CTX (Fig. S6). Although differential expression between cell lines corresponding to par ticular subtypes of BC is evident, it is doubtful these cell lines accurately represent the response of BC tumor tissue; thus, we are investigating whether differences in myeloid cell infiltrates reflect distinct molecular subtypes of BC and to what extent these differ in residual tumors from CTX treated patients.

It is important to acknowledge that leukocyte composition within tumors responding to CTX likely differs substantially from residual or recurrent tumors from patients that have received CTX, given what is known regarding immune responses to CTX induced cell death (28). However, we recently reported that in mammary carcinomas of MMTV PyMT mice, blockade of the CSF1 CSF1R pathway critical for TAM recruitment improved response to CTX through a CD8$^+$ T cell dependent effect (6). Thus, even though the findings presented herein are based on a small dataset of heterogeneous tumor subtypes, and our results may be biased because of sample selection favoring large and/or less CTX responsive tumors among the CTX treated group, the clear distinctions in the myeloid profiles between CTX naive and CTX treated tumors is provocative and indicates that a CSF1 targeted strategy may be a promising approach to enhance therapeutic efficacy of cytotoxic CTX, particularly for treatment of refractory BC. Moreover, given the increase in granulocytic populations within tumors resistant to CTX, and the involvement of these cells in regulating immune responses in chronic in flammatory diseases (58 62), these populations may also be functionally relevant, and targeting common pathways of im mune suppression within the tumor microenvironment may provide additional therapeutic opportunities to increase efficacy of neoadjuvant CTX.

Materials and Methods

Tissues were collected at the time of surgery from consenting patients at the University of California, San Francisco under approval from the institutional review board. Tumor and ipsilateral nonadjacent normal tissues were collected by a certified pathologist (A.A.) and were prepared for analysis on the day of resection. The percent of macrophages and CD8$^+$ T cells has been reported for a subset of the patients described here (6). Flow cytometry, immunohisto chemistry, and immunofluorescence were performed as described (6), with detailed methods contained in *SI Materials and Methods*, and a list of anti bodies available in Tables S2 and S3. Statistical differences between two in dependent groups were determined by using Student's *t* test via Prism 4.0 software (GraphPad Software).

ACKNOWLEDGMENTS. We thank Erin Bowlby for compiling patient data. This work was supported by a Department of Defense Breast Cancer Research Program Fellowship (to B.R.); a grant from the Breast Cancer Research Foundation (to H.S.R.); National Institutes of Health/National Cancer Institute Grants R01CA130980, R01CA132566, R01CA140943, and P50CA58207; a Dr. Susan Love Research Foundation Instructional grant; and Department of Defense Grants W81XWH 06 1 0416 and PR080717 (to L.M.C.).

1. DeNardo DG, et al. (2009) CD4(+) T cells regulate pulmonary metastasis of mammary carcinomas by enhancing protumor properties of macrophages. *Cancer Cell* 16:91–102.
2. Ménard S, et al. (1997) Lymphoid infiltration as a prognostic variable for early-onset breast carcinomas. *Clin Cancer Res* 3:817–819.
3. Pupa SM, et al. (1996) Macrophage infiltrate and prognosis in c-erbB-2-overexpressing breast carcinomas. *J Clin Oncol* 14:85–94.
4. Bingle L, Brown NJ, Lewis CE (2002) The role of tumour-associated macrophages in tumour progression: Implications for new anticancer therapies. *J Pathol* 196:254–265.
5. Mukhtar RA, Nseyo O, Campbell MJ, Esserman LJ (2011) Tumor-associated macrophages in breast cancer as potential biomarkers for new treatments and diagnostics. *Expert Rev Mol Diagn* 11:91–100.
6. DeNardo DG, et al. (2011) Leukocyte complexity in breast cancer predicts overall survival and functionally regulates response to chemotherapy. *Cancer Discovery* 1:54–67.
7. Esserman LJ, et al. (2006) Magnetic resonance imaging captures the biology of ductal carcinoma in situ. *J Clin Oncol* 24:4603–4610.
8. Volodko N, Reiner A, Rudas M, Jakesz R (1998) Tumour-associated macrophages in breast cancer and their prognostic correlations. *Breast* 7:99–105.
9. Lee AH, Happerfield LC, Bobrow LG, Millis RR (1997) Angiogenesis and inflammation in invasive carcinoma of the breast. *J Clin Pathol* 50:669–673.
10. Uzzan B, Nicolas P, Cucherat M, Perret GY (2004) Microvessel density as a prognostic factor in women with breast cancer: A systematic review of the literature and meta-analysis. *Cancer Res* 64:2941–2955.
11. Tsutsui S, et al. (2005) Macrophage infiltration and its prognostic implications in breast cancer: The relationship with VEGF expression and microvessel density. *Oncol Rep* 14:425–431.
12. Bolat F, et al. (2006) Microvessel density, VEGF expression, and tumor-associated macrophages in breast tumors: Correlations with prognostic parameters. *J Exp Clin Cancer Res* 25:365–372.
13. Chen JJ, et al. (2005) Tumor-associated macrophages: The double-edged sword in cancer progression. *J Clin Oncol* 23:953–964.
14. Leek RD, et al. (1996) Association of macrophage infiltration with angiogenesis and prognosis in invasive breast carcinoma. *Cancer Res* 56:4625–4629.
15. Campbell MJ, et al. (2010) Proliferating macrophages associated with high grade, hormone receptor negative breast cancer and poor clinical outcome. *Breast Cancer Res Treat* 128:703–711.
16. Robinson BD, et al. (2009) Tumor microenvironment of metastasis in human breast carcinoma: A potential prognostic marker linked to hematogenous dissemination. *Clin Cancer Res* 15:2433–2441.
17. Guy CT, Cardiff RD, Muller WJ (1992) Induction of mammary tumors by expression of polyomavirus middle T oncogene: A transgenic mouse model for metastatic disease. *Mol Cell Biol* 12:954–961.
18. Lin EY, Nguyen AV, Russell RG, Pollard JW (2001) Colony-stimulating factor 1 promotes progression of mammary tumors to malignancy. *J Exp Med* 193:727–740.
19. Lin EY, et al. (2006) Macrophages regulate the angiogenic switch in a mouse model of breast cancer. *Cancer Res* 66:11238–11246.
20. Stockmann C, et al. (2008) Deletion of vascular endothelial growth factor in myeloid cells accelerates tumorigenesis. *Nature* 456:814–818.
21. Lin EY, et al. (2007) Vascular endothelial growth factor restores delayed tumor progression in tumors depleted of macrophages. *Mol Oncol* 1:288–302.
22. Wyckoff J, et al. (2004) A paracrine loop between tumor cells and macrophages is required for tumor cell migration in mammary tumors. *Cancer Res* 64:7022–7029.
23. Wyckoff JB, et al. (2007) Direct visualization of macrophage-assisted tumor cell intravasation in mammary tumors. *Cancer Res* 67:2649–2656.
24. Doedens AL, et al. (2010) Macrophage expression of hypoxia-inducible factor-1 alpha suppresses T-cell function and promotes tumor progression. *Cancer Res* 70:7465–7475.
25. Aspord C, et al. (2007) Breast cancer instructs dendritic cells to prime interleukin 13-secreting CD4+ T cells that facilitate tumor development. *J Exp Med* 204:1037–1047.
26. Pedroza-Gonzalez A, et al. (2011) Thymic stromal lymphopoietin fosters human breast tumor growth by promoting type 2 inflammation. *J Exp Med* 208:479–490.
27. Gocheva V, et al. (2010) IL-4 induces cathepsin protease activity in tumor-associated macrophages to promote cancer growth and invasion. *Genes Dev* 24:241–255.
28. Zitvogel L, Apetoh L, Ghiringhelli F, Kroemer G (2008) Immunological aspects of cancer chemotherapy. *Nat Rev Immunol* 8:59–73.
29. Allan CP, Turtle CJ, Mainwaring PN, Pyke C, Hart DN (2004) The immune response to breast cancer, and the case for DC immunotherapy. *Cytotherapy* 6:154–163.
30. Qian BZ, Pollard JW (2010) Macrophage diversity enhances tumor progression and metastasis. *Cell* 141:39–51.
31. Pulford KA, Sipos A, Cordell JL, Stross WP, Mason DY (1990) Distribution of the CD68 macrophage/myeloid associated antigen. *Int Immunol* 2:973–980.
32. Kunz-Schughart LA, et al. (2003) [The "classical" macrophage marker CD68 is strongly expressed in primary human fibroblasts]. *Verh Dtsch Ges Pathol* 87:215–223.
33. Hintzen RQ, et al. (1994) Characterization of the human CD27 ligand, a novel member of the TNF gene family. *J Immunol* 152:1762–1773.
34. Hamann D, et al. (1997) Phenotypic and functional separation of memory and effector human CD8+ T cells. *J Exp Med* 186:1407–1418.
35. Okada R, Kondo T, Matsuki F, Takata H, Takiguchi M (2008) Phenotypic classification of human CD4+ T cell subsets and their differentiation. *Int Immunol* 20:1189–1199.
36. Nelson BH (2010) CD20+ B cells: The other tumor-infiltrating lymphocytes. *J Immunol* 185:4977–4982.
37. Liu W, et al. (2006) CD127 expression inversely correlates with FoxP3 and suppressive function of human CD4+ T reg cells. *J Exp Med* 203:1701–1711.
38. Kunkel EJ, et al. (2002) Expression of the chemokine receptors CCR4, CCR5, and CXCR3 by human tissue-infiltrating lymphocytes. *Am J Pathol* 160:347–355.
39. Kim CH, et al. (2001) Rules of chemokine receptor association with T cell polarization in vivo. *J Clin Invest* 108:1331–1339.
40. Beatty GL, et al. (2011) CD40 agonists alter tumor stroma and show efficacy against pancreatic carcinoma in mice and humans. *Science* 331:1612–1616.
41. Demaria S, et al. (2001) Development of tumor-infiltrating lymphocytes in breast cancer after neoadjuvant paclitaxel chemotherapy. *Clin Cancer Res* 7:3025–3030.
42. Denkert C, et al. (2010) Tumor-associated lymphocytes as an independent predictor of response to neoadjuvant chemotherapy in breast cancer. *J Clin Oncol* 28:105–113.
43. Bates GJ, et al. (2006) Quantification of regulatory T cells enables the identification of high-risk breast cancer patients and those at risk of late relapse. *J Clin Oncol* 24:5373–5380.
44. Ladoire S, et al. (2008) Pathologic complete response to neoadjuvant chemotherapy of breast carcinoma is associated with the disappearance of tumor-infiltrating foxp3+ regulatory T cells. *Clin Cancer Res* 14:2413–2420.
45. de Kruijf EM, et al. (2010) The predictive value of HLA class I tumor cell expression and presence of intratumoral Tregs for chemotherapy in patients with early breast cancer. *Clin Cancer Res* 16:1272–1280.
46. Macchetti AH, et al. (2006) Tumor-infiltrating CD4+ T lymphocytes in early breast cancer reflect lymph node involvement. *Clinics (Sao Paulo)* 61:203–208.
47. Sheu BC, et al. (2008) Clinical significance of tumor-infiltrating lymphocytes in neoplastic progression and lymph node metastasis of human breast cancer. *Breast* 17:604–610.
48. Mahmoud SM, et al. (2011) Tumor-infiltrating CD8+ lymphocytes predict clinical outcome in breast cancer. *J Clin Oncol* 29:1949–1955.
49. Gottfried E, et al. (2008) Expression of CD68 in non-myeloid cell types. *Scand J Immunol* 67:453–463.
50. Pilling D, Fan T, Huang D, Kaul B, Gomer RH (2009) Identification of markers that distinguish monocyte-derived fibrocytes from monocytes, macrophages, and fibroblasts. *PLoS ONE* 4:e7475.
51. Shao DD, Suresh R, Vakil V, Gomer RH, Pilling D (2008) Pivotal Advance: Th-1 cytokines inhibit, and Th-2 cytokines promote fibrocyte differentiation. *J Leukoc Biol* 83:1323–1333.
52. Azambuja D, et al. (May 2, 2011) Lack of association of tumor-associated macrophages with clinical outcome in patients with classical Hodgkin's lymphoma. *Ann Oncol*, 10.1093/annonc/mdr157.
53. Sharma M, et al. (2010) Analysis of stromal signatures in the tumor microenvironment of ductal carcinoma in situ. *Breast Cancer Res Treat* 123:397–404.
54. Beck AH, et al. (2009) The macrophage colony-stimulating factor 1 response signature in breast carcinoma. *Clin Cancer Res* 15:778–787.
55. Trimboli AJ, et al. (2009) Pten in stromal fibroblasts suppresses mammary epithelial tumours. *Nature* 461:1084–1091.
56. Erez N, Truitt M, Olson P, Arron ST, Hanahan D (2010) Cancer-associated fibroblasts are activated in incipient neoplasia to orchestrate tumor-promoting inflammation in an NF-kappaB-dependent manner. *Cancer Cell* 17:135–147.
57. Kalluri R, Zeisberg M (2006) Fibroblasts in cancer. *Nat Rev Cancer* 6:392–401.
58. Schmielau J, Finn OJ (2001) Activated granulocytes and granulocyte-derived hydrogen peroxide are the underlying mechanism of suppression of T-cell function in advanced cancer patients. *Cancer Res* 61:4756–4760.
59. Fridlender ZG, et al. (2009) Polarization of tumor-associated neutrophil phenotype by TGF-beta: "N1" versus "N2" TAN. *Cancer Cell* 16:183–194.
60. Eller K, et al. (2011) IL-9 production by regulatory T cells recruits mast cells that are essential for regulatory T cell-induced immune suppression. *J Immunol* 186:83–91.
61. Galli SJ, Nakae S, Tsai M (2005) Mast cells in the development of adaptive immune responses. *Nat Immunol* 6:135–142.
62. Perrigoue JG, et al. (2009) MHC class II-dependent basophil-CD4+ T cell interactions promote T(H)2 cytokine-dependent immunity. *Nat Immunol* 10:697–705.

Supporting Information

Ruffell et al. 10.1073/pnas.1104303108

SI Materials and Methods

Flow Cytometry. Freshly resected tissue was manually minced and then incubated for 45 min at 37 °C in DMEM (Invitrogen) with 2.0 mg/mL Collagenase A (Roche) and 50 units/mL DNase I (Roche). Single cell suspensions were prepared by filtering through 70 μm nylon strainers (BD Biosciences), and $<10^6$ cells were incubated for 30 min on ice with Fc Receptor Binding Inhibitor (eBioscience) diluted 1/10 in PBS containing Live Dead Aqua (1:500, Invitrogen). Cells were then incubated for 30 min in PBS containing 1.0 mM EDTA and 5% FCS along with manufacturers' suggested dilutions of fluorescently labeled primary monoclonal antibodies (Table S2). After washing once, cells were fixed with BD Cytofix for 30 min on ice, washed again, and stored at 4 °C until analysis with an LSRII flow cytometer (BD Bioscience). Before intracellular FoxP3 staining, cells were instead fixed with the FoxP3 Fixation/Permeabilization system (eBioscience) according to the manufacturer's instructions.

Immunohistochemistry. Sections (5 μm) of formalin fixed, paraffin embedded tissues were deparaffinized with xylene, rehydrated, immersed in antigen retrieval citra (BioGenex), then heated for 7 min at maximum power in a microwave, followed by a 30 min incubation in the heated buffer. After washing 3 times in PBS and surrounding tissues with a hydrophobic Super Pap Pen (The Binding Site), peroxidase activity and nonspecific binding was blocked with appropriate components of the Thermo Scientific Ultravision Detection Kit according to the manufacturer's instructions. After a second blocking step with PBS containing 5% goat serum, 2.5% BSA, and 0.1% Tween 20, unlabeled primary antibodies (Table S3) were diluted according to manufacturers' recommendations and added to sections overnight at 4 °C. After washing, antibodies were detected by using the appropriate components of the Thermo Scientific Ultravision Detection Kit according to manufacturer's instructions. After development with liquid DAB, slides were washed in H_2O, counterstained briefly with 1% Methyl Green, dehydrated, and mounted with Cytoseal (Thermo Scientific). Representative images and quantitative image analysis was done by using the Aperio ScanScope CS Slide Scanner (Aperio Technologies) system with a 20× or 40× objective to capture whole slide images. Positive staining was assessed with the nuclear default algorithm (Aperio).

Immunofluorescence. Sections (10 μm) of PFA fixed, sucrose protected, OCT embedded tissues were thawed at 37 °C for 10 min, permeabilized with 100% ice cold acetone for 10 min, washed in PBS, and then blocked with goat blocking buffer for 2 h. To use two primary antibodies from the same species, one antibody was added at a 100 fold reduced dilution overnight at 4 °C in 0.5× blocking buffer, and after washing, slides were incubated with a biotinylated anti mouse or rabbit secondary (Vector Laboratories) for 30 min. The signal from the diluted antibody was then amplified with a TSA indirect kit (Perkin Elmer) according to manufacturer's instructions. After extensive washing, additional primary antibodies were added overnight at 4 °C. After another round of washing, goat anti mouse Alexa 488, donkey anti rabbit or anti mouse Alexa 546, and streptavidin Alexa 647 (1/500, Invitrogen) were used to detect all three antibodies. To use three primary murine antibodies, slides were blocked with 5.0 μg/mL mouse IgG1 and IgG2a (BioLegend) for 30 min after detection of the first primary antibody with anti mouse Alexa 647. Slides were then incubated with two primary antibodies directly conjugated to either FITC or Cy3 for 3 h, washed, and incubated with goat anti FITC Alexa 488 (Invitrogen). Slides were mounted with ProLong Gold with DAPI anti fade mounting medium (Invitrogen) overnight, and images were acquired by using a LSM510 Confocal Laser Scanning Microscope (Carl Zeiss).

Real-Time PCR. Culture and exposure of human BC cell lines to CTX agents was performed as described (1). mRNA was isolated from cells by using the RNeasy mini kit (Qiagen), contaminating DNA was removed by DNase I (Invitrogen) digestion, and reverse transcription into cDNA was performed by using Super Script III (Invitrogen) according to the manufactures' directions. Real time PCR was performed by using the Taqman system after a preamplification step with TaqMan PreAmp (Applied Biosystems) according to the manufacturer's instructions.

1. DeNardo DG, et al. (2011) Leukocyte complexity in breast cancer predicts overall survival and functionally regulates response to chemotherapy. *Cancer Discovery* 1: 54–67.

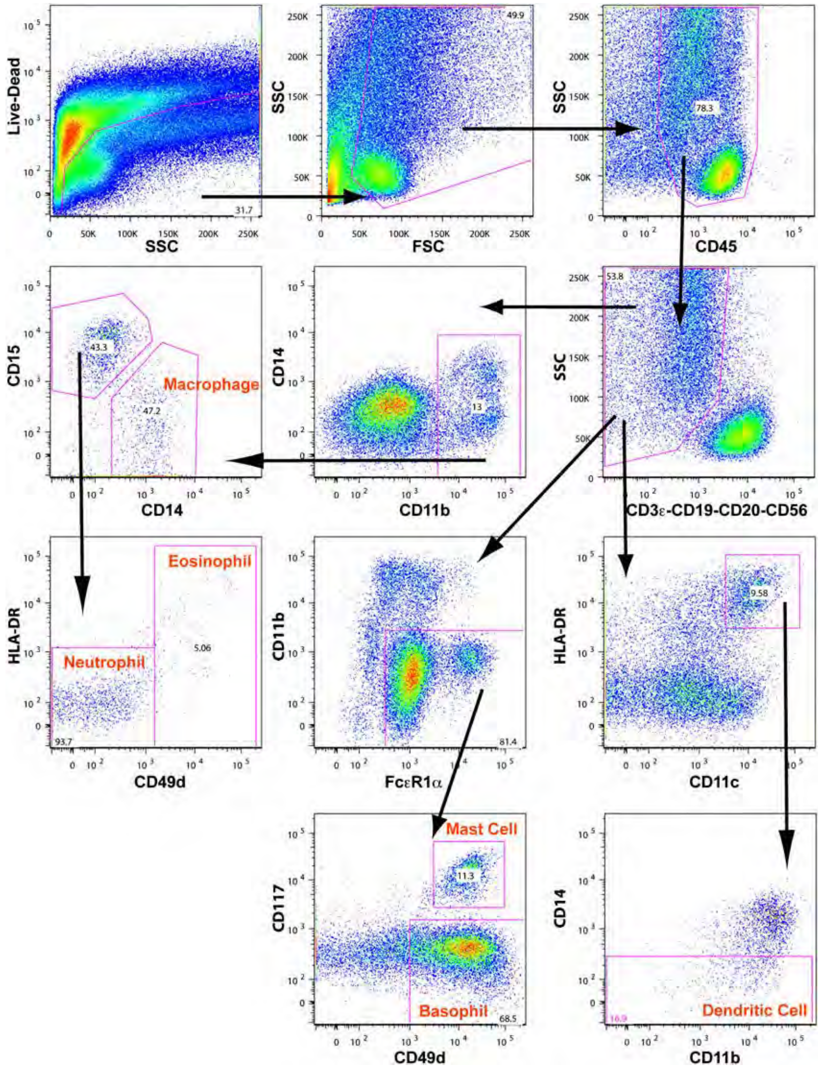

Fig. S1. Gating strategy for identification of myeloid lineage populations. Starting from the upper left, arrows indicate directionality of subgates. Markers are indicated to the left and bottom of each polychromatic dot plot. Identified populations are marked in red text.

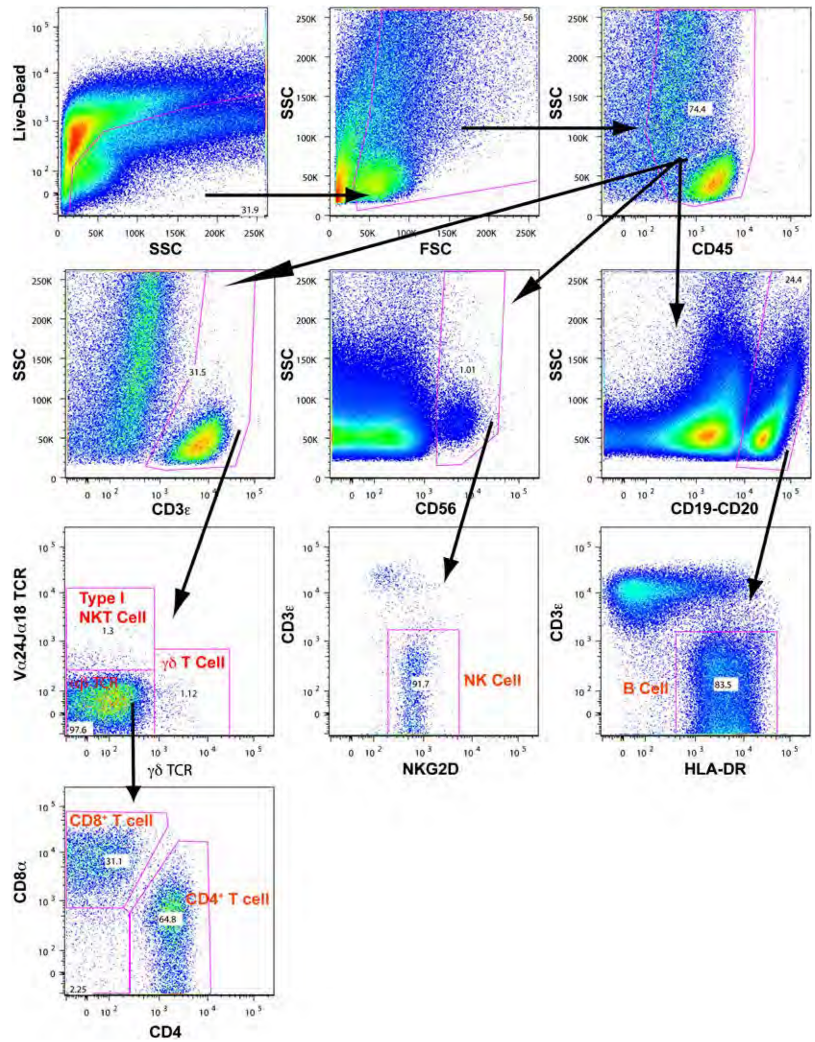

Fig. S2. Gating strategy for identification of lymphocyte populations. Starting from the upper left, arrows indicate directionality of subgates. Markers are indicated to the left and bottom of each polychromatic dot plot. Identified populations are marked in red text.

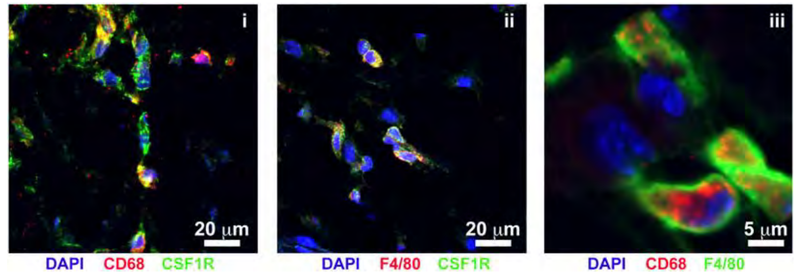

Fig. S3. Immunofluorescent staining in murine mammary tumors for CD68 (red; *i* and *iii*), CSF1R (green; *i* and *ii*) or F4/80 (red, *ii*; green, *iii*).

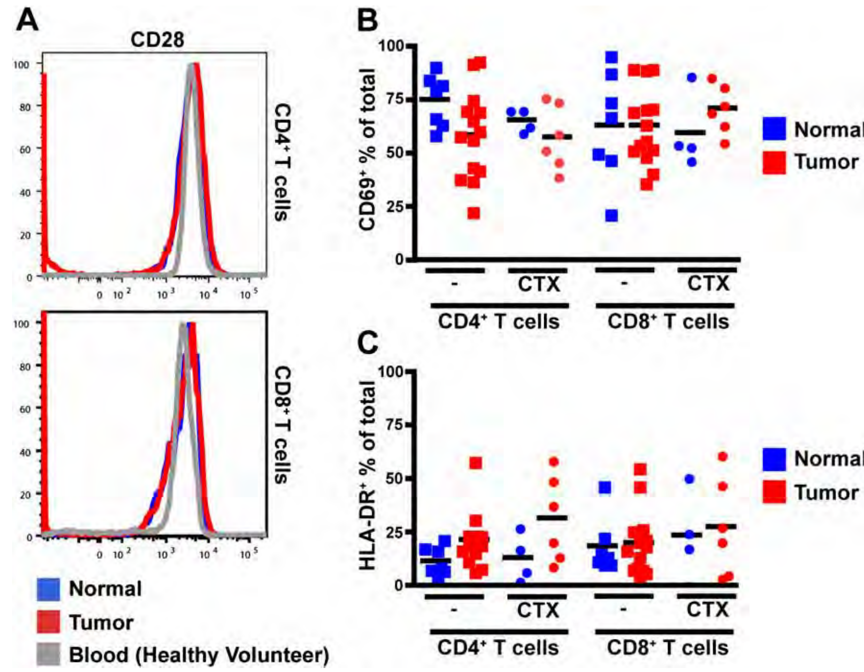

Fig. S4. Activation marker expression on T lymphocytes. (*A*) Representative histograms of CD28 expression for $CD3^+CD4^+$ (*Upper*) or $CD3^+CD8^+$ (*Lower*) T cells isolated from a single CTX treated patient with both normal (blue) and tumor (red) tissue. (*B* and *C*) Percent of CD69 expressing (*B*) or HLA DR expressing (*C*) T cells from all samples.

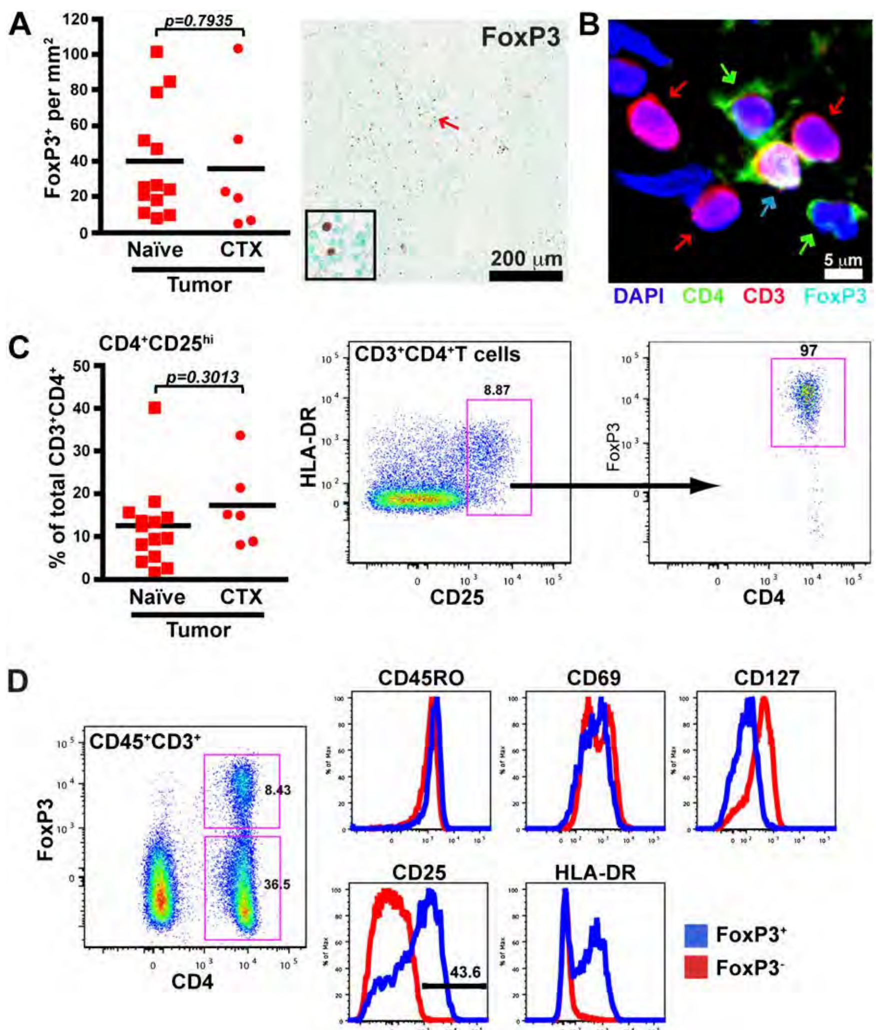

Fig. S5. Presence of CD4^{+}FoxP3^{+} regulatory T cells within tumors. (*A*) Number of FoxP3 positive cells per area as determined by automated counting (*Left*) with a representative stained section shown (*Right*). (*B*) Immunofluorescent staining of tumors for CD4 (green), CD3 (red), and FoxP3 (teal). Arrows indicate CD3^{+}CD4 FoxP3 (red), CD3^{+}CD4^{+}FoxP3 (green), and CD3^{+}CD4^{+}FoxP3^{+} (teal) cells. (*C*) Percent of CD25^{hi} cells within the CD3^{+}CD4^{+} T cell population (*Left*) with a representative polychromatic dot plot demonstrating FoxP3 staining within this population (*Right*). (*D*) Representative histograms of CD3^{+}CD4^{+}FoxP3 (red) and CD3^{+}CD4^{+}FoxP3^{+} cells (blue) showing expression of CD45RO, CD69, CD25, CD127, and HLA DR.

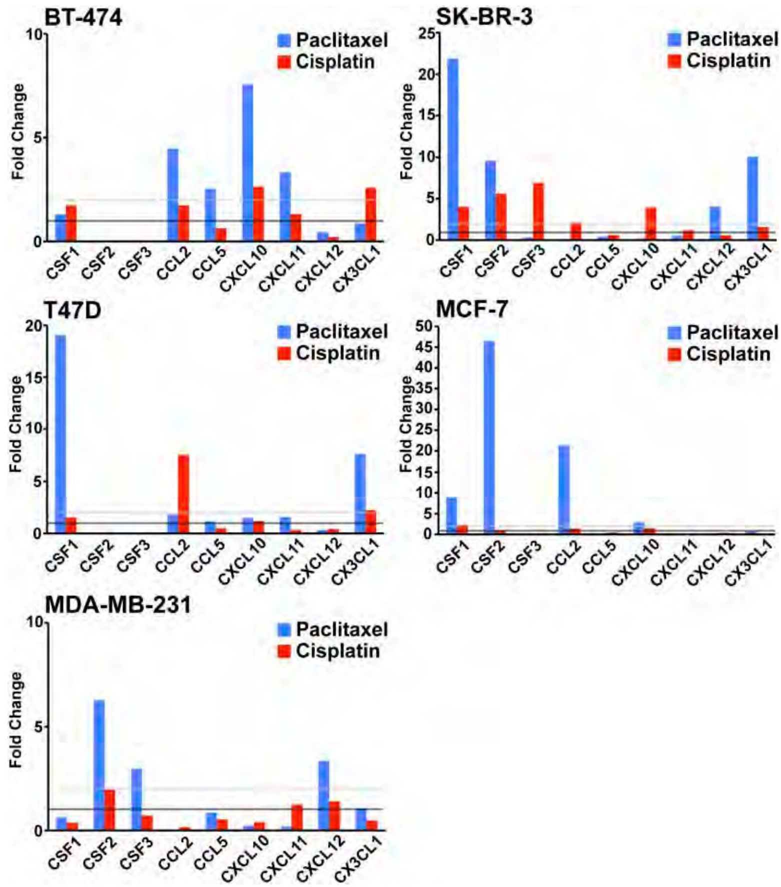

Fig. S6. CTX induces chemokine gene expression changes in human breast cancer cell lines. Relative gene expression compared with untreated controls after in vitro exposure to 25 nM paclitaxel or cisplatin for 24 h. Data represent an average of three replicates. Absence of bars for treated samples indicates un detectable gene expression in control. Fold change of 1× is shown with black horizontal bar, and 2× change is shown with gray horizontal bar.

Table S1. Patient information for evaluated tissue samples. ER, PR, and Her2 status is shown as grade, with percent positivity for ER/PR, and Her2 (evaluated by FISH) shown in parentheses

Age	Histology	Grade	ER	PR	Her2	Tumor size, cm	Node	Neoadjuvant Therapy
63	IDC	3	0 (0)	0 (0)	0 (1.1)	1.6		None
56	IDC	3	3+ (95)	3+ (90)	0	2.6	+	None
57	IDC	2	3+ (99)	2 3+ (25)	0	0.9	+	None
61	IDC	3	3+ (99)	3+ (60)	2+ (1.0)	4.8	+	None
78	IDC	3	3+ (30)	1 3+ (40)	3+	2.2	+	None
54	ILC	2	3+ (30)	3+ (30)	0	7.0	+	None
78	IDC	3	3+ (100)	0 (0)	2+ (1.0)	2.2		None
55	ILC	3	3+ (95)	0 (0)	2+ (1.6)	7.3	+	None
76	IDC	2	0 (0)	0 (0)	2+ (1.2)	5.1		None
65	IDC	2	1 3+ (90)	1 3+ (60)	0	9.0	+	None
74	IDC	2	1+ (1)	0 (0)	2+ ( )	0.8	+	None
65	ILC	2	3+ (100)	1 3+ (60)	0	1.1		Tamoxifen
59	ILC	2	3+ (100)	1+ (10)	0	7.0	+	None
71	ILC	1	3+ (95)	0 (0)	0	3.0		None
73	IDC	2	3+ (100)	2 3+ (50)	3+	9.8 (4.2)	+ (+)	Docetaxel, Carboplatin, Trastuzumab
66	IDC	3	0 (0)	0 (0)	0 (1.7)	10 (9.6)	+ (+)	Valproic Acid, 5 FU, Epirubicin, Cyclophosphamide
49	IDC	3	3+ (90)	0 (0)	2+ (2.3)	4.3 (4.3)	( )	Paclitaxol, Doxorubicin, Cyclophosphamide
39	IDC	2	3+ (95)	0 (0)	2+ (1.1)	8.0 (9.9)	+ (+)	Docetaxel, Doxorubicin, Cyclophosphamide
38	IDC	2	0 (0)	0 (0)	3+	3.5 (9.2)	+ (+)	Doxorubicin, Cyclophosphamide, Trastuzumab, Lapatinib
51	IDC	3	2+ (20)	0 (0)	2+ (1.0)	3.9 (4.2)	( )	Valproic Acid, 5 FU, Epirubicin, Anastrozole

Tumor size and node status are shown following neoadjuvant CTX in parentheses.

Table S2. Antibodies used for flow cytometry

Antigen	Clone	Fluorophore	Company	Catalog no.
CD3ε	OKT3	PerCP eFluor 710	eBioscience	46 0037 42
CD3ε	OKT3	PerCP Cy5.5	eBioscience	45 0037 42
CD4	RPA T4	Qdot 655	Invitrogen	Q10007
CD4	RPA T4	PE	BioLegend	300508
CD8α	RPA T8	APC eFluor 780	eBioscience	47 0088 42
CD8α	RPA T8	Qdot 605	Invitrogen	Q10009
CD11b	ICRF44	PE Cy7	eBioscience	25 0118 42
CD11c	3.9	Alexa 700	eBioscience	56 0116 73
CD14	61D3	Qdot 655	Invitrogen	Q10056
CD15	W6D3	Alexa 647	BioLegend	323012
CD19	HIB19	Alexa 700	eBioscience	56 0199 73
CD19	HIB19	PerCP Cy5.5	eBioscience	45 0199 73
CD20	2H7	Alexa 700	BioLegend	302322
CD20	2H7	PerCP Cy5.5	BioLegend	302326
CD25	BC96	PE Cy5	BioLegend	302608
CD25	BC96	PE Cy7	eBioscience	25 0259 42
CD27	O323	Alexa700	eBioscience	56 0279 73
CD28	CD28.2	PE Cy7	eBioscience	25 0289 42
CD45	HI30	Qdot 705	Invitrogen	Q10062
CD45	HI30	APC 780	eBioscience	47 0459 42
CD45RA	HI100	Qdot 605	Invitrogen	Q10047
CD45RO	UCHL1	Alexa700	BioLegend	304218
CD49d	9F10	PE Cy5	BioLegend	304306
CD56	HCD56	PE Cy5	BioLegend	318308
CD56	HCD56	PerCP Cy5.5	BioLegend	318322
CD69	FN50	FITC	eBioscience	11 0699 73
CD85g	17G10.2	APC	eBioscience	17 5179 42
CD86	IT2.2	PE Cy5	eBioscience	15 0869 73
CD117	YB5.B8	PE	eBioscience	12 1179 42
CD127	eBioRDR5	650NC	eBioscience	95 1278 42
CCR4	TG6	PE Cy7	BioLegend	335405
CCR5	HEK/1/85a	PE	BioLegend	313708
CCR7	TG8	Alexa 647	BioLegend	335603
CXCR3	TG1	Alexa 647	BioLegend	334903
FcεR1	AER 37	FITC	eBioscience	11 5899 73
FoxP3	PCH101	PE Cy5	eBioscience	15 4776 42
HLA DR	L243	eFluor450	eBioscience	48 9952 42
γδ TCR	B1.1	Alexa 647	BioLegend	331214
Vα24Jα18	6B11	PE	eBioscience	12 5806 42

Table S3. Antibodies used for immunohistochemistry and immunofluorescence

Antigen	Species	Dilution	Company	Catalog no.
CD3	Rabbit	1/150	Thermo Scientific	RM 9107 S1
CD4	Mouse	1/20	Thermo Scientific	MS 1528 S1
CD8	Mouse	1/100	Thermo Scientific	MS 457 S1
CD20	Mouse	1/50	Abcam	Ab9475
CD31 FITC	Mouse	1/10	BioLegend	303104
CD45	Mouse	1/100	eBioscience	14 0459 82
CD45 FITC	Mouse	1/10	BioLegend	304003
CD68	Mouse	1/100	Thermo Scientific	MS 397 P
CSF1R	Rabbit	1/100	Abcam	61137
Pan keratin Alexa 488	Mouse	1/100	Cell Signaling	4523
FoxP3	Mouse	1/40	eBioscience	14 4777 82
Granzyme B	Mouse	1/50	Thermo Scientific	MS 1157 S1

Published OnlineFirst July 26, 2011; DOI:10.1158/1078-0432.CCR-10-3420

Clinical Cancer Research

MRI of Tumor-Associated Macrophages with Clinically Applicable Iron Oxide Nanoparticles

Heike E. Daldrup-Link, Daniel Golovko, Brian Ruffell, et al.

Clin Cancer Res 2011;17:5695-5704. Published OnlineFirst July 26, 2011.

Published OnlineFirst July 26, 2011; DOI:10.1158/1078-0432.CCR-10-3420

Clinical Cancer Research

MRI of Tumor-Associated Macrophages with Clinically Applicable Iron Oxide Nanoparticles

Heike E. Daldrup-Link[1], Daniel Golovko[2], Brian Ruffell[3], David G. DeNardo[3], Rosalinda Castaneda[1], Celina Ansari[1], Jianghong Rao[1], Grigory A. Tikhomirov[1], Michael F. Wendland[4], Claire Corot[5], and Lisa M. Coussens[3]

Abstract

Purpose: The presence of tumor associated macrophages (TAM) in breast cancer correlates strongly with poor outcome. The purpose of this study was to develop a clinically applicable, noninvasive diagnostic assay for selective targeting and visualization of TAMs in breast cancer, based on magnetic resonancel and clinically applicable iron oxide nanoparticles.

Experimental Design: F4/80 negative mammary carcinoma cells and F4/80 positive TAMs were incubated with iron oxide nanoparticles and were compared with respect to magnetic resonance signal changes and iron uptake. MMTV PyMT transgenic mice harboring mammary carcinomas underwent nanoparticle enhanced magnetic resonance imaging (MRI) up to 1 hour and 24 hours after injection. The tumor enhancement on MRIs was correlated with the presence and location of TAMs and nanoparticles by confocal microscopy.

Results: *In vitro* studies revealed that iron oxide nanoparticles are preferentially phagocytosed by TAMs but not by malignant tumor cells. *In vivo*, all tumors showed an initial contrast agent perfusion on immediate postcontrast MRIs with gradual transendothelial leakage into the tumor interstitium. Twenty four hours after injection, all tumors showed a persistent signal decline on MRIs. TAM depletion via αCSF1 monoclonal antibodies led to significant inhibition of tumor nanoparticle enhancement. Detection of iron using 3,3′ diaminobenzidine enhanced Prussian Blue staining, combined with immunodetection of CD68, localized iron oxide nanoparticles to TAMs, showing that the signal effects on delayed MRIs were largely due to TAM mediated uptake of contrast agent.

Conclusion: These data indicate that tumor enhancement with clinically applicable iron oxide nanoparticles may serve as a new biomarker for long term prognosis, related treatment decisions, and the evaluation of new immune targeted therapies. *Clin Cancer Res; 17(17); 5695 704. ©2011 AACR.*

Introduction

Although breast cancer has not historically been linked to underlying inflammation or infection, it exhibits tumor associated inflammation marked by infiltration of leuko cytes into developing tumors where increases in some leu kocyte subsets parallels disease progression (1 3). In the majority of cases, however, the natural immunity to cancer that is present is not protective, but instead fosters progres sion. Studies in transgenic mouse models of mammary carcinogenesis revealed that tumor associated macrophages (TAM) promote tumor growth and enhance pulmonary metastasis by high level expression of epidermal growth factor (EGF) and activation of EGF regulated signaling in mammary epithelial cells (MEC) critical for invasive tumor growth and metastatic dissemination (4). Histopathologic and flow cytometric evaluations have revealed that TAMs are the most abundant innate immune cell present in murine mammary carcinomas and in human breast cancers (2, 5). TAM presence in several types of human cancer, including breast, correlates with increased vascular density and worse clinical outcome (6 11). A clinically reliable noninvasive *in vivo* imaging test that could reliably detect and quantify TAMs could be employed as a novel, widely applicable prognostic assay for stratifying individual patients to more aggressive and/or TAM targeted therapies.

Intravenously injected superparamagnetic iron oxide (SPIO) nanoparticles are effective contrast agents for mag netic resonance imaging (MRI). SPIO are phagocytosed by macrophages in various target tissues depending on their particle size and composition. Relatively large SPIO with

Authors' Affiliations: [1]Department of Radiology, Molecular Imaging Pro gram at Stanford, Stanford University, Stanford, California; [2]Department of Medicine, University of Massachusetts Medical School, Worcester, Mas sachusetts; [3]Department of Pathology, Helen Diller Family Comprehensive Cancer Center; [4]Department of Radiology and Biomedical Imaging, Uni versity of California San Francisco, San Francisco, California; and [5]Guer bet Group, Paris, France

Corresponding Author: Heike E. Daldrup Link, Molecular Imaging Pro gram at Stanford, Stanford University, 725 Welch Road, Stanford, CA 94304. Phone: 650 723 8996; Fax: 650 723 8402; E mail: heiked@stanford.edu

doi: 10.1158/1078 0432.CCR 10 3420

Translational Relevance

The presence of tumor associated macrophages (TAM) in adenocarcinomas correlates strongly with poor outcome in patients with breast cancer. Our data indicate that the Food and Drug Administration (FDA) approved iron oxide nanoparticle compound ferumoxytol (Fera heme) is preferentially phagocytosed by TAMs, but not by neoplastic tumor cells. *In vivo*, ferumoxytol adminis tration was associated with an initial tumor perfusion, followed by tumor retention and persistent magnetic resonance enhancement at 24 hours after intravenous administration, which correlated with phagocytosed nanoparticles in TAMs. Together, these data indicate that ferumoxytol enhancement may serve as a new bio marker for long term prognosis and related treatment decisions that will support ongoing development of new immune targeted therapies. Since ferumoxytol is FDA approved as an iron supplement, this application is immediately clinically applicable as an imaging approach via an "off label" use.

hydrodynamic diameters in the order of 80 to 150 nm are rapidly phagocytosed by macrophages of the reticulo endothelial system (RES), such as liver, spleen, and bone marrow, whereas ultra small SPIO (USPIO) with diameters of less than 50 nm escape RES phagocytosis to some extent, leading to a prolonged blood pool circulation and accu mulation in inflamed tissues and tumors due to transen dothelial leak and macrophage phagocytosis (12 14).

The goal of this study was to utilize novel USPIO to develop an immediately clinically applicable molecular imaging approach for enhanced imaging of TAMs in breast cancer. Our imaging technique relies on the iron supple ment ferumoxytol (Feraheme), recently Food and Drug Administration approved for intravenous treatment of iron deficiency in patients (15 17). Ferumoxytol is also a USPIO compound, providing a strong signal effect on MRIs and thus exerting properties of an magnetic resonance contrast agent (18 21). On the basis of these properties, we postu lated that ferumoxytol would be phagocytosed by TAMs in breast cancer, thereby enabling selective detection of TAMs on delayed, postperfusion MRIs.

Materials and Methods

Contrast agents

Three USPIO nanoparticle compounds were investi gated: (i) Ferumoxytol (Feraheme, AMAG Pharmaceuticals Inc.) is a USPIO nanoparticle applied for intravenous treatment of iron deficiency in patients with impaired renal function (15, 16, 20, 22, 23). Ferumoxytol consists of an iron oxide core and a carboxydextran coating. Ferumoxytol has a mean hydrodynamic diameter of 30 nm, an r_1 relaxivity of 38 $s^{-1}mM^{-1}$, and an r_2 relaxivity of 83 $s^{-1}mM^{-1}$ at 0.94T and at 37°C. Ferumoxytol was conju gated to fluorescein isothiocyanate (FITC; Ferumoxytol FITC) for detection by immunofluorescent microscopy. (ii) P904 (Guerbet Group, Paris, France) is a USPIO com pound currently in phase I clinical trials in Europe with plans for global distribution (24 27). P904 consists of an iron oxide core and a hydrophilic coating by a monomeric organic molecule with 20 hydroxylic groups. P904 has a mean hydrodynamic diameter of 21 nm, an r_1 of 14 $s^{-1}mM^{-1}$, and an r_2 relaxivity of 92 $s^{-1}mM^{-1}$ at 1.5 T and 37°C. (iii) P1133 (Guerbet) is a preclinical USPIO with potential future clinical development (24). P1133 is based on P904 but also incorporates 8 to 10 folate moieties per nanoparticle in its coating, added via an amino PEG derivative of folic acid coupled on its *g* carboxylic moiety to the carboxylate bearing iron core. P1133 has a mean hydrodynamic diameter of 26 nm, an r_1 relaxivity of 12 $s^{-1}mM^{-1}$, and an r_2 relaxivity of 95 $s^{-1}mM^{-1}$ at 1.5 T and 37°C.

Animal model

This study was approved by the animal care and use committees at the respective institutions. MMTV PyMT mice that spontaneously develop multifocal, multiclonal mammary adenocarcinomas were used at 12 to 14 weeks of life (28). Seven animals each received intravenous injec tions of ferumoxytol, P904, or P1133. Six additional ani mals received injections of P1133 + free folic acid. Animal age, weight, and tumor size were not significantly different between experimental groups that received different con trast agents ($P > 0.05$). Additional experiments were carried out in 7 postpubertal female FVB/n mice (10 12 weeks), which received injections of 50,000 PyMT derived tumor cells into the right lower mammary fat pad for induction of orthotopic tumors. Three of these animals were treated with anti colony stimulating factor (CSF) 1 monoclonal anti body (mAb), clone 5A1, purified by the UCSF Hybridoma core using the ATCC hybridoma (#CRL 2702). The animals received an intraperitoneal injection of 2 mg of anti CSF1 mAb, consisting of a 1 mg starting dose followed by 0.5 mg chaser doses on day 5 and 8, and ferumoxytol enhanced MRI on day 9. Three additional animals served as controls and received intraperitoneal injections of PBS at the corre sponding time points above, followed by ferumoxytol enhanced MRI. One additional mouse received 3 subse quent MRIs at 0, 1, and 24 hours without any contrast agent injection to confirm that tumors did not show any changes in magnetic resonance signal over a 2 day observation period. For all animals, MRI experiments were carried out when mammary tumors reached an approximate size of 1.0 cm.

Macrophage isolation and *in vitro* labeling

Tumors from MMTV PyMT mice at day 90 to 95, or PyMT orthotopic tumors, were isolated and digested in collagenase and DNAse (Roche Applied Sciences), strained over a cell strainer (BD Falcon, BD Biosciences), and incubated with phycoerythrin (PE) conjugated rat anti mouse F4/80 antibody (clone CI:A3 1, Caltag). Cells were then incubated with anti PE magnetic beads and isolated

Published OnlineFirst July 26, 2011; DOI:10.1158/1078-0432.CCR-10-3420

over a magnetic column to provide F4/80$^+$ cells (macrophages and monocytes) and F4/80$^-$ cell fractions (malignant mammary epithelial cells and other stromal populations). In a previous study, we reported that F4/80$^+$ cells represent Ly6G$^-$Ly6C$^-$CD11b$^+$F4/80$^+$ TAMs (2). A total of 4×10^6 of both F4/80$^+$ and F4/80$^-$ cells were plated onto cell culture dishes in DMEM supple mented with 10% fetal calf serum. A total of 200 µg [Fe]/mL of either Ferumoxytol, P1133, or P904 were added to the cell culture medium. Additional samples were incu bated with P1133 + 1.67 µmol/mL of free folic acid, a dose that corresponds to 10 times the dose of folic acid engrafted onto P1133. Cells were incubated overnight at standard cell culture conditions (37°C, 5% CO_2). The next day, nonadherent cells were discarded and adherent cells were removed via a cell lifter. Removed cells were washed 3 times in PBS and resuspended in 400 µL of ficoll at a density of 1.07 g/mL and placed into 2.0 mL conical tubes for imaging. Experiments were done in duplicates.

In vitro cell imaging and data analysis

For *in vitro* imaging of nanoparticle loaded cells, a clin ical 3T scanner was used (Signa Excite HD, GE Medical Systems) with a standard wrist coil (USA Instruments). Test tubes were immersed in a water bath and a multiecho spin echo sequence was obtained with the following para meters: TE 15, 30, 45, 60 ms, TR 2000 ms, FOV 8 × 8 cm, matrix 256 × 196 pixels, slice thickness 2 mm, and 2 acquisitions. Image processing was done by using MRVision software (MR Vision Co.). T2 relaxation times were calculated assuming a monoexponential signal decay and using nonlinear least square curve fitting on a pixel by pixel basis.

Determination of cell iron content

After imaging, cell samples were digested overnight in trypsin and placed in 10% HNO_3. Inductively coupled plasma optical emission spectroscopy (ICP OES) was done to quantify the iron content per sample (Perkin Elmer).

In vivo imaging

Animals were randomly assigned to MRI when their tumor reached a size of approximately 1.0 cm. Imaging of MMTV PyMT mice before and after injection of different nanoparticles was done with a 2 T Omega CSI II magnetic resonance scanner (Bruker Instruments) and imaging of mice before and after anti CSF1 mAb treatment was done with a 1 T desktop magnetic resonance scanner (Aspect M2 Compact High Performance MR System). Animals were anesthetized with isofluorane and placed on a recirculating water warming pad in a dedicated radiofrequency coil for high resolution MRI. A butterfly cannula filled with hepar inized saline solution was introduced into the tail vein and left in place. T1, T2, and T2* weighted imaging sequences were obtained with the following parameters: T1 Spinecho (SE): TR 500 ms, TE 12 ms; T2 SE: TR 2000 2500 ms, TE 15, 30, 45, 60 ms (2T), and TE 20, 40, 60, 80 ms (1T); T2* Gradient echo (GE): TR 240 ms, TE 10 ms, flip angle 30 degrees (2T). MRIs were obtained with a field of view (FOV) of 3 × 3 cm (2T) or 6 × 6 cm (1T), a matrix of 128 × 128 or 200 × 200 pixels, and a slice thickness of 1 to 2 mm.

Following precontrast T1, T2, and T2* weighted imaging, 24 PyMT animals received intravenous injections of 0.5 mmol [Fe]/kg ferumoxytol ($n = 7$), P904 ($n = 7$), P1133 ($n = 7$), P1133 + 2.35 mmol/kg free folic acid (100 times the dose of folate engrafted onto P1133; $n = 3$), or P1133 + 0.235 mmol/kg free folic acid (10 times the dose of folate engrafted onto P1133; $n = 3$). Additional tumor bearing mice after anti CSF1 mAb treatment ($n = 3$) or controls ($n = 3$) were injected with 0.5 mmol [Fe]/kg ferumoxytol. After contrast media injection, without repo sitioning the mouse, 6 subsequent multiecho T2 SE sequences were obtained over the course of an hour, followed by T1 and T2* weighted images. Mice were removed from the scanner, allowed to wake up, and imaged 24 hours later with T1, T2, and T2* weighted sequences. T2 relaxation times of the tumor were calculated based on multiecho SE sequences and converted to R2 relaxation rates (R2 = 1/T2), which is proportional to contrast agent concentration. The relative change in R2 data between pre and postcontrast MRIs, ΔR2 (%), was determined as a quantitative measure of tumor contrast enhancement.

Histology

After the last MRI, at 24 hours postcontrast media injec tion, mice were sacrificed, and mammary tumors explanted and placed in optimal cutting temperature (OCT) com pound on dry ice for histologic processing. Samples were cut onto slides and warmed to room temperature, followed by fixation in 100% ice cold acetone. Some samples were then washed in H_2O, and iron deposits in the tissue were detected using the Accustain Iron Stain Kit (Sigma Aldrich) according to the manufacturer's instructions, followed by signal enhancement with Fast 3,3′ diaminobenzidine (DAB, Vector Laboratories) for 2 minutes. After blocking sections with PBS containing 5% goat serum and 2.5% bovine serum albumin (blocking buffer), sections were incubated overnight at 4°C with 0.5× blocking buffer containing either rabbit anti mouse folate receptor α (1:100, Abcam) or rat anti mouse folate receptor β (1:8, kind gift from Prof. Matsuyama, Kagoshima University, Japan; ref. 29). Staining for folate receptor β was enhanced using a biotinylated anti rat secondary antibody (1:200, Vector Laboratories) and the Tyramide Signal Amplifica tion kit (Perkin Elmer). After extensive washing, sections were incubated overnight with FITC conjugated rat anti mouse CD68 (1:50, Serotec), followed by Alexa 488 con jugated goat anti FITC and either Alexa 546 conjugated donkey anti rabbit or Alexa 546 conjugated Streptavidin (1:500, Invitrogen). For detection of Ferumoxytol FITC, sections were stained with rat anti mouse CD68 (1:100, Serotec), washed, and then incubated with a combination of Alexa 546 conjugated donkey anti rat and Alexa 488 conjugated goat anti FITC. All slides were mounted using ProLong Gold with DAPI (Invitrogen) and analyzed using an LSM510 confocal microscope (Zeiss).

Statistics

Statistical analysis comparing the differences of tumor relaxation rates between mice receiving different contrast agents was done with a Wilcoxon rank sum test. A *t* test was used to determine the significance of differences between different cell samples and differences between age and tumor size of mice. A *P* value of less than 0.05 was considered significant.

Results

F4/80 positive TAMs phagocytose USPIO *in vitro*

Following incubation with the iron oxide nanoparticle ferumoxytol, F4/80$^+$ TAMs showed a markedly decreased signal on T2 weighted MRIs, whereas F4/80$^-$ cells showed minimal signal changes compared with untreated controls (Fig. 1A). Calculation of changes in relaxation rates (ΔR) as quantitative measures of the magnetic resonance signal enhancement (Fig. 1B) corroborated the qualitative find ings with significantly higher ΔR2 data for ferumoxytol exposed F4/80$^+$ TAMs compared with ferumoxytol exposed F4/80$^-$ cells consisting primarily of carcinoma cells ($P > 0.05$). Determination of iron content in the samples revealed that increased iron uptake was respon sible for the observed relaxation rate changes (Fig. 1C).

Since both TAMs and malignant epithelial cells highly express the folate receptor, folate linked USPIO have been recently developed for "tumor targeted imaging" (24, 30, 31). F4/80$^+$ TAMs incubated with folate engrafted P1133 nanoparticles showed significantly stronger visual and quantitative magnetic resonance signal enhancement as compared with ferumoxytol and P904 (Fig. 1). However, folate engraftment also leads to significantly increased nanoparticle uptake and magnetic resonance enhancement of F4/80$^-$ populations. The P1133 induced signal effect was inhibited by coincubation with free folic acid to P904 levels (Fig. 1), thus indicating that folate targeting mediates increased USPIO uptake *in vitro*.

Ferumoxytol leads to persistent tumor enhancement on delayed, postperfusion MRIs and corresponds to specific nanoparticle retention in TAMs

We investigated 90 day old MMTV PyMT mice bearing late stage mammary adenocarcinomas before and after intravenous injection of ferumoxytol, as well as syngeneic mice with PyMT derived orthotopic mammary tumors. All tumors showed an initial negative (dark) enhancement on immediate postcontrast T2 weighted MRIs, which was most pronounced in the tumor periphery and increased slowly and gradually up to 1.0 hour postinjection (p.i.). This corresponds to an initial blood pool perfusion of USPIO with slow, gradual transendothelial leakage of the nanoparticles into the tumor interstitium (32 35). At 24 hour p.i. of ferumoxytol, all tumors showed a per sistent signal decline, which was most pronounced in tumor centers (Fig. 2). We used DAB enhanced Prussian Blue staining for detection of iron, and immunodetection of CD68$^+$ TAMs in tissue sections of mammary tumors

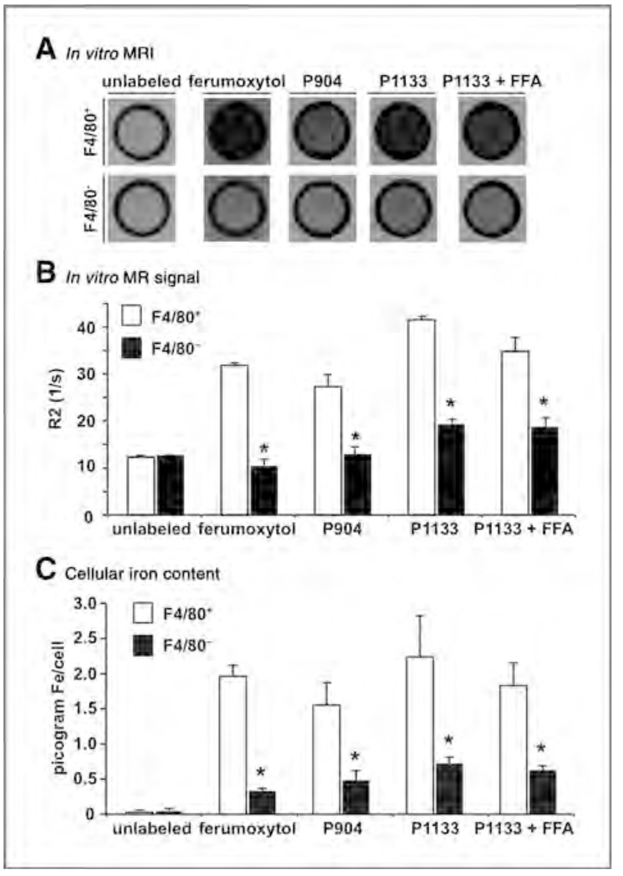

Figure 1. *In vitro* MRIs of iron oxide nanoparticle labeled cells with corresponding quantitative magnetic resonance signal enhancement and spectrometry data. A, axial T2 weighted MRIs through test tubes containing F4/80$^+$ versus F4/80 cells labeled overnight with Ferumoxytol, P904, P1133 alone, or P1133 with free folic acid (FFA). Cells were kept in suspension in ficoll solution and test tubes were placed in a water bath to avoid artifacts by surrounding air (which would cause a dark magnetic resonance signal). Image parameters: 3 Tesla, SE 2000/60 (TR/TE in ms). B, corresponding R2 relaxation rates that quantitatively measure the magnetic resonance signal effect of iron oxide nanoparticle labeled F4/80$^+$ versus F4/80 cells, displayed as mean ± SD from duplicate experiments. C, iron content of the same cell samples as shown in B, as determined by ICP OES.

localized ferumoxytol to CD68$^+$ TAMs (Fig. 3A). As it was difficult to show selective uptake using DAB generated contrast due to high background, we also generated fer umoxytol FITC to show colocalization by immunofluor escence using an Alexa 488 conjugated anti FITC antibody. As shown in Figure 3B, ferumoxytol was specifically found within CD68$^+$ TAMs, but not keratin 18 expressing malig nant epithelial cells. Although ferumoxytol was not found within all TAMs, these results indicate that the magnetic resonance signal effects on delayed MRIs were largely due to TAM mediated uptake of contrast agent.

USPIO mediated TAM enhancement on delayed MRIs can be increased by folate receptor targeting of nanoparticles

To determine whether folate receptor targeting could enhance the MRIs, we obtained additional MRIs of

Published OnlineFirst July 26, 2011; DOI:10.1158/1078-0432.CCR-10-3420

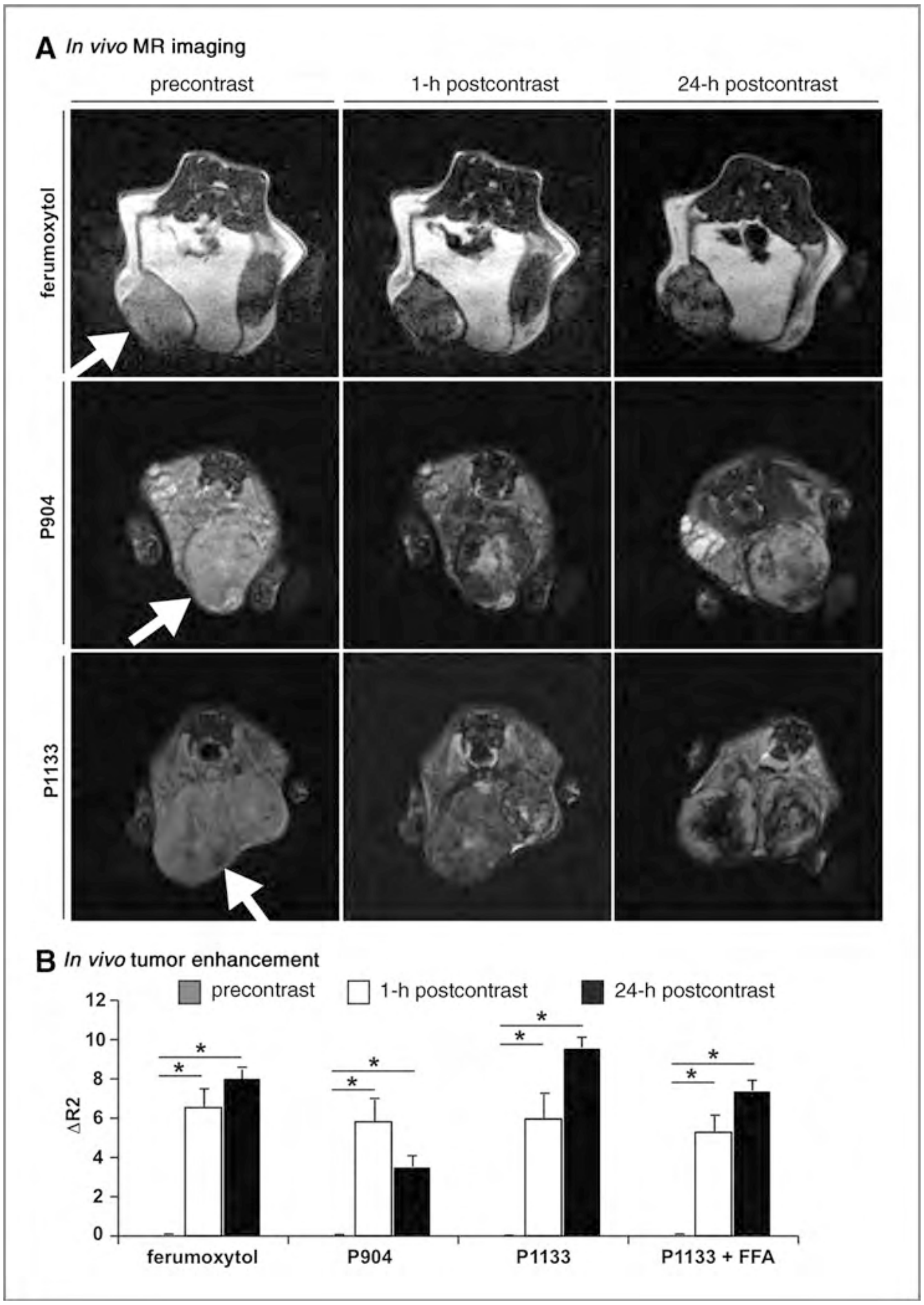

Figure 2. *In vivo* MRI of iron oxide nanoparticles. A, T2 weighted SE images of representative mammary tumors in MMTV PyMT mice prior to (precontrast) 1 and 24 hours after administration of 0.5 mmol [Fe]/kg of ferumoxytol, P904 or P1133. The iron oxide nanoparticle based contrast agents cause a negative (dark) signal effect in the tumor tissue on these scans (arrows point to tumors). B, quantitation of magnetic resonance signal enhancement (delta R2 measurement) of mammary tumors in MMTV PyMT mice before and after iron oxide nanoparticle administration, displayed as means ± SD ($n = 7$ mice/group, except P1133 + FFA which contained 3 mice). Note that all tumors show a nanoparticle retention at 24 hours, which is most pronounced for the folate linked nanoparticle P1133.

MMTV PyMT mice with late stage mammary adenocarci nomas injected with the folate engrafted USPIO P1133, the nontargeted analogue P904, or P1133 plus free folic acid. P1133 and P904 caused a nonspecific tumor perfusion effect on T2 weighted images during the first hour p.i., which was not significantly different as compared with tumor bearing mice injected with ferumoxytol (Fig. 2). Delayed MRIs showed a significantly stronger persistent tumor signal decline at 24 hour p.i. of P1133 compared with ferumoxytol ($P < 0.05$).

In vivo inhibition experiments with free folic acid are limited due to rapid liver uptake and renal elimination of free folic acid (36). Inhibition experiments with free folic acid at a 10 times increased dose as compared with the folate dose delivered with P1133 resulted in a minor, albeit not significant inhibition of the P1133 induced tumor enhancement ($P > 0.05$). Inhibition experiments with higher folic acid doses proved toxic in tumor bearing mice, similar to previous reports (37). However, delayed MRIs showed significantly less tumor enhancement at 24 hour

Published OnlineFirst July 26, 2011; DOI:10.1158/1078-0432.CCR-10-3420

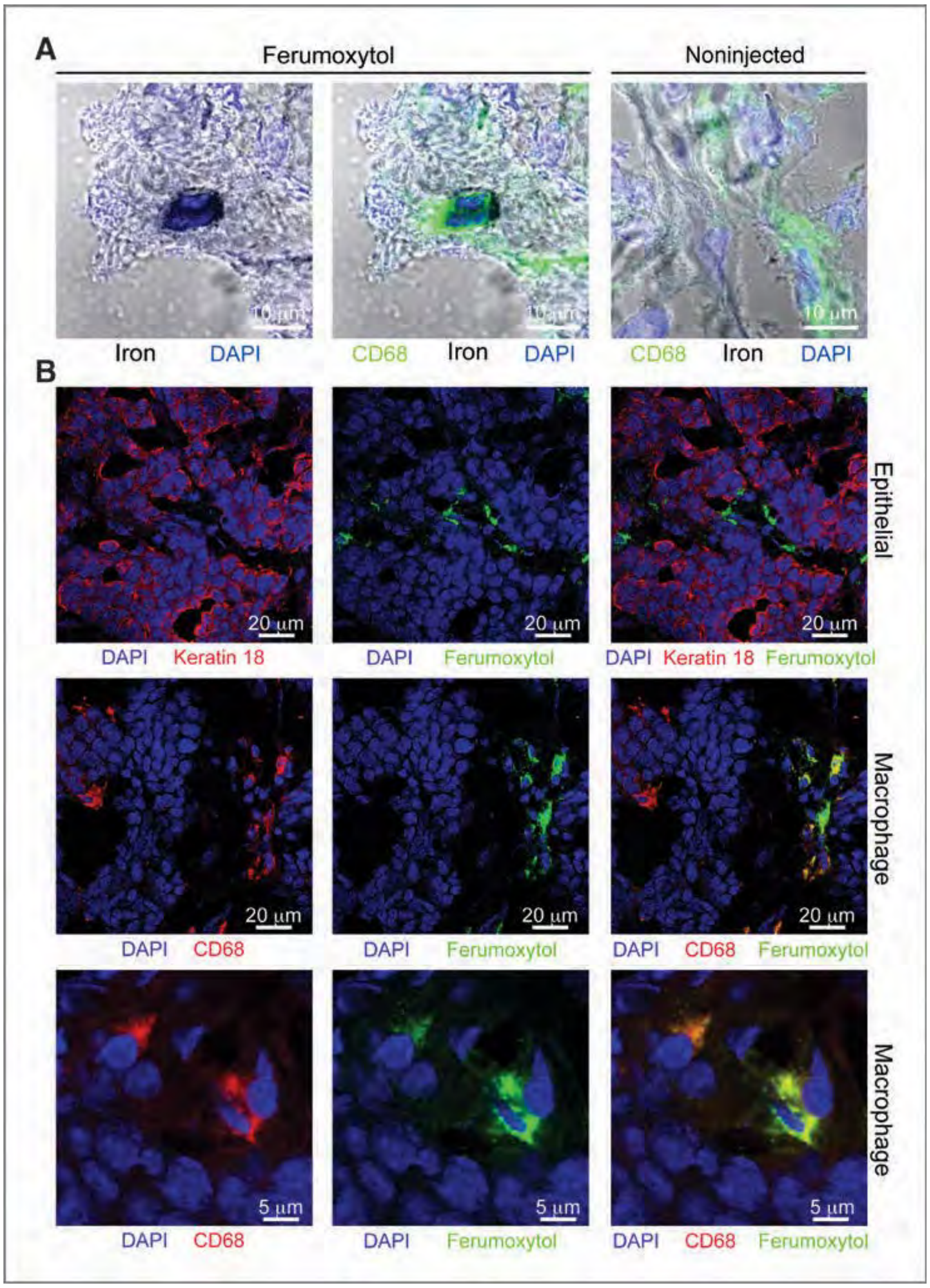

Figure 3. Uptake of ferumoxytol by TAMs *in vivo*. A, localization within OCT embedded mammary tumors of ferumoxytol (iron; black contrast) to $CD68^+$ macrophages (green) using phase contrast of DAB staining and confocal microscopy. B, localization of ferumoxytol FITC (green) to $CD68^+$ macrophages (red) but not Keratin 18^+ carcinoma cells (red) within mammary tumors. Scale bars are shown in images.

p.i. of folate free P904 compared with folate linked P1133 ($P < 0.05$; Fig. 2). Because P1133 and P904 are chemically identical except for folate engraftment on P1133, this data indicates increased nanoparticle uptake via folate receptor targeting.

We next evaluated TAMs versus epithelial cells for expres sion of α and β folate receptor in mammary tumors and revealed folate receptor α staining throughout epithelium, with no expression detectable on $CD68^+$ TAMs (Fig. 4A). In contrast, expression of folate receptor β was observed exclusively on $CD68^+$ cells, although these represented only a portion of the total $CD68^+$ TAMs found within tumors (Fig. 4B) and seemed to be primarily associated with vascular and peripheral regions of mammary tumors. Consistent with the MRIs, Prussian Blue staining for iron was more prominent within tumors from mice injected with P1133 compared with P904 or ferumoxytol (Fig. 4C). Furthermore, although some iron staining was observed in areas that did not seem occupied by TAMs (blue arrow), this was minor compared with staining within stromal areas likely enriched with TAMs (red arrow). Thus, while folate engraftment did increase uptake of USPIOs by cells

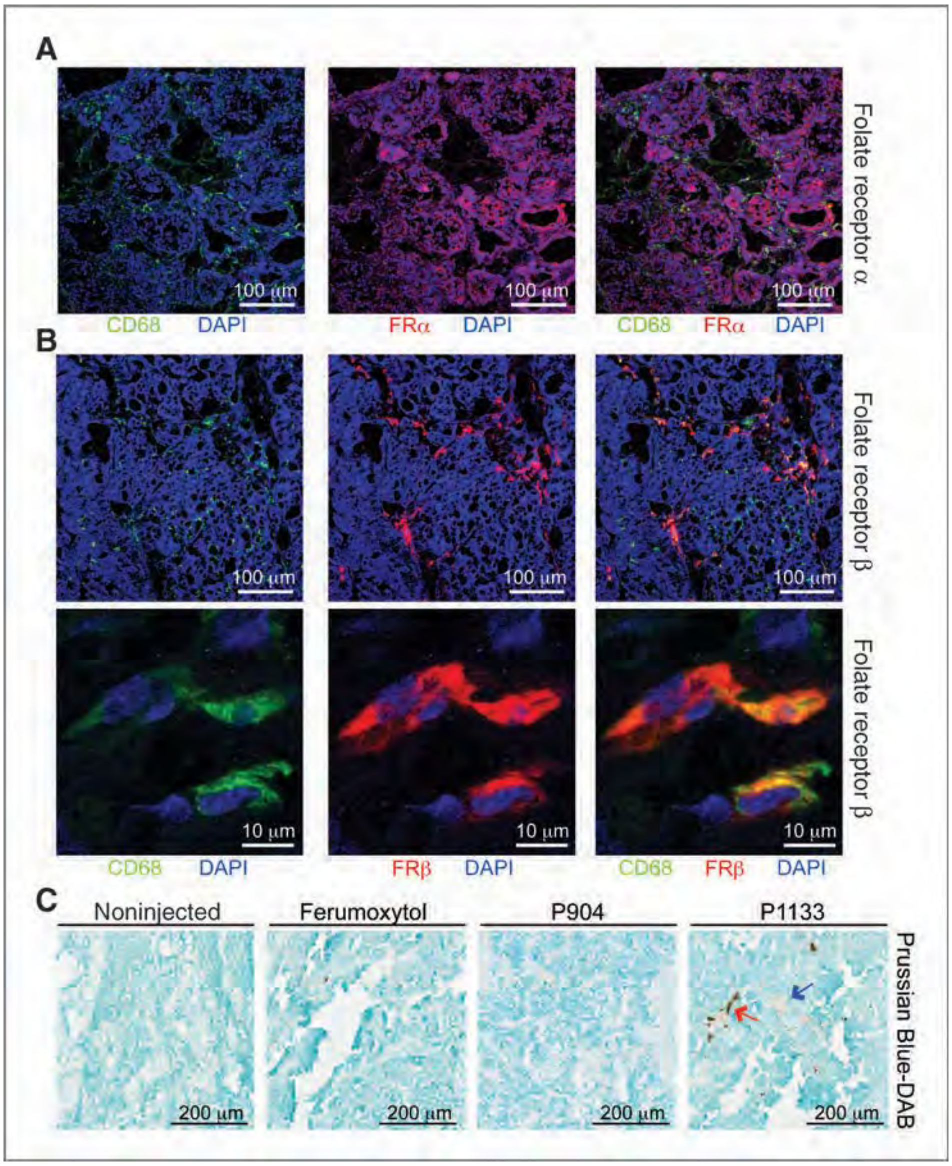

Figure 4. Folate receptor expression and folate targeted uptake of nanoparticles. A, staining for folate receptor α (FRα; red) and $CD68^+$ macrophages (green) shows that expression of FRα is localized to carcinoma cells within mammary tumors. B, a subpopulation of $CD68^+$ macrophages (green) expresses folate receptor β (FRβ; red staining). C, Prussian Blue staining for iron with DAB enhancement within mammary tumors from mice injected with ferumoxytol, P904, or P1133. Scale bars are shown in images.

other than TAMs, these results indicate that folate modi fication of USPIOs may still improve their clinical use as evaluators of TAM presence within tumors.

Ferumoxytol enhanced MRI detects TAM depletion after anti CSF1 mAb treatment

Imaging data from a control mouse that underwent 3 subsequent MRIs at 0, 1, and 24 hours without any contrast agent injection confirmed that MMTV PyMT tumors do not show any intrinsic changes in magnetic resonance signal within a 2 day observation period. Mice treated with anti CSF1 mAb showed a similar ferumoxytol tumor perfusion effect compared with untreated controls during the first hour after intrave nous ferumoxytol injection. However, at 24 hour p.i., anti CSF1 mAb treated tumors showed less magnetic resonance contrast effects and significantly smaller ΔR2 enhancement data compared with untreated con trols (Fig. 5A). Corresponding confocal microscopy eva luations confirmed TAM depletion of anti CSF1 mAb treated tumors (Fig. 5B), indicating that ferumoxytol enhanced MRI is related to TAM density.

Discussion

Results from this study show that ferumoxytol can be used as a reliable tool to quantitatively monitor macro phage presence in tumors, suggesting that this imaging technique can be readily investigated as a surrogate mea sure to predict outcomes for patients with breast cancer, and applied to monitor TAM targeted therapies now in clinical trials.

Published OnlineFirst July 26, 2011; DOI:10.1158/1078-0432.CCR-10-3420

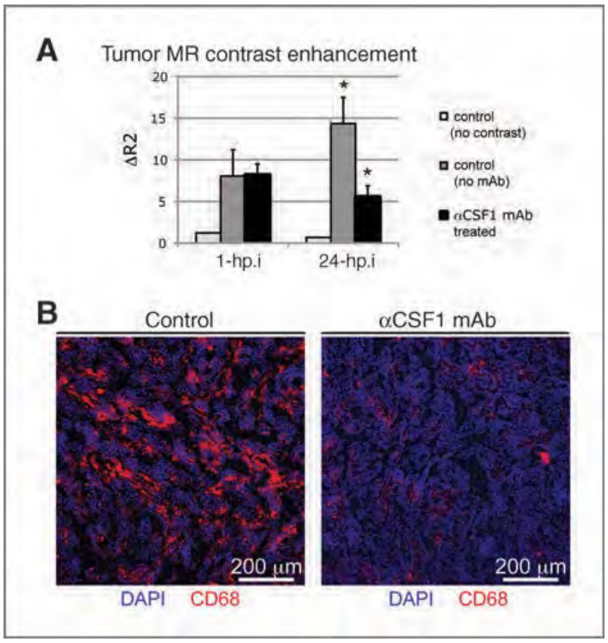

Figure 5. Ferumoxytol enhanced MRI detects TAM depletion noninvasively *in vivo*. A, quantitative magnetic resonance signal enhancement (delta R2 measurement) of MMTV PyMT mammary tumors before and after iron oxide nanoparticle administration, displayed as mean ± SD of 3 mice treated with anti CSF1 mAb or PBS control. An additional control mouse underwent serial magnetic resonance without any contrast agent injection to confirm that MMTV PyMT tumors do not show any intrinsic changes in magnetic resonance signal within a 2 day observation period. Note that mice treated with anti CSF1 mAb showed significantly smaller ΔR2 enhancement data compared with untreated controls. B, corresponding confocal microscopy evaluations confirmed TAM depletion within anti CSF1 mAb treated tumors.

To the best of our knowledge, this is the first report of utilizing a clinically applicable nanoparticle for TAM detection by MRI. Other investigators have reported TAM detection with nanoparticles that are not clinically applicable, for either MRI (38) or optical imaging (39). In addition, there have been reports of radiotracer based approaches for TAM detection by positron emission tomography (PET; ref. 39). The latter is associated with radiation exposure and therefore not used routinely for breast imaging. MRI, on the other hand, is radiation free, established for breast cancer detection, and integrates near microscopic anatomic resolution, high sensitivity, and excellent soft tissue contrast. Although histologic methods for quantifying TAMs are more precise, they are invasive, limited to one or few observations, and not representative of the whole tumor in the case of biopsies.

Preclinical and clinical evidence indicates that chronic presence of diverse leukocyte subsets within the stroma of breast cancers promotes tumor growth and metastasis (3, 40, 41). TAMs play a significant protumorigenic role in this context by augmenting neoplastic cell survival and motility via elaboration of cytokines, chemokines, proteases, and reactive oxygen species (3, 4, 42, 43). TAMs also potentiate pulmonary metastasis of mammary adenocarcinomas through enhanced angiogenesis via regulation of VEGF bioavailability and supplying epidermal growth factor (EGF) to mammary epithelium (5, 44), in addition to suppression of protective adaptive immune responses (3, 42, 43, 45, 46). Exuberant macrophage recruitment to breast cancer has been reported to be strongly associated with poor prognosis, both in animal models and in patients (2 4, 42 44). Although phagocytotic capacity can be altered by *in vitro* polarization of macrophages, we have no evidence that ferumoxytol uptake corresponds to a particular TAM phenotype. Regardless, aggressive human breast cancers have been reported to contain few (if any) T_H1 polarized macrophages (47), and in the MMTV PyMT transgenic model in particular, TAMs are strongly T_H2 polarized by interleukin 4 (2).

Ferumoxytol enhancement is a new, noninvasive indicator for TAM tumor infiltration, which may serve as a novel biomarker for breast cancers with poor outcome and may be utilized to stratify tumors with high TAM infiltration for immune targeted therapies. There have been multiple approaches for specific targeting and/or blockade of TAMs for therapeutic purposes (29, 48, 49), some of which are currently in clinical trials based on experimental data showing that genetic, immunologic, or pharmacologic blockade of CSF1, or its receptor (CSF1R), decreases TAM presence in tissues and in experimental solid tumors, correlating with diminished tumor angiogenesis, and reduced primary tumor growth and pulmonary metastasis (50 54). Because these therapies are not cytotoxic, biomarkers of their efficiency at inducing macrophage depletion would be of great clinical benefit. Moreover, since clinical trials of new therapeutic drugs and new combination therapies are expensive and take years to complete, the immediate value and impact of imaging TAMs and/or TAM depletion via MRI would be immense.

We recognize several limitations with this approach. Studies reported herein were done with ferumoxytol doses of 0.5 mmol/kg. Previously described ferumoxytol doses in humans were in the order of 0.035 0.072 mmol/kg (18, 19). Iron oxide nanoparticles are generally applied in higher doses in rodents as opposed to humans to compensate for the relatively shorter blood half life in rodents. However, future clinical applications must show if the currently applied dose in patients is sufficient for TAM detection, or if the dose can be safely increased. Of note, ferumoxytol showed an excellent safety profile in more than 700 patients (17). Larger superparamagnetic iron oxide nanoparticles (SPIO, diameter >50 nm) provide higher cellular uptake via *ex vivo* labeling. However, SPIOs are rapidly phagocytosed by macrophages in liver, spleen, and bone marrow and do not reach TAMs *in vivo*. USPIOs, on the other hand, are not as quickly recognized by the RES and have a longer circulation time, and can therefore leak into tumor interstitium, where they can be phagocytosed by TAMs. Thus, for "*in vivo* TAM labeling," USPIOs are advantageous (32, 33).

As shown by our data, an alternative approach to increase the sensitivity of MRI would be to utilize folate engrafted nanoparticles. Although such particles are currently not available for clinical use, precursors of such compounds are currently entering clinical trials and thus folate engrafted derivatives may become clinically avail able in the future. Folate engraftment enhances nanopar ticle uptake via the folate receptor β, which is highly expressed on TAMs (31). Several investigators including us have reported uptake of USPIO and folate engrafted USPIO by neoplastic cells, which may be a confounding variable when aiming for TAM detection (24, 55, 56). However, data presented here reveal that the ferumoxytol and P1133 uptake in malignant epithelial cells is signifi cantly lower as compared with macrophage uptake, leading to negligible interferences of our imaging approach.

In conclusion, we have shown that iron oxide nanopar ticle enhanced MRI can be utilized to detect TAMs in a mouse model of mammary carcinogenesis. Ferumoxytol is a clinically available nanoparticle that can be readily applied for TAM imaging in patients with breast cancer via an "off label" use. Macrophage detection may be enhanced by using folate engrafted nanoparticles that may become available for clinical use in the near future. Clinical studies are underway to evaluate these findings in patients.

Disclosure of Potential Conflicts of Interest

C. Corot works for Guerbet Research and provided contrast agents for this study. She was not involved in data analyses. The other authors disclosed no potential conflicts of interest.

Acknowledgments

The authors thank the UCSF Helen Diller Family Comprehensive Cancer Center Laboratory for Cell Analysis and Mouse Pathology shared resource core facilities and members of the Daldrup-Link and Coussens laboratories for critical discussion.

Grant Support

This work was supported by fellowships from the American Cancer Society to D.G. DeNardo and the Department of Defense Breast Cancer Research Program to B. Ruffell, grants from the NIH/NCI (R01CA130980, R01CA132566, R01CA140943, and P50 CA58207), and the Department of Defense (W81XWH-06-1-0416, PR080717) to L.M. Coussens, grants from the NIH/NCI (R01CA140943 and R21CA156124), Bay Area Breast Cancer Specialized Program of Research Excellence (P50 CA 58207), and a pilot grant from the Stanford Center for Cancer Nanotechnology Excellence and Translation (CCNE-T; NIH/NCI U54 CA151459) to H.E. Daldrup-Link, and grant P50 CA114747 to J. Rao.

The costs of publication of this article were defrayed in part by the payment of page charges. This article must therefore be hereby marked *advertisement* in accordance with 18 U.S.C. Section 1734 solely to indicate this fact.

Received December 23, 2010; revised July 12, 2011; accepted July 14, 2011; published OnlineFirst July 26, 2011.

References

1. de Visser KE, Eichten A, Coussens LM. Paradoxical roles of the immune system during cancer development. Nature Reviews Cancer 2006;6:24 37.
2. DeNardo DG, Barreto JB, Andreu P, Vasquez L, Tawfik D, Kolhatkar N, et al. CD4+ T cells regulate pulmonary metastasis of mammary carcinomas by enhancing protumor properties of macrophages. Cancer Cell 2009;16:91 102.
3. DeNardo DG, Coussens LM. Inflammation and breast cancer. Balancing immune response: crosstalk between adaptive and innate immune cells during breast cancer progression. Breast Cancer Res 2007;9:212.
4. Pollard JW. Tumour educated macrophages promote tumour pro gression and metastasis. Nat Rev Cancer 2004;4:71 8.
5. DeNardo DG, Johansson M, Coussens LM. Immune cells as media tors of solid tumor metastasis. Cancer Metastasis Rev 2008;27:11 8.
6. Bolat F, Kayaselcuk F, Nursal TZ, Yagmurdur MC, Bal N, Demirhan B, et al. Microvessel density, VEGF expression, and tumor associated macrophages in breast tumors: correlations with prognostic para meters. J Exp Clin Cancer Res 2006;25:365 72.
7. Campbell MJ, Tonlaar NY, Garwood ER, Huo D, Moore DH, Khramt sov AI, et al. Proliferating macrophages associated with high grade, hormone receptor negative breast cancer and poor clinical outcome. Breast Cancer Res Treat 2011;128:703 11.
8. Chen JJ, Lin YC, Yao PL, Yuan A, Chen HY, Shun CT, et al. Tumor associated macrophages: the double edged sword in cancer pro gression. J Clin Oncol 2005;23:953 64.
9. Steidl C, Lee T, Shah SP, Farinha P, Han G, Nayar T, et al. Tumor associated macrophages and survival in classic Hodgkin's lym phoma. N Engl J Med 2010;362:875 85.
10. Tsutsui S, Yasuda K, Suzuki K, Tahara K, Higashi H, Era S, et al. Macrophage infiltration and its prognostic implications in breast cancer: the relationship with VEGF expression and microvessel den sity. Oncol Rep 2005;14:425 31.
11. Zhang J, Patel L, Pienta KJ. CC chemokine ligand 2 (CCL2) promotes prostate cancer tumorigenesis and metastasis. Cytokine Growth Factor Rev 2010;21:41 8.
12. Rosenblum LT, Kosaka N, Mitsunaga M, Choyke PL, Kobayashi H. *In vivo* molecular imaging using nanomaterials: General *in vivo* charac teristics of nano sized reagents and applications for cancer diagnosis (Review). Mol Membr Biol 2010;27:274 85.
13. Gossuin Y, Gillis P, Hocq A, Vuong QL, Roch A. Magnetic resonance relaxation properties of superparamagnetic particles. Wiley Interdiscip Rev Nanomed Nanobiotechnol 2009;1:299 310.
14. Corot C, Robert P, Idee JM, Port M. Recent advances in iron oxide nanocrystal technology for medical imaging. Adv Drug Deliv Rev 2006;58:1471 504.
15. Landry R, Jacobs PM, Davis R, Shenouda M, Bolton WK. Pharma cokinetic study of ferumoxytol: a new iron replacement therapy in normal subjects and hemodialysis patients. Am J Nephrol 2005; 25:400 10.
16. Lu M, Cohen MH, Rieves D, Pazdur R. FDA report: Ferumoxytol for intravenous iron therapy in adult patients with chronic kidney disease. Am J Hematol 2010;85:315 9.
17. Schwenk MH. Ferumoxytol: a new intravenous iron preparation for the treatment of iron deficiency anemia in patients with chronic kidney disease. Pharmacotherapy 2010;30:70 9.
18. Li W, Salanitri J, Tutton S, Dunkle EE, Schneider JR, Caprini JA, et al. Lower extremity deep venous thrombosis: evaluation with ferumoxytol enhanced magnetic resonance imaging and dual contrast mechanism preliminary experience. Radiology 2007; 242:873 81.
19. Li W, Tutton S, Vu AT, Pierchala L, Li BS, Lewis JM, et al. First pass contrast enhanced MR angiography in humans using feru moxytol, a novel ultrasmall superparamagnetic iron oxide (USPIO) based blood pool agent. J Magn Reson Imaging 2005;21:46 52.
20. Neuwelt EA, Várallyay CG, Manninger S, Solymosi D, Haluska M, Hunt MA, et al. The potential of ferumoxytol nanoparticle magnetic reso nance imaging, perfusion, and angiography in central nervous system malignancy: a pilot study. Neurosurgery 2007;60:601 11; discussion 611 602.

Published OnlineFirst July 26, 2011; DOI:10.1158/1078-0432.CCR-10-3420

21. Simon GH, von Vopelius Feldt J, Fu Y, Schlegel J, Pinotek G, Wend land MF, et al. Ultrasmall supraparamagnetic iron oxide enhanced magnetic resonance imaging of antigen induced arthritis: a compara tive study between SHU 555 C, ferumoxtran 10, and ferumoxytol. Invest Radiol 2006;41:45 51.

22. Balakrishnan VS, Rao M, Kausz AT, Brenner L, Pereira BJ, Frigo TB, et al. Physicochemical properties of ferumoxytol, a new intravenous iron preparation. Eur J Clin Invest 2009;39:489 96.

23. Pai AB, Nielsen JC, Kausz A, Miller P, Owen JS. Plasma pharmaco kinetics of two consecutive doses of ferumoxytol in healthy subjects. Clin Pharmacol Ther 2010;88:237 42.

24. Meier R, Henning TD, Boddington S, Tavri S, Arora S, Piontek G, et al. Breast cancers: MR imaging of folate receptor expression with the folate specific nanoparticle P1133. Radiology 2010;255:527 35.

25. Sigovan M, Bessaad A, Alsaid H, Lancelot E, Corot C, Neyran B, et al. Assessment of Age Modulated Vascular Inflammation in ApoE / Mice by USPIO Enhanced Magnetic Resonance Imaging. Invest Radiol 2010;45:702 7.

26. Sigovan M, Boussel L, Sulaiman A, Sappey Marinier D, Alsaid H, Desbleds Mansard C, et al. Rapid clearance iron nanoparticles for inflammation imaging of atherosclerotic plaque: initial experience in animal model. Radiology 2009;252:401 9.

27. Wang ZJ, Boddington S, Wendland M, Meier R, Corot C, Daldrup Link H, et al. MR imaging of ovarian tumors using folate receptor targeted contrast agents. Pediatr Radiol 2008;38:529 37.

28. Guy CT, Cardiff RD, Muller WJ. Induction of mammary tumors by expression of polyomavirus middle T oncogene: a transgenic mouse model for metastatic disease. Mol Cell Biol 1992;12:954 61.

29. Nagai T, Tanaka M, Tsuneyoshi Y, Xu B, Michie SA, Hasui K, et al. Targeting tumor associated macrophages in an experimental glioma model with a recombinant immunotoxin to folate receptor beta. Cancer Immunol Immunother 2009;58:1577 86.

30. Kim S, Lee J. Folate targeted drug delivery systems prepared by nano comminution. Drug Dev Ind Pharm 2011;37:131 8.

31. Puig Kröger A, Sierra Filardi E, Domínguez Soto A, Samaniego R, Corcuera MT, Gómez Aguado F, et al. Folate receptor beta is expressed by tumor associated macrophages and constitutes a marker for M2 anti inflammatory/regulatory macrophages. Cancer Res 2009;69:9395 403.

32. Daldrup Link HE, Rydland J, Helbich TH, Bjørnerud A, Turetschek K, Kvistad KA, et al. Quantification of breast tumor microvascular per meability with feruglose enhanced MR imaging: initial phase II multi center trial. Radiology 2003;229:885 92.

33. Daldrup Link HE, Simon GH, Brasch RC. Imaging of tumor angiogen esis: current approaches and future prospects. Curr Pharm Des 2006;12:2661 72.

34. Turetschek K, Huber S, Floyd E, Helbich T, Roberts TP, Shames DM, et al. MR imaging characterization of microvessels in experimental breast tumors by using a particulate contrast agent with histopatho logic correlation. Radiology 2001;218:562 9.

35. Turetschek K, Roberts TP, Floyd E, Preda A, Novikov V, Shames DM, et al. Tumor microvascular characterization using ultrasmall super paramagnetic iron oxide particles (USPIO) in an experimental breast cancer model. J Magn Reson Imaging 2001;13:882 8.

36. Steinberg SE, Campbell CL, Hillman RS. Kinetics of the normal folate enterohepatic cycle. J Clin Invest 1979;64:83 8.

37. Parchure M, Ambaye RY, Lalitha VS, Gokhale SV. Acute toxicity of folic acid in mice. Experientia 1985;41:72 3.

38. Leimgruber A, Berger C, Cortez Retamozo V, Etzrodt M, Newton AP, Waterman P, et al. Behavior of endogenous tumor associated macro phages assessed *in vivo* using a functionalized nanoparticle. Neo plasia 2009;11:459 68, 452 p following 468.

39. Nahrendorf M, Keliher E, Marinelli B, Waterman P, Feruglio PF, Fexon L, et al. Hybrid PET optical imaging using targeted probes. Proc Natl Acad Sci U S A 2010;107:7910 5.

40. Coussens LM, Werb Z. Inflammation and cancer. Nature 2002; 420:860 7.

41. Ruffell B, DeNardo DG, Affara NI, Coussens LM. Lymphocytes in cancer development: polarization towards pro tumor immunity. Cyto kine Growth Factor Rev 2010;21:3 10.

42. Leek RD, Lewis CE, Whitehouse R, Greenall M, Clarke J, Harris AL, et al. Association of macrophage infiltration with angiogenesis and prognosis in invasive breast carcinoma. Cancer Res 1996;56: 4625 9.

43. van Netten JP, Ashmed BJ, Cavers D, Fletcher C, Thornton IG, Antonsen BL, et al. 'Macrophages' and their putative significance in human breast cancer. Br J Cancer 1992;66:220 1.

44. Lin EY, Nguyen AV, Russell RG, Pollard JW. Colony stimulating factor 1 promotes progression of mammary tumors to malignancy. J Exp Med 2001;193:727 40.

45. Lin EY, Li JF, Gnatovskiy L, Deng Y, Zhu L, Grzesik DA, Qian H, et al. Macrophages regulate the angiogenic switch in a mouse model of breast cancer. Cancer Res 2006;66:11238 46.

46. Crowther M, Brown NJ, Bishop ET, Lewis CE. Microenvironmental influence on macrophage regulation of angiogenesis in wounds and malignant tumors. J Leukoc Biol 2001;70:478 90.

47. Solinas G, Germano G, Mantovani A, Allavena P. Tumor associated macrophages (TAM) as major players of the cancer related inflamma tion. J Leukoc Biol 2009;86:1065 73.

48. Luo Y, Zhou H, Krueger J, Kaplan C, Lee SH, Dolman C, et al. Targeting tumor associated macrophages as a novel strategy against breast cancer. J Clin Invest 2006;116:2132 41.

49. Zeisberger SM, Odermatt B, Marty C, Zehnder Fjällman AH, Ballmer Hofer K, Schwendener RA, et al. Clodronate liposome mediated depletion of tumour associated macrophages: a new and highly effective antiangiogenic therapy approach. Br J Cancer 2006;95: 272 81.

50. Conway JG, McDonald B, Parham J, Keith B, Rusnak DW, Shaw E, et al. Inhibition of colony stimulating factor 1 signaling *in vivo* with the orally bioavailable cFMS kinase inhibitor GW2580. Proc Natl Acad Sci U S A 2005;102:16078 83.

51. Manthey CL, Johnson DL, Illig CR, Tuman RW, Zhou Z, Baker JF, et al. JNJ 28312141, a novel orally active colony stimulating factor 1 receptor/FMS related receptor tyrosine kinase 3 receptor tyro sine kinase inhibitor with potential utility in solid tumors, bone metastases, and acute myeloid leukemia. Mol Cancer Ther 2009;8: 3151 61.

52. Nowicki A, Szenajch J, Ostrowska G, Wojtowicz A, Wojtowicz K, Kruszewski AA, et al. Impaired tumor growth in colony stimulating factor 1 (CSF 1) deficient, macrophage deficient op/op mouse: evi dence for a role of CSF 1 dependent macrophages in formation of tumor stroma. Int J Cancer 1996;65:112 9.

53. Priceman SJ, Sung JL, Shaposhnik Z, Burton JB, Torres Collado AX, Moughon DL, et al. Targeting distinct tumor infiltrating myeloid cells by inhibiting CSF 1 receptor: combating tumor evasion of antiangio genic therapy. Blood 2010;115:1461 71.

54. DeNardo D, et al. Leukocyte complexity predicts breast cancer survival and functionally regulates response to chemotherapy. Cancer Discovery 2011;1:54 67.

55. Choi H, Choi SR, Zhou R, Kung HF, Chen IW. Iron oxide nanoparticles as magnetic resonance contrast agent for tumor imaging via folate receptor targeted delivery. Acad Radiol 2004;11:996 1004.

56. Sun C, Sze R, Zhang M. Folic acid PEG conjugated superparamag netic nanoparticles for targeted cellular uptake and detection by MRI. J Biomed Mater Res A 2006;78:550 7.

Leukocyte Complexity Predicts Breast Cancer Survival and Functionally Regulates Response to Chemotherapy

David G. DeNardo[1], Donal J. Brennan[2], Elton Rexhepaj[2], Brian Ruffell[1], Stephen L. Shiao[3], Stephen F. Madden[4], William M. Gallagher[2], Nikhil Wadhwani[1], Scott D. Keil[1], Sharfaa A. Junaid[1], Hope S. Rugo[5,6], E. Shelley Hwang[6,7], Karin Jirström[8], Brian L. West[9], and Lisa M. Coussens[1,6]

ABSTRACT Immune-regulated pathways influence multiple aspects of cancer development. In this article we demonstrate that both macrophage abundance and T-cell abundance in breast cancer represent prognostic indicators for recurrence-free and overall survival. We provide evidence that response to chemotherapy is in part regulated by these leukocytes; cytotoxic therapies induce mammary epithelial cells to produce monocyte/macrophage recruitment factors, including colony stimulating factor 1 (CSF1) and interleukin-34, which together enhance CSF1 receptor (CSF1R)–dependent macrophage infiltration. Blockade of macrophage recruitment with CSF1R-signaling antagonists, in combination with paclitaxel, improved survival of mammary tumor–bearing mice by slowing primary tumor development and reducing pulmonary metastasis. These improved aspects of mammary carcinogenesis were accompanied by decreased vessel density and appearance of antitumor immune programs fostering tumor suppression in a $CD8^+$ T-cell–dependent manner. These data provide a rationale for targeting macrophage recruitment/response pathways, notably CSF1R, in combination with cytotoxic therapy, and identification of a breast cancer population likely to benefit from this novel therapeutic approach.

SIGNIFICANCE: These findings reveal that response to chemotherapy is in part regulated by the tumor immune microenvironment and that common cytotoxic drugs induce neoplastic cells to produce monocyte/macrophage recruitment factors, which in turn enhance macrophage infiltration into mammary adenocarcinomas. Blockade of pathways mediating macrophage recruitment, in combination with chemotherapy, significantly decreases primary tumor progression, reduces metastasis, and improves survival by $CD8^+$ T-cell–dependent mechanisms, thus indicating that the immune microenvironment of tumors can be reprogrammed to instead foster antitumor immunity and improve response to cytotoxic therapy. *Cancer Discovery; 1(1); 54–67. ©2011 AACR.*

Authors' Affiliations: [1]Departments of Pathology, [3]Radiation Oncology, [5]Medicine, and [7]Surgery, and [6]Helen Diller Family Comprehensive Cancer Center, University of California, San Francisco; [2]University College Dublin School of Biomolecular and Biomedical Science, University College Dublin Conway Institute, Belfield, and [4]National Institute for Cellular Biotechnology, Dublin City University, Glasnevin, Dublin, Ireland; [8]Center for Molecular Pathology, Department of Laboratory Medicine, Lund University, Skåne University Hospital, Malmö, Sweden; and [9]Plexxikon Inc., Berkeley, California

Current affiliation for Dr. DeNardo: Department of Medicine, Washington University, St. Louis, Missouri

Note: Supplementary data for this article are available at Cancer Discovery Online (http://www.aacrjournals.org).

Corresponding Author: Lisa M. Coussens, Department of Pathology, University of California, San Francisco, 513 Parnassus Avenue, HSW450C, San Francisco, CA 94143. Phone: 415-502-6318; Fax: 415-514-0878; E-mail: Lisa.Coussens@ucsf.edu

doi: 10.1158/2159-8274.CD-10-0028

INTRODUCTION

Tumor-associated macrophages (TAM) have been identified as regulators of solid tumor development based on their capacity to enhance angiogenic, invasive, and metastatic programming of neoplastic tissue (1, 2). Colony stimulating factor-1 (CSF1) is a key cytokine involved in recruitment and activation of tissue macrophages, exerting these effects through binding to a high-affinity receptor tyrosine kinase, the cFMS/CSF1 receptor (CSF1R; ref. 3). A second CSF1R ligand, interleukin 34 (IL-34), possesses similar binding affinities and regulates macrophage recruitment to tissues, but exhibits distinct tissue distribution characteristics (4).

Macrophage presence in several types of human cancer, including breast, ovarian, non–small cell lung cancer, and Hodgkin's lymphoma, correlates not only with increased vascular density but also a worse clinical outcome (1, 5, 6). Accordingly, a CSF1-response gene signature was identified in human breast cancer that predicts risk of recurrence and metastasis, and is similarly predictive for clinical outcome in colon cancer and leiomyosarcoma (7–9). On the basis of these findings, it seems reasonable to postulate that blockade of the molecular programs enhancing macrophage recruitment or protumor bioactivity in tumors may represent tractable targets for anticancer therapy. Accordingly, genetic or pharmacologic blockade of CSF1 or its receptor has been reported to decrease macrophage presence in tissues and in some experimental solid tumors, correlating with diminished tumor angiogenesis, reduced primary tumor growth, and pulmonary metastasis (1, 2).

Experimental studies have recently revealed that B and T lymphocytes can exert protumor activity indirectly by regulating the bioactivity of myeloid cells, including macrophages, monocytes, and mast cells, resulting in resistance to endocrine therapies and development of metastasis (10–13). We reported that in the absence of a significant $CD8^+$ CTL response, $CD4^+$ T-effector lymphocytes potentiate mammary adenocarcinoma metastasis by directly enhancing the protumor bioactivity of TAMs (11). On the basis of these results, we hypothesized that human breast cancers containing leukocytic infiltrates dominated by $CD4^+$ T lymphocytes and $CD68^+$ macrophages, without significant $CD8^+$ T-cell infiltration, would have a higher relative risk for metastasis and therefore reduced overall survival (OS) of patients. In this article, we report on an immune signature consisting of $CD68^{high}/CD4^{high}/CD8^{low}$ that significantly correlates with reduced OS for patients with breast cancer. Moreover, to demonstrate the biologic significance of this signature, we investigated a combination of standard-of-care chemotherapy and agents that block TAM infiltration of mammary tumors in an aggressive transgenic mouse model of mammary adenocarcinoma development [MMTV–polyoma middle T (PyMT) mice; ref. 14], in which late-stage carcinogenesis and pulmonary metastasis are regulated by CSF1 and tissue macrophages (15). We found that when TAM presence in mammary adenocarcinomas was minimized, antitumor immunity and $CD8^+$ CTL infiltration were enhanced; together, this improved chemosensitivity and resulted in reduced primary tumor development, significant decrease in pulmonary metastases, and improved OS, when compared with treatment using standard chemotherapy alone.

RESULTS

Single Immune Marker Analysis of Leukocyte Infiltration Predicts Breast Cancer Survival

In previous studies, we demonstrated that in the absence of a significant $CD8^+$ CTL response, $CD4^+$ T lymphocytes indirectly promoted invasion and metastasis of mammary adenocarcinomas by directly regulating the protumor bioactivities of TAMs (11). From these data, we predicted that infiltration of primary human breast cancer by $CD4^+$ and $CD8^+$ T lymphocytes and $CD68^+$ macrophages would correlate with aspects of breast cancer regulating OS. To address this issue, we analyzed $CD4^+$, $CD8^+$, and $CD68^+$ leukocyte density in tissue microarrays consisting of tumor tissue obtained at the time of primary surgery from 179 treatment-naïve breast cancer patients (Fig. 1A). We employed a fully automated nuclear algorithm to quantify $CD4^+$, $CD8^+$, and $CD68^+$ cells following immunohistochemical (IHC) detection. For survival analyses, high and low thresholds for each marker were established using a classification and regression decision tree analysis with 10-fold cross-validation (16). Kaplan-Meier analyses indicated that, as single variables, "high" $CD4^+$ T-cell density ($P = 0.032$) and "low" $CD8^+$ T-cell density ($P = 0.012$) correlated with reduced OS, whereas $CD68^+$ cell density alone showed no statistical significance (Fig. 1B). However, analysis of $CD68^+$ and $CD8^+$ immune cell infiltration demonstrated an inverse association between stromal infiltration by $CD68^+$ macrophages and $CD8^+$ T lymphocytes in human breast cancer tissues (Spearman's rho, −0.38; $P < 0.001$; Supplementary Table S1).

Three-Marker Immune Signature Is Prognostic for Breast Cancer Survival

Heterotypic interactions between diverse leukocyte populations often determine the outcome of immune responses in tissues (17). As such, we proposed that combined analysis of CD4, CD8, and CD68 would allow for improved prognostic stratification of breast cancer patients by assessing both antitumor immunity (i.e., $CD8^+$ density) and protumor immunity (i.e., high $CD4^+$ and $CD68^+$ leukocyte density). Thus, we predicted that an immune profile characterized by $CD68^{low}/CD4^{low}/CD8^{high}$ would represent primary breast cancer controlled by local resection, with improved OS and relapse-free survival (RFS). In contrast, an immune response characterized by $CD68^{high}/CD4^{high}/CD8^{low}$ would instead represent a population of patients at risk for distant metastasis and thus reduced OS. A classification and regression tree algorithm was used to define the signature in the screening cohort (Cohort I, $n = 179$; Supplementary Fig. S1). High and low thresholds for each marker were established by decision tree analysis with 10-fold cross-validation

Figure 1. CD68/CD4/CD8 immune signature is an independent prognostic indicator of breast cancer survival. **A**, high-magnification images (40×; 80× for inlays) of human breast cancer tissue sections showing immunoreactivity for representative CD68⁺, CD4⁺, and CD8⁺ leukocyte infiltration. **B**, automated analysis of CD68⁺, CD4⁺, and CD8⁺ immune cell detection, revealing relationship between leukocyte density and OS. Kaplan-Meier estimate of OS comparing autoscore leukocyte high- and low-infiltration groups is shown; 179 samples from Cohort I were used for analyses, and log-rank (Mantel-Cox) *P* values are denoted for difference in OS. **C** and **D**, Kaplan-Meier estimate of RFS, comparing CD68^{high}/CD4^{high}/CD8^{low} and CD68^{low}/CD4^{low}/CD8^{high} immune profiles as assigned by random forest clustering to identify optimal thresholds using Cohort I (**C**). Identified CD68^{high}/CD4^{high}/CD8^{low} and CD68^{low}/CD4^{low}/CD8^{high} immune profiles were used to stratify a second independent cohort, Cohort II (**D**). Cohort I (n = 179) and Cohort II (n = 498) samples were assessed, and the log-rank (Mantel-Cox) *P* value is denoted for difference in RFS. **E** and **F**, results from multivariate Cox regression analysis of RFS for the CD68/CD4/CD8 signature in Cohort I (**E**) and Cohort II (**F**). Hazard ratios (HR) and *P* values are shown for all characteristics. **G** and **H**, RFS in node-positive breast cancer predicted by CD68/CD4/CD8 immune signature. Kaplan-Meier estimates of RFS comparing CD68^{high}/CD4^{high}/CD8^{low} and CD68^{low}/CD4^{low}/CD8^{high} immune profiles as assigned by random forest clustering of breast cancer tissues. breast cancers were stratified into node-negative (**G**) and node-positive (**H**) patients and analyzed for RFS. The log-rank (Mantel-Cox) *P* value is denoted for difference in RFS.

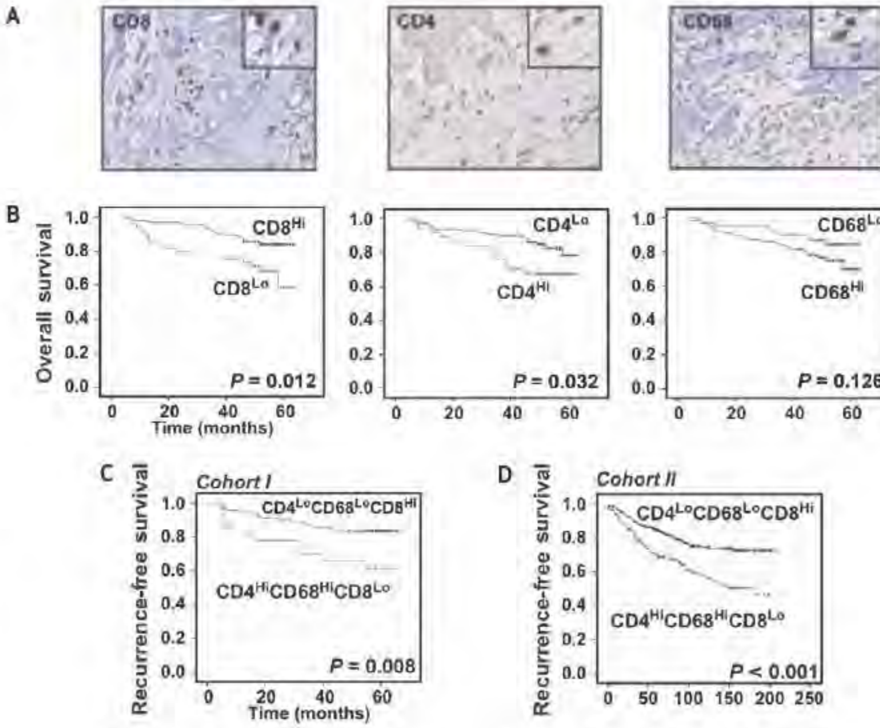

E

RFS cohort I	HR	P value
Immune signature	2.788	0.050
Grade	1.266	0.681
Nodal status	5.081	0.003
Size	1.038	0.001
Ki67	0.262	0.233
Age	1.033	0.072
ER	0.264	0.069
PR	1.349	0.637
Her2	6.170	0.001

F

RFS cohort II	HR	P value
Immune signature	2.368	0.001
Grade	2.024	0.010
Nodal status	2.724	<0.001
Size	0.998	0.748
Ki67	1.441	0.237
Age	0.998	0.784
ER	1.523	0.194
PR	0.327	<0.001
Her2	0.965	0.785

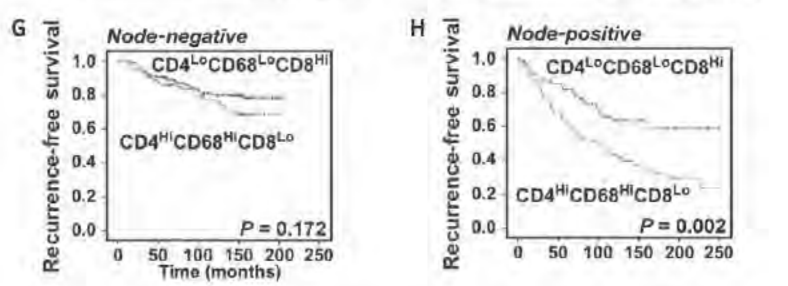

of each tree model (16). All patients were categorized as having either a CD68^{high}/CD4^{high}/CD8^{low} or a CD68^{low}/CD4^{low}/CD8^{high} immune signature, and the same thresholds were then applied to a validation cohort (Cohort II, n = 498 patients, primary tumor samples). Kaplan-Meier analysis in the 2 independent cohorts (totaling 677 patients) showed significantly reduced OS and RFS in patients whose tumors harbored the CD68^{high}/CD4^{high}/CD8^{low} signature (Fig. 1C and D; Supplementary Fig. S2A and B). Multivariate Cox regression analysis revealed that the CD68^{high}/CD4^{high}/CD8^{low} signature was an independent predictor of decreased OS and RFS after controlling for grade, nodal status, tumor size, estrogen receptor (ER), progesterone receptor (PR), HER2, and Ki-67 status in both cohorts (Fig. 1E and F; Supplementary Tables S2–S5), indicating that the immune signature predicted OS independently of established histopathologic parameters.

Three-Marker Immune Signature Is an Independent Predictor of RFS in Node-Positive Patients

The OS of breast cancer patients is greatly reduced if metastasis to regional or draining lymph nodes is present at the time of primary tumor detection. Therefore, node-positive patients require aggressive treatment with neoadjuvant or adjuvant systemic chemotherapy, or targeted therapies such as anti-estrogens or trastuzumab. To assess whether immune infiltration by macrophages and T lymphocytes affected the survival of this high-risk group, we examined the impact of the CD68/CD4/CD8 signature following stratification for nodal status. Whereas the CD68/CD4/CD8 signature was not predictive in node-negative patients (Fig. 1G), Kaplan-Meier analysis of Cohort II demonstrated significantly reduced RFS in node-positive patients whose tumors harbored the CD68^{high}/CD4^{high}/CD8^{low} signature

(Fig. 1H). Multivariate Cox regression analysis revealed that the CD68^{high}/CD4^{high}/CD8^{low} signature was an independent predictor of decreased RFS after controlling for grade, tumor size, ER, PR, HER2, and Ki-67 status (Supplementary Table S6), indicating that the immune signature predicts RFS independently of established histopathologic parameters. Thus, tumor infiltration by macrophages and T lymphocytes may influence breast cancer recurrence in lymph node–positive patients, a group often aggressively treated with neoadjuvant and adjuvant chemotherapy.

Cytotoxic Therapies Induce TAM Recruitment and CSF1 and IL-34 Cytokine Expression

These findings led us to hypothesize that blocking TAM infiltration in breast cancer patients bearing the CD68^{high}/CD4^{high}/CD8^{low} signature might enhance antitumor T-cell responses and facilitate CD8$^+$ CTL infiltration and/or repolarization of CD4$^+$ T-cell responses toward T-helper 1 cell (T_H1). Consistent with this hypothesis, we found an inverse association between stromal infiltration by CD68$^+$ macrophages and CD8$^+$ T lymphocytes in human breast cancer tissues (Spearman's rho, –0.38; $P < 0.001$; Supplementary Table S1). On the basis of this observation, we postulated that chemosensitivity might in part be regulated by TAM and/or CD8$^+$ T-cell presence in breast cancer tissue. To address this, we initially evaluated leukocyte infiltration in a small cohort of freshly isolated breast tumors from women who had received neoadjuvant chemotherapy, compared with those undergoing primary surgery without preoperative treatment (Supplementary Table S7). We found a higher percentage of CD45$^+$CD11b$^+$CD14$^+$ macrophages in breast cancer from women who had received neoadjuvant chemotherapy than in tumors from women treated with surgery alone (Fig. 2A). In contrast, we observed no difference in tumor-infiltrating CD45$^+$CD3$^+$CD8$^+$ T lymphocytes between the 2 groups (Supplementary Fig. S3A).

To determine whether TAM presence in breast cancers was directly enhanced by chemotherapy, we evaluated leukocyte responses in MMTV-PyMT mice, a transgenic mouse model of mammary carcinogenesis, following treatment with paclitaxel (PTX; Supplementary Fig. S4). We found that infiltration of mammary tumors by CD45$^+$CD11b$^+$Ly6C^{low}Ly6G$^-$F4/80$^+$ TAMs was significantly increased following PTX treatment, with no significant change in the presence of CD3$^+$CD8$^+$ T lymphocytes (Fig. 2B; Supplementary Fig. S3B). Similar PTX-induced TAM recruitment was observed in syngeneic orthotopic PyMT-derived tumors (Supplementary Fig. S3C). Consistent with our hypothesis, PTX treatment of MMTV-PyMT mice only modestly slowed primary tumor growth (Fig. 2B). For studies herein, we defined TAMs as CD45$^+$CD11b$^+$Ly6G$^-$Ly6C^{low}F4/80$^+$, monocytic immature myeloid cells (iMC) as CD45$^+$CD11b$^+$Ly6G$^-$Ly6C^{high}, and granulocytic iMCs/neutrophils as CD45$^+$CD11b$^+$Ly6G^{high}Ly6C$^+$ (Supplementary Fig. S5A and B), in agreement with previously published studies (18, 19).

To reveal molecular mediators involved in regulating PTX-induced TAM recruitment, we examined mRNA expression of several monocyte/macrophage cytokines and chemokines in murine mammary epithelial carcinoma cells (MEC) following exposure to several forms of cytotoxic therapy *in vitro*. *CSF1, CCL8/MCP2,* and *IL34* mRNAs were increased in MMTV-PyMT–derived MECs following exposure to PTX (Fig. 2C). Of these, *CSF1* and *IL34* mRNAs were also increased following exposure to either CDDP or ionizing radiation (Fig. 2D; Supplementary Fig. S3D). Increased mRNA expression was not merely a response of malignant PyMT-derived MECs (pMEC), because a similar induction was also observed in nontransgenic MECs exposed to PTX in culture (Fig. S3E). Similarly, *CSF1* mRNA expression was also induced by PTX and CDDP in 5 of 6 human breast cancer cell lines reflecting the major subtypes of breast cancer (Fig. 2E). *In vivo, CSF1* mRNA was increased in mammary tissue of MMTV-PyMT mice following treatment with either PTX or ionizing radiation (Fig. 2F; Supplementary Fig. S3F). Together, these data indicate that induction of *CSF1* (and *IL34*) mRNA and subsequent TAM recruitment into mammary tissue represent a common response of MECs to cytotoxic agents.

Blockade of Chemotherapy-Induced TAM Recruitment

To determine whether tumor-infiltrating TAMs also regulate sensitivity of MECs to cytotoxic therapy, we blocked TAM infiltration *in vivo* with immunologic and pharmacologic agents (Supplementary Fig. S4) and evaluated myeloid cell infiltration of tumors from treated mice (Supplementary Fig. S5). Mice bearing orthotopic mammary tumors were treated with neutralizing monoclonal antibodies (mAb) CSF1 (clone 5S1) or CD11b (clone M1/70), or a competitive ATP inhibitor with potent (nM) specificity for CSF1 and cKIT receptor tyrosine kinases (PLX3397), either as a monotherapy or in combination with PTX. CD11b is an integrin cell adhesion molecule expressed on granulocytes, macrophages, monocytes, dendritic cells (DC), and natural killer cells that in part regulates transendothelial migration of cells into tissue and tumor parenchyma. PLX3397 has 10- to 100-fold selectivity for cKIT and CSF1R, as opposed to other related kinases, such as KDR (see Supplementary Fig. S6A and Methods; ref. 20).

Fluorescence-activated cell sorting analysis of the predominant myeloid subtypes infiltrating mammary tumors revealed that either as monotherapy, or in combination with PTX, CD45$^+$CD11b$^+$Ly6C$^-$Ly6G$^-$F4/80$^+$ TAM recruitment was significantly diminished following treatment with either αCSF1 mAb or PLX3397, with no effect on infiltration of CD45$^+$CD11b$^+$LY6G^{high} iMCs or CD45$^+$CD11b$^{low/-}$Ly6C$^-$CD22$^-$Ly6G$^-$CD11c^{high}MHCII^{high} DCs (Fig. 3A and B; Supplementary Fig. S5A and B). Treatment with aCD11b mAb decreased both TAM and iMC infiltration (Fig. 3A). Analysis of the maturation and differentiation status of TAMs remaining in mammary tumor tissue following αCSF1 or PLX3397 treatment revealed no significant change in CD11b, CD11c, F4/80, CD45, or MHCII expression (Supplementary Fig. S5B). However, examination of mammary tumor sections revealed a population of perivascular CSF1-independent F4/80$^+$ TAMs remaining (Fig. 3C). Blockade of TAM recruitment was a direct effect of CSF1/CSF1R blockade: *In vitro* CSF1R inhibition efficiently blocked CD11b$^+$ monocyte chemotaxis in response to control or PTX-treated pMEC–conditioned medium, with no effect on chemotaxis of CD3$^+$ T lymphocytes (Fig. 3D; Supplementary Fig. S3G). These results were mirrored *in vivo*; treatment of late-stage MMTV-PyMT mice with PLX3397 significantly inhibited both steady-state and PTX-induced tumor infiltration by CD45$^+$CD11b$^+$Ly6C$^-$Ly6G$^-$F4/80$^+$ TAMs (Fig. 3E; Supplementary Fig. S5) without altering TAM maturation/differentiation (Supplementary Fig. S6B).

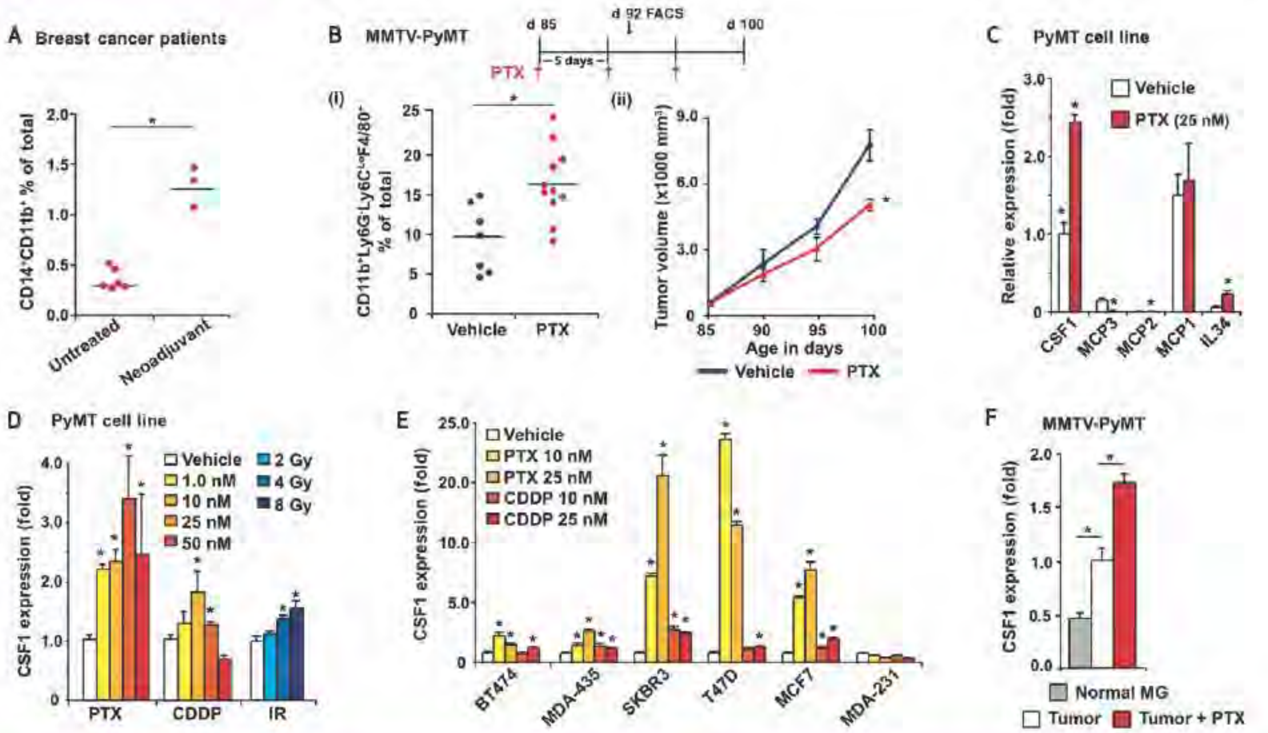

Figure 2. Cytotoxic therapy induces macrophage recruitment, as well as *CSF1* and *IL-34* mRNA expression. **A,** macrophage percentage in fresh human primary breast cancer tissues, depicted as mean of $CD45^+CD11b^+CD14^+$ macrophages as a percentage of total cells (analyzed by flow cytometry). "Neo-adjuvant" denotes patients who received chemotherapy prior to surgical resection of their primary breast cancer, as opposed to those who did not, denoted as "untreated"; *, statistically significant differences ($P = 0.004$) between the 2 groups. **B,** PTX-induced *CSF1* mRNA expression regulates tumor infiltration of macrophages and limits PTX response. (i), TAM percentage in mammary tumors of MMTV-PyMT mice following PTX treatment with mean number of $CD45^+Ly6G^-Ly6C^-CD11b^+F4/80^+$ TAMs as a percentage of total cells shown (analyzed by flow cytometry); (ii), primary tumor growth reduced by treatment with PTX. The 85-day-old MMTV-PyMT mice were treated with PTX and total tumor burden per animal was assessed every 5 days until endpoint. Treatment schematic is depicted at top, and data are displayed as mean tumor burden ±SEM; *, statistically significant differences between controls and PTX-treated mice (>8 mice/group). **C,** expression of monocyte/macrophage chemoattractants following chemotherapy. Quantitative reverse transcriptase PCR (qRT-PCR) analyses of *CSF1, MCP1, MCP2, MCP3,* and *IL34* expression in MMTV-pMECs–derived MECs treated with PTX for 24 hours ex vivo, expressed as mean fold change, compared with controls. Samples were assayed in triplicate for each tested condition; *, statistically significant differences between control and PTX-treated groups. **D,** Dose-dependent expression of *CSF1* following chemotherapy or radiation therapy. qRT-PCR analysis of mRNA expression in MMTV-PyMT–derived pMECs 24 hours after treatment with either cisplatin (CDDP), PTX, or a single dose of ionizing radiation, expressed as mean fold change, compared with control ±SEM. Drug and radiation doses are shown. Samples were assayed in triplicate for each tested condition; *, statistically significant differences between control and the indicated treatment. **E,** *CSF1* expression induced by chemotherapy in human breast carcinoma cell lines. qRT-PCR analysis of mRNA expression in BT474, MDA-MB-435, SKBR3, T47D, MCF7, and MDA-MB-231 at 24 hours after treatment with either CDDP or PTX, expressed as mean fold change, compared with vehicle-treated cells ±SEM. Chemotherapeutic doses are denoted. Samples were assayed in triplicate for each condition; *, statistically significant differences between control and indicated treatment. **F,** *CSF1* expression induced by cytotoxic therapy in MMTV-PyMT mammary tumors. qRT-PCR analysis of mRNA expression isolated from normal mammary tissue or MMTV-PyMT mammary tumors from mice treated with either PTX (10 mg/kg) every 5 days, or ionizing radiation (single dose of 8 Gy), expressed as mean fold change, compared with vehicle-treated tumors (4 mice/group). SE is depicted; *, statistically significant differences ($P < 0.05$, Mann-Whitney) for all gene expression analyses (**C–F**).

We next treated 80-day-old MMTV-PyMT mice, or mice bearing syngeneic orthotopic PyMT-derived tumors (~1.0 cm) with αCSF1, αCD11b, or PLX3397 (vs controls) for 5 days, followed by 4 cycles of PTX (10 mg/kg, i.v.; Supplementary Fig. S4). Primary tumor burden at study endpoints (2.0 cm primary tumors or 100 days of age) was significantly reduced in mice treated with combined αCSF1/PTX, αCD11b/PTX, or PLX3397/PTX therapy, compared to mice treated with these as single agents (Fig. 4A and B; Supplementary Fig. S7A). Similar results were observed in syngeneic mice bearing orthotopic PyMT-derived mammary tumors receiving combined PLX3397/carboplatin (CBDCA) therapy (Fig. 4B).

Mammary tumors in MMTV-PyMT mice progress through well-defined stages of cancer development, similar to progression of breast cancer in women, including tissue with florid ductal hyperplasia, ductal carcinoma *in situ* with early stromal invasion, and poorly differentiated invasive ductal carcinoma (15, 21). Using this staging criterion, we observed that mammary tumors arising in MMTV-PyMT mice treated with combined PLX3397/PTX therapy exhibited decreased development of late-stage carcinoma, compared with tumors in age-matched mice treated with either PTX or PLX3397 as monotherapy (Fig. 4C; Supplementary Fig. S7B). Moreover, the late-stage carcinomas that did develop in PLX3397/PTX-treated mice contained large areas of necrosis (Supplementary Fig. S7C) characterized by increased presence of apoptotic cells, as measured by cleaved caspase 3-positivity (Fig. 4D) with no accompanying change in epithelial proliferation (Supplementary Fig. S7D).

Decreased Vascular Density Accompanies Improved Chemosensitivity

It is known that TAMs provide VEGF to developing mammary tumors and thereby regulate angiogenic programming of tissue (22–24). Chemosensitivity to CDDP in MMTV-PyMT mice is in part regulated by myeloid-derived VEGF (25); thus, we sought to determine if TAM depletion altered VEGF expression and/

or density of $CD31^+$ vessels in MMTV-PyMT mice treated with PTX. Whereas total *VEGF* mRNA expression was significantly reduced by PLX3397 (Fig. 4E), this 70% reduction did not correlate with a change in vascular density (Fig. 4F). In contrast, combined PLX3397/PTX therapy resulted in a significant reduction in $CD31^+$ vessel density within mammary tumors, paralleling induction of apoptosis and necrosis (Fig. 4F).

CSF1-Signaling Blockade Enhances Antitumor Immunity and CTL Infiltration in Response to Chemotherapy

Because analysis of human breast cancer tissues revealed that high stromal TAM density inversely correlated with $CD8^+$ T-cell infiltration (Supplementary Table S1), we predicted that depletion of TAMs would enhance $CD8^+$ CTL infiltration and thereby foster an antitumor immune microenvironment. Analyses of tumor-infiltrating T lymphocytes in mice treated with αCSF1/PTX or PLX3397/PTX by flow cytometry or IHC revealed significantly increased presence of $CD4^+$ and $CD8^+$ T cells in mammary tumors (Fig. 5A and B; Supplementary Fig. S8A). Consistent with these findings, cytokine mRNA expression in mammary tissue derived from PLX3397/PTX-treated MMTV-PyMT mice revealed increased mRNA expression of cytotoxic effector molecules, including *IFN-γ*, *granzyme A*, *granzyme B*, *perforin-1*, and the type 1 DC effector molecules *IL12p35* and *IFN-α* (Fig. 5C). In contrast, expression of the immunosuppressive molecule *arginase-1* was

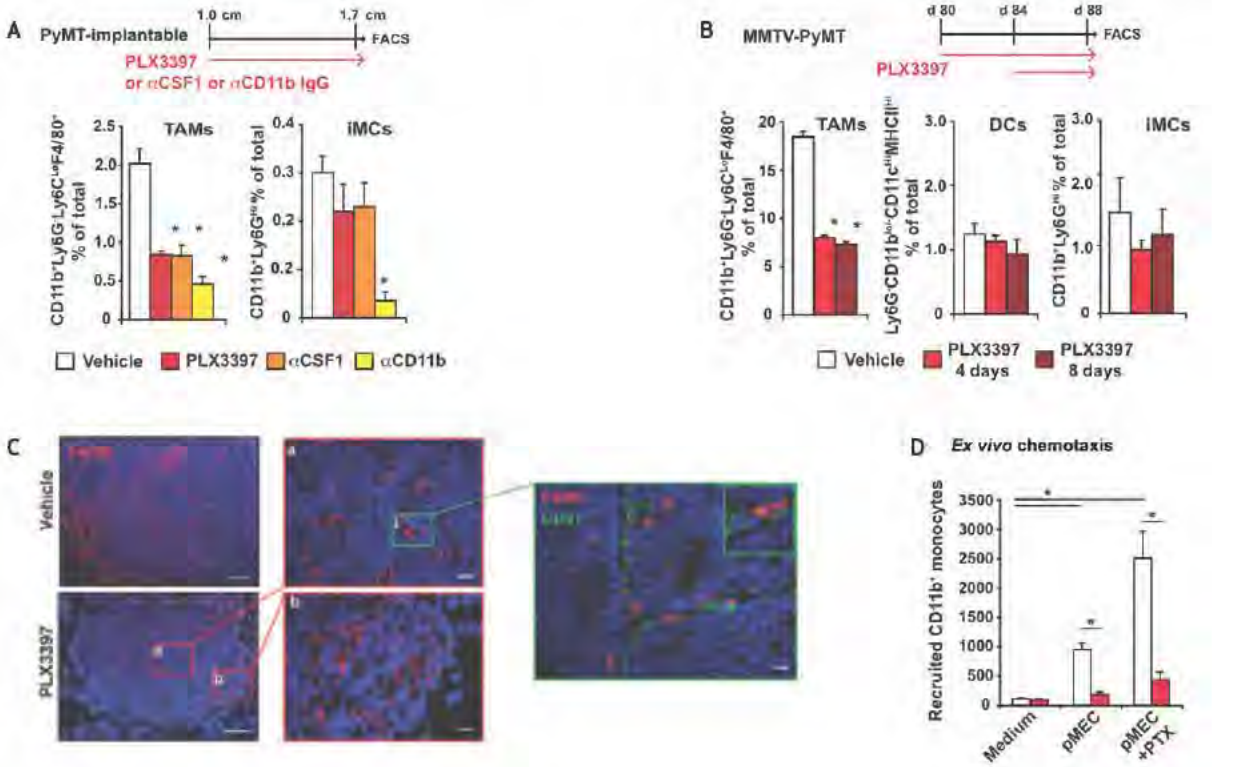

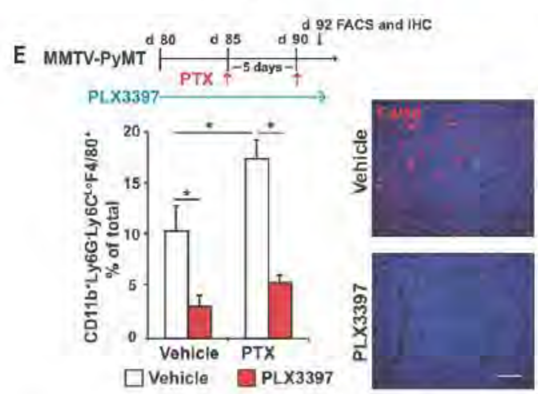

Figure 3. Cytotoxic therapy induces CSF1-dependent macrophage recruitment. **A,** analysis of TAM depletion following CSF1/CSF1R blockade. Mice bearing 1.0-cm orthotopic PyMT-derived tumors were treated either with αCSF1 or αCD11b neutralizing immunoglobulins (Ig) or with PLX3397. Treatment regimen is shown, and flow cytometric analysis of tumor-infiltrating $D45^+Ly6G^-Ly6C^{low}CD11b^+F4/80^+$ macrophages and $CD45^+CD11b^+Ly6G^{high}$ iMCs is depicted as mean percentage of total cells ±SEM. **B,** selective depletion of TAMs following CSF1R kinase blockade. MMTV-PyMT mice (either 80 or 84 days old) were treated with PLX3397 for 4 or 8 days. Treatment regimen is shown, and flow cytometric analysis of tumor-infiltrating $CD45^+Ly6G^-Ly6C^{low}CD11b^+F4/80^+$ TAMs, $CD45^+Ly6G^-Ly6C^{low}CD11b^{low/-}CD11c^{high}$MHCIIHi DCs, and $CD45^+CD11b^+$Ly6GHi iMCs in mammary tumors is depicted as mean percentage of total cells ±SEM. **C,** perivascular TAMs resisting PLX3397. Representative images of $F4/80^+$ cell staining of mammary tumors from 90-day-old MMTV-PyMT mice treated with PLX3397 (vs control) for 8 days. Insets (a and b) show F4/80 staining in tumor stroma and tumor interior; (i), costaining for F4/80 (red) and CD31 (green); scale bar, 500 μm, 100 μm (a and b); 25 μm (i). **D,** peripheral blood lymphocyte (PBL) migration in response to conditioned medium from MMTV-PyMT MECs treated with either vehicle or PTX (25 nM for 24 hours), evaluated by Boyden chamber assay. $CD45^+CD11b^+$ peripheral blood monocytes after migration to the lower chamber, in the presence or absence of PLX3397 (50 nM), as quantified by flow cytometry. Data are depicted as mean cell number assayed in triplicate. **E,** PTX-induced TAM recruitment inhibited by PLX3397. TAM density in mammary tumors removed from MMTV-PyMT mice following treatment with PTX ± PLX3397. Treatment regimen is shown with mouse age, and data are depicted as mean number of $CD45^+Ly6G^-Ly6C^-CD11b^+F4/80^+$ TAMs as a percentage of total cells ±SEM (analyzed by flow cytometry, >5 mice/group). Representative IHC staining for F4/80 (red) and nuclear DNA (blue) from the same cohort of animals is shown. Scale bar, 500 μm; *, statistically significant differences ($P < 0.05$, Mann-Whitney) in **A–E**.

decreased by PLX3397/PTX therapy (Fig. 5C). This reprogramming of the immune microenvironment was accompanied by increased tumor infiltration of CD45$^+$CD11b$^{low/-}$CD19$^-$Ly6G$^-$Ly6C^{low}CD11c^{high}MHCII^{high} DCs (Fig. 5D), indicating that combined treatment of MMTV-PyMT mice with PLX3397/PTX fostered an antitumor immune response by T lymphocytes expressing high levels of cytotoxic effector molecules.

Given these findings, we assessed the capacity of TAMs (isolated from mammary tumors of MMTV-PyMT mice) to directly repress CD8$^+$ T-cell activation *in vitro*. Using carboxyfluorescein succinimidyl ester (CFSE) dilution as a marker for T-cell proliferation, we found that CD45$^+$CD11b$^+$F4/80$^+$Ly6G$^-$Ly6C^{low} TAMs significantly repressed CD8$^+$ T-cell activation and proliferation in a dose-dependent manner (Fig. 5E) that was reflective of the altered ratio of TAMs to CD8$^+$ T cells in mammary tumors of untreated versus PLX3397/PTX-treated MMTV-PyMT mice (Fig. 5F).

One mechanism by which TAMs may suppress CD8$^+$ T cells involves expression of inhibitory B7 family members that interact with "checkpoint" receptors expressed on infiltrating CD8 T cells. In particular, growing interest has been expressed in the PD1- PDL1 ligand system, in which PDL1/B7-H1 expression by TAMs represents a major source of the inhibitory PD1 ligand. Thus, we evaluated TAMs isolated from mammary tumors for expression of PDL1/B7-H1 and PDL2/B7-DC, as well as costimulatory molecules CD80 and CD86, and MHCII. TAMs expressed high levels of MHCII and B7-H1, but relatively lower levels of CD80 and CD86, indicating a possible role in inducing tolerance/anergy in tumor antigen-specific CD4$^+$ and CD8$^+$ T lymphocytes (Supplementary Fig. S5C).

Macrophage Depletion Enhances Chemotherapeutic Response in a CD8$^+$ CTL-Dependent Manner

To determine whether increased chemosensitivity of mammary tumors in PLX3397/PTX-treated mice was dependent on enhanced CD8$^+$ T-cell response, we depleted CD8$^+$ T cells from late-stage MMTV-PyMT mice treated with PTX or PLX3397 or both. Findings from this study revealed that the improved outcome with enhanced chemosensitivity resulting

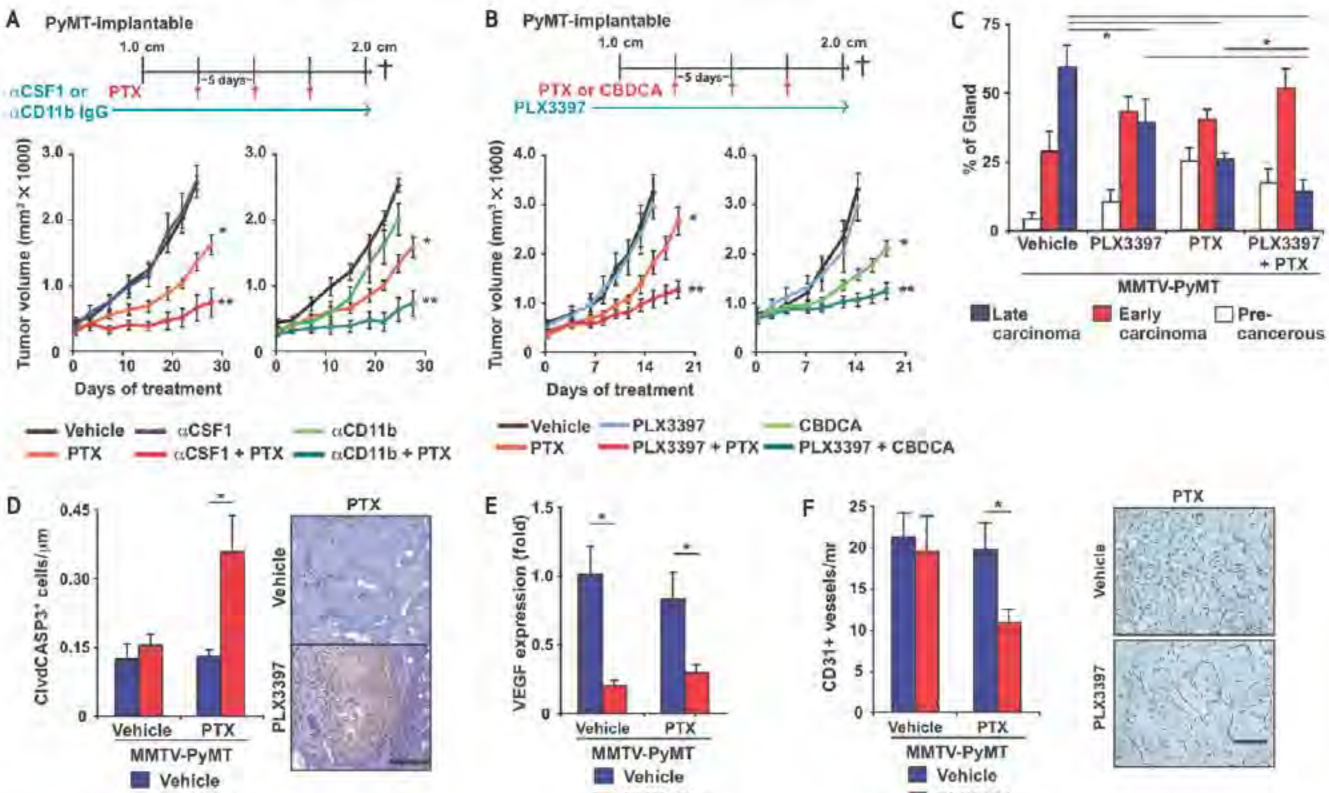

Figure 4. Macrophage depletion improves response to chemotherapy. **A** and **B**, primary tumor growth reduced by treatment with macrophage-depleting agents in combination with chemotherapy. Orthotopic PyMT-derived tumors were grown to a median diameter of 1.0 cm, and mice were then treated with PTX, CBDCA, and/or αCSF1, αCD11b neutralizing Igs ± PLX3397 for 21 or 28 days, with total tumor burden per animal assessed every 2 to 3 days. Treatment regimens are depicted for all cohorts, and data displayed as mean tumor burden ±SEM; *, statistically significant differences between vehicle- and PTX-treated mice. **, significant differences between mice treated with PTX alone and mice treated with PTX/PLX3397 or αCSF1 or αCD11b in combination. **C**, histologic stage analysis of MMTV-PyMT tumors. Tumors from 100-day-old MMTV-PyMT mice treated with PTX or PLX3397 or both were assessed for the presence of premalignant tissue and early- and late-stage carcinoma; data expressed as mean percentage of total gland area ±SEM. **D**, quantification of cleaved caspase-3-positive cells in mammary tumors of MMTV-PyMT mice treated with PTX or PLX3397 or both versus control (vehicle). Graph depicts mean positive cells per μm^2 of tumor tissue. Representative images show cleaved caspase-3-positive cells (brown staining) in tumors of MMTV-PyMT mice; scale bar, 500 μm. **E**, *VEGF* mRNA expression assessed by qRT-PCR of tumor tissue from MMTV-PyMT mice treated with vehicle or PTX or PLX3397 or both. Graph depicts mean fold change in gene expression compared with vehicle-treated control group. **F**, quantification of CD31$^-$ positive vessels in mammary tumors from MMTV-PyMT mice treated with PTX or PLX3397 or both, versus control (vehicle). Data represent the mean number of CD31$^+$ positive vessels per mm^2 of carcinoma tissue. Representative photomicrographs show CD31-positive vessels (brown staining); scale bar, 400 μm; *, statistically significant differences ($P < 0.05$, Mann-Whitney) in **C–F**.

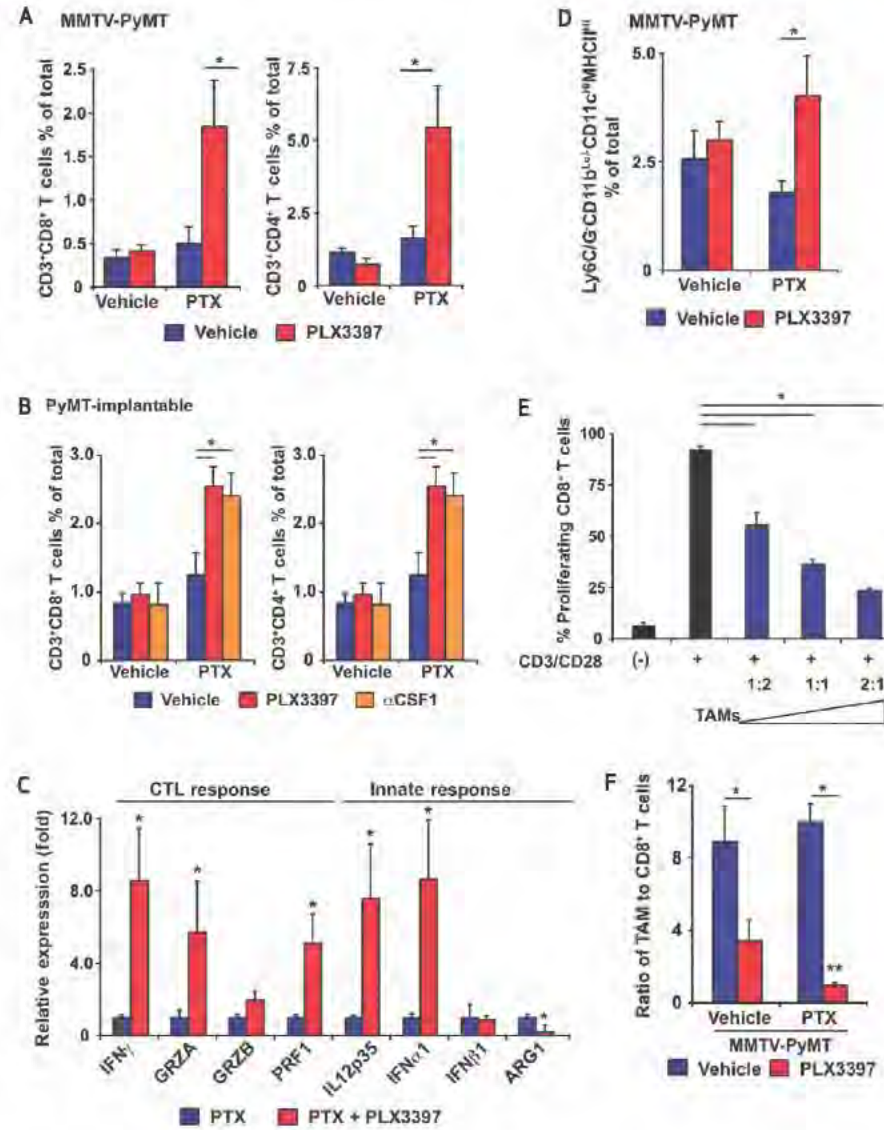

Figure 5. PTX in combination with PLX397 induces antitumor T-cell response. **A** and **B**, tumor infiltration by T lymphocytes enhanced by combined PTX and CSF1 or CSF1R blockade. Flow cytometric analyses of tumor infiltrating $CD3^+CD8^+$ and $CD3^+CD4^+$ T lymphocytes depicted as the mean number of positive cells, assessed as a percentage of total cells following treatment of MMTV-PyMT mice with PTX or PLX3397 or both (**A**), or treatment of mice having orthotopic PyMT-derived tumors with combined PTX/αCSF1 or PTX/PLX3397 (**B**), compared with controls. Mean values ±SEM are depicted. **C**, cytokine mRNA expression assessed in orthotopic PyMT-derived tumors from mice treated with PTX alone or in combination with PLX3397. Graph depicts mean fold change in mRNA expression compared with PTX treatment group (5 animals/group). SEM is depicted. **D**, tumor infiltration by DCs enhanced by combined PTX/PLX3397. Flow cytometric analysis of tumor-infiltrating $CD45^+Ly6G^-Ly6C^{low}CD11b^{low/-}CD11c^{high}MHCII^{high}$ DCs depicted as mean percentage of positive cells as a percentage of total cells from MMTV-PyMT mice treated with PTX or PLX3397 or both, versus controls. **E**, $CD8^+$ T-lymphocyte activation repressed by TAMs. Purified T cells were loaded with CFSE and activated *in vitro* by plate-bound CD3/28 and cocultured with the indicated ratio of $CD45^+Ly6G^-Ly6C^{Low}CD11b^+F4/80^+$ TAMs isolated from late-stage mammary tumors of MMTV-PyMT mice. Data are depicted as the percentage of live $CD8^+$ T lymphocytes exhibiting CFSE dilution after 60 hours. Data are representative of 2 independent experiments run in triplicate. Error bars represent SEM. **F**, analysis of the ratio of tumor-infiltrating $CD45^+Ly6G^-Ly6C^{low}CD11b^+F4/80^+$ TAMs to $CD3^+CD8^+$ T lymphocytes depicted as mean ratio (TAM/CD8 CTL) ±SEM from MMTV-PyMT mice treated with vehicle or with PTX and/or PLX3397. *, statistically significant differences ($P < 0.05$, Mann-Whitney) in **A**–**F**. **, statistically significant differences ($P < 0.05$, Mann-Whitney) between PLX3397-treated groups in **F**.

from combined PLX3397/PTX therapy was indeed a $CD8^+$ T-cell–dependent response (Fig. 6A and B; Supplementary Fig. S8B). We found that CD8 depletion also resulted in increased tumor grade and decreased presence of cleaved caspase-3–positive cells in mice that had received combined PLX3397/PTX therapy (Fig. 6C and D). Taken together, these data indicate that the enhanced cytotoxic response elicited by CSF1R-signaling blockade was $CD8^+$ T-cell–dependent.

Combined Macrophage Depletion and Chemotherapy Blocks Metastasis in a CD8-Dependent Manner

Long-term survival of breast cancer patients is often limited by disseminated metastases following surgical resection of primary tumors. Analysis of leukocyte profiles in human breast cancers demonstrated that OS, and thus presumably metastatic spread, were regulated by the spectrum of tumor-infiltrating T lymphocytes and macrophages present. In MMTV-PyMT mice, although neither CSF1R-signaling blockade nor PTX therapy alone inhibited development of pulmonary metastasis, mice receiving combined PLX3397/PTX exhibited >85% reduction in pulmonary metastases that was in part $CD8^+$ T-cell–dependent (Fig. 6E).

Macrophages and CD8 Infiltration Predicts Survival and Chemotherapeutic Response

Overall, our data indicated that in the absence of TAMs, antitumor $CD8^+$ CTLs bolster response to chemotherapy and thereby influence outcome; thus, we predicted that TAM and CD8 T-cell ratios would correlate with pathologic responses in patients with breast cancer. Accordingly, we analyzed *CD68* and *CD8a* mRNA expression in a cohort of 311 patients constructed from 2 independent datasets (26, 27). All patients provided fine-needle aspirates (FNA) prior to neoadjuvant chemotherapy, and pathologic response was assessed at the time of definitive surgery. *CD8* mRNA expression in FNA samples correlated with pathologic complete response (pCR; $R = 0.216$; $P < 0.001$); however, CD68 did not. With median expression as a threshold, examination of both *CD8* and *CD68* mRNA revealed 3 groups—CD68 > CD8, CD68 < CD8, and CD68 = CD8 (denoted $CD68^{high}/CD8^{low}$, $CD68^{low}/CD8^{high}$, and CD68/

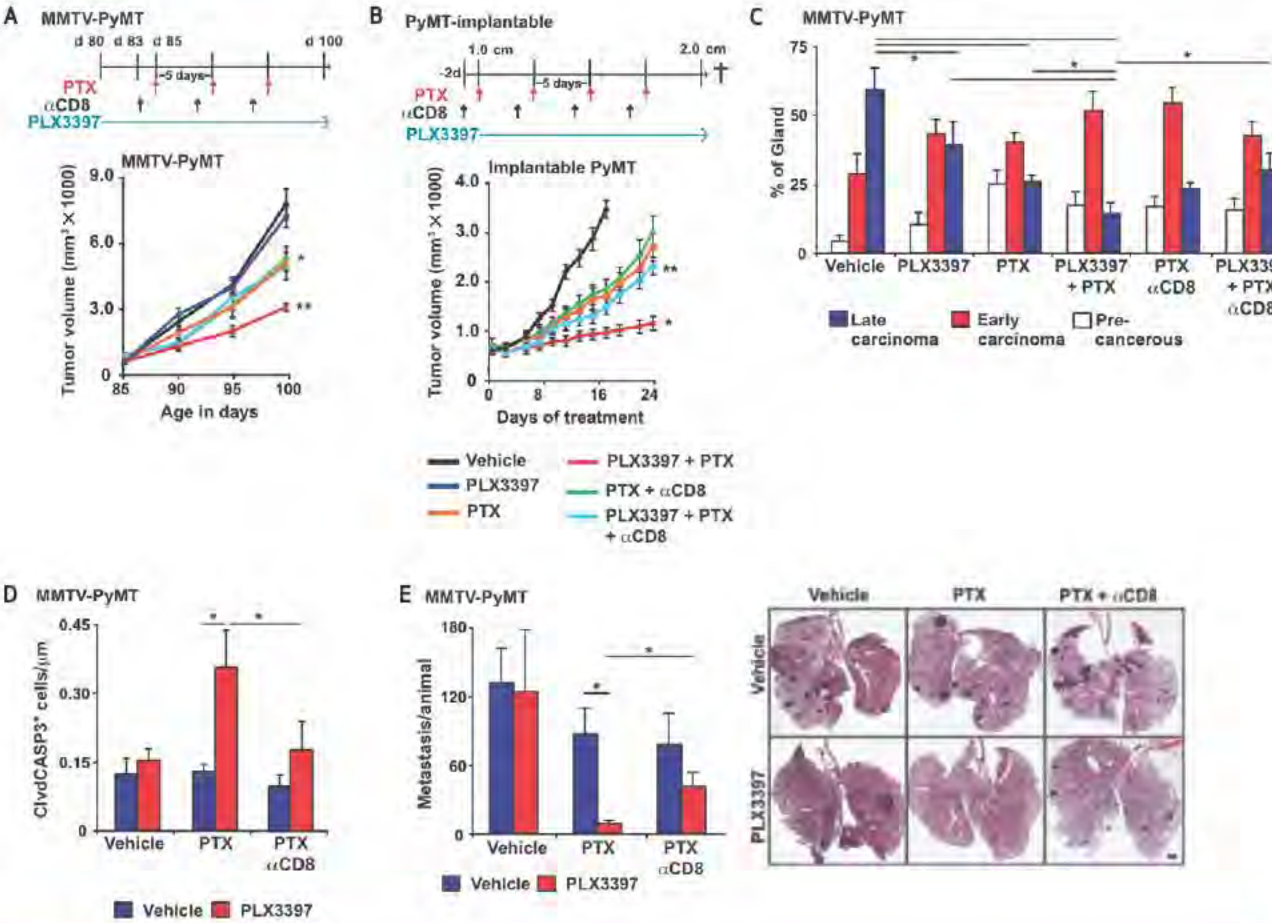

Figure 6. Combined PLX3397 and PTX treatment inhibits metastasis in a CD8-dependent manner. **A** and **B**, improved outcome following PLX3397/PTX treatment dependent on $CD8^+$ T cells. **A**, 85-day-old MMTV-PyMT mice were treated with PTX or PLX3397 or both, as well as anti-CD8 IgG. Total tumor burden per animal was assessed every 5 days. **B**, orthotopic PyMT-derived tumors were grown to a median diameter of 1.0 cm, at which time mice were treated with PTX or PLX3397 or both in combination with anti-CD8 or control IgG for 21 days, and total tumor burden per animal was assessed every 2 to 3 days. Treatment regimens are depicted along with SEM; *, statistically significant differences between mice treated with PTX alone and those treated with PLX3397/PTX. **, significant differences between mice treated with PLX3397/PTX and those treated with anti-CD8 and PTX/PLX3397/control IgG. **C**, histologic stage analysis of MMTV-PyMT tumors. Tumors from 100-day-old MMTV-PyMT mice treated with anti-CD8 IgG or with PTX and/or PLX3397 were assessed for presence of premalignant tissue and early- and late-stage carcinoma; data expressed as mean percentage of total gland area ±SEM. **D**, quantification of cleaved caspase-3–positive cells in mammary tumors of MMTV-PyMT mice treated with anti-CD8 IgG or with PTX and/or PLX3397 versus control (vehicle). Graph depicts mean positive cells per μm^2 of tumor tissue. **E**, quantification of metastatic foci per lung section per mouse from 100-day-old MMTV-PyMT mice treated with PTX and/or PLX3397 and/or anti-CD8 IgG, versus controls. Each lung was serially sectioned, 6 sections 100 µm apart were stained with hematoxylin and eosin (H&E), and the total number of metastatic foci (>8 cells) was quantified per mouse ($n \geq 10$ mice per cohort). SEM is depicted. *, Statistically significant differences ($P < 0.05$, Mann-Whitney). Representative photomicrographs of lung tissue sections reveal metastatic foci from 100-day-old MMTV-PyMT mice treated with vehicle or with PTX and/or PLX3397. Scale bar, 500 µm.

$CD8^{equal}$, respectively)—with the $CD68^{high}/CD8^{low}$ group correlating with a significantly lower rate of pCR (7%) and the $CD68^{low}/CD8^{high}$ exhibiting the highest rate of pCR at 27% (Fig. 7A). Thus, the ratio of *CD68/CD8a* expression represents a predictive response biomarker for neoadjuvant chemotherapy.

We next evaluated *CD68* and *CD8a* mRNA expression in breast cancers representing ~4000 patients assembled from 22 retrospective gene expression datasets (Supplementary Table S8). Median expression for both *CD8* and *CD68* was used to determine high and low groups. All patients were categorized as either $CD68^{high}/CD8^{low}$ or $CD68^{low}/CD8^{high}$. Kaplan-Meier estimates of survival demonstrated significantly reduced OS in the $CD68^{high}/CD8^{low}$ group (Fig. 7B). Not surprisingly, these gene expression results were validated using Kaplan-Meier analysis of OS on IHC data from Cohort I and II stratified for $CD68^{high}/CD8^{low}$ or $CD68^{low}/CD8^{high}$ (Supplementary Fig. S9A and B).

Because breast cancer represents a spectrum of distinct molecular subtypes (luminal A, luminal B, HER2-positive, basal type/triple negative), possessing distinct histopathologic and molecular features and correlating with differential responses to therapy and outcome (28–30), we evaluated *CD68/CD8* expression within breast cancer subtypes. $CD68^{high}/CD8^{low}$ expression correlated with reduced OS for breast cancer patients whose tumors were classified as either basal or HER2-positive (Fig. 7C; Supplementary Fig. S10).

DISCUSSION

The immune microenvironment in which a tumor evolves influences multiple parameters of the tumorigenic process. In this article we demonstrate that the immune microenvironment in breast cancer is a predictor of RFS and OS. Moreover, we provide evidence that response to chemotherapy is in part regulated by the immune microenvironment and that cytotoxic therapies induce neoplastic cells to produce monocyte/macrophage recruitment factors, including CSF1 and IL-34, which in turn enhance CSF1R-dependent macrophage infiltration into mammary adenocarcinomas. This is significant in light of our finding that blockade of the CSF1-signaling pathway mediating TAM recruitment, in combination with chemotherapy, decreases primary tumor progression, reduces metastasis, and improves survival—a $CD8^+$ T-cell–dependent outcome resulting from a reprogrammed immune microenvironment that fosters antitumor immunity. These data provide a compelling rationale for combinatorial therapies targeting TAM recruitment, notably CSF1R-mediated signaling pathways, in combination with cytotoxic therapy for breast cancer.

The Immune Microenvironment in Breast Cancer Predicts Outcome

In a previous study, we reported that T-helper 2 (T_H2)-$CD4^+$ T-effector cells regulate TAM bioactivity and thereby promote late-stage mammary carcinogenesis and development of pulmonary metastasis (11). We now extend these findings and demonstrate that the complexity of $CD8^+$ T lymphocytes, $CD4^+$ T lymphocytes (presumably T_H2 or T regulatory cells or both), and $CD68^+$ TAMs is a predictive biomarker for OS and RFS in node-positive breast cancer (Fig. 1). Retrospective clinical studies have previously revealed that the ratio of $CD4^+$ to $CD8^+$ T lymphocytes, or T_H2 to T_H1 $CD4^+$ T cells, infiltrating breast cancer correlates with increased tumor grade, lymph node metastasis, and reduced OS (31). Unsupervised expression profiling of breast cancer-associated stroma revealed a gene signature predictive of good prognostic outcome (>98% 5-year survival) that was functionally enriched for genes suggestive of CTL and natural killer cell activity (32). Moreover, elucidation of a CSF1-response gene expression signature in breast cancer demonstrated that CSF1 signaling correlates with response to therapy and OS (7–9). In this article, we revealed that not only does increased macrophage density correlate with poor outcome (Fig. 1), as reported by others, as well (5, 31, 33), but also the ratio of macrophages/*CD68* to $CD8^+$ T lymphocytes/*CD8a* in breast cancer is inversely correlated, an important finding when considering that TAMs can also suppress antitumor immunity. These findings indicate that our immune-based signature may be a useful predictor of recurrence and poor OS for multiple breast cancer subtypes, and, as such, may improve existing gene expression-based prognostic profiling to evaluate risk.

Breast Cancer CSF1 and CSF1R Expression

Our findings demonstrate that macrophage CSF1R signaling is necessary for their recruitment following induction of *CSF1* mRNA and interaction with ligand in carcinoma cells treated with chemotherapy (Fig. 3). Recent studies by Patsialou and colleagues (34) demonstrated that in some human breast carcinoma cell lines, specifically MDA-MB231, steady-state *CSF1R* mRNA is expressed at high levels and autocrine CSF1-CSF1R signaling enhances invasion (44). Notably, MDA-MB231 cells in our studies did not respond to CTX with increased *CSF1* mRNA expression (Fig. 3), likely because these cells already express 10- to 50-fold higher levels of *CSF1* mRNA than do other breast cancer cell lines evaluated (data not shown). Carcinoma cells isolated from MMTV-PyMT mice do not express significant levels of *CSF1R* mRNA (15, 22), indicating that CSF1R blockade in MMTV-PyMT mice influences myeloid biology, as opposed to MECs.

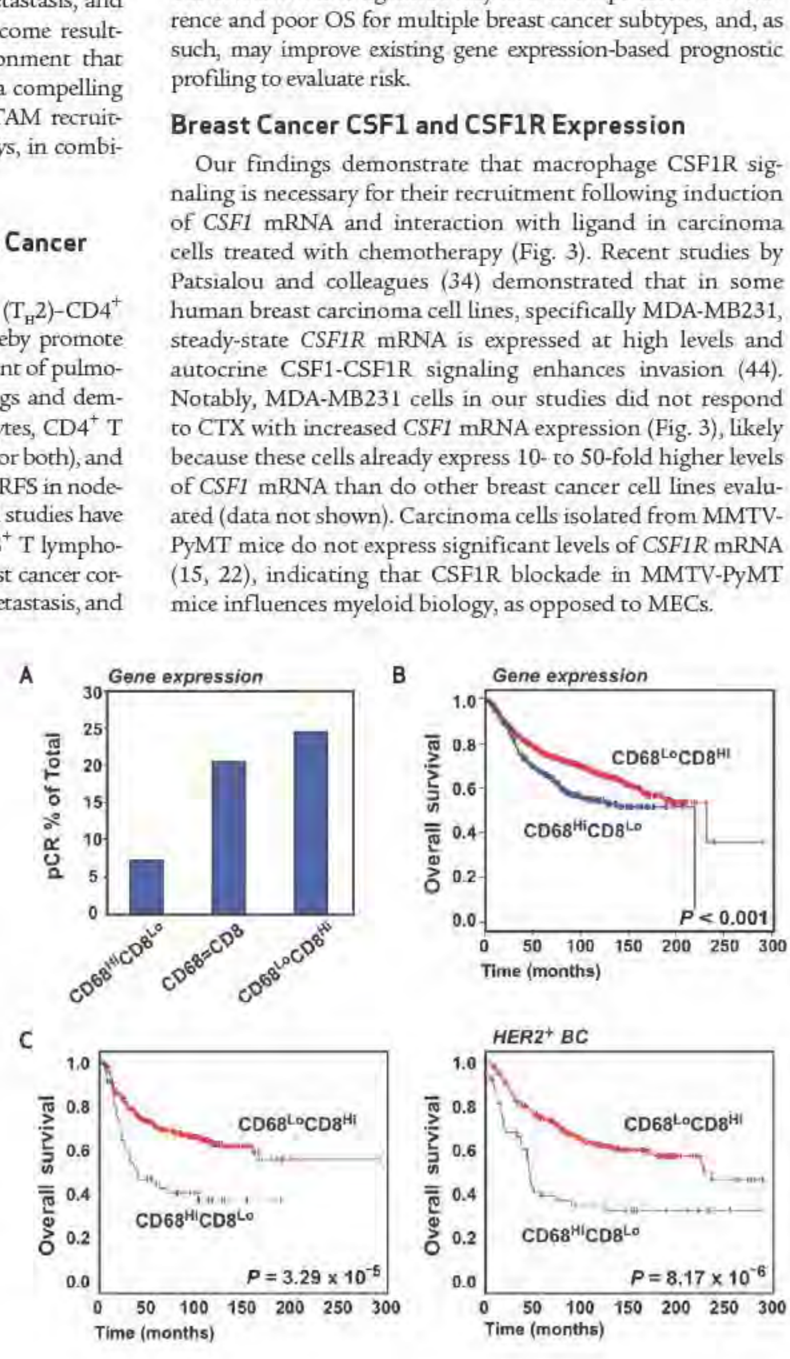

Figure 7. Ratio of *CD68* to *CD8* predicts patient survival and response to neoadjuvant chemotherapy. **A,** frequency of pCR in a cohort of 311 patients constructed from 2 independent datasets. All patients received FNAs prior to neoadjuvant chemotherapy and pathologic response was assessed at definitive surgery. With median expression as a threshold, examination of *CD8a* and *CD68* mRNA in FNA samples revealed 3 separate groups: CD68 > CD8, CD68 < CD8, and CD68 = CD8 (denoted $CD68^{high}/CD8^{low}$, $CD68^{low}/CD8^{high}$, and $CD68/CD8^{equal}$, respectively). Analysis of the rate of pCR in the groups is shown. **B,** Kaplan-Meier estimate of survival, comparing $CD68^{high}/CD8^{low}$ and $CD68^{low}/CD8^{high}$ immune profiles as assessed by mRNA expression from 3,872 patient samples assembled from 14 different platforms. Median expression for both *CD8* and *CD68* was used to determine high and low groups within each of the 22 individual datasets. Once a sample was assigned to a particular group, the 22 datasets were combined and a global survival analysis was performed. The log-rank (Mantel-Cox) *P* value is shown for difference in survival. **C,** Kaplan-Meier estimate of survival, comparing $CD68^{high}/CD8^{low}$ and $CD68^{low}/CD8^{high}$ immune profiles as assessed by mRNA expression from 3872 patient samples for tumors stratified into basal and $HER2^+$ breast cancer. The log-rank (Mantel-Cox) *P* value is shown for difference in survival.

Immunosuppressive Macrophages and Chemosensitivity

Development and progression of pulmonary metastases in mammary carcinoma is impaired in mice containing a recessive null mutation in the *CSF1* gene (15, 35). Similarly, blockade of CSF1R signaling impairs aspects of mammary carcinogenesis (36) and metastases (37). We used αCSF1 mAb and PLX3397, a novel small-molecular-weight tyrosine kinase inhibitor, to efficiently deplete $CD11b^+Ly6G^-Ly6C^{low}F4/80^+$ TAMs (70%) without altering the presence of $CD11b^+Ly6G^{high}F4/80^-$ iMCs or perivascular $F4/80^+$ macrophages in mammary tumor stroma (Fig. 3).

Malignant mammary epithelial cells from MMTV-PyMT mice express high levels of CSF1, which directly regulates TAM recruitment (and EGF expression) and induction of macrophage HIF1α (11, 38, 39). We previously reported that IFN-γ^+ $CD8^+$ CTL activity is impaired by myeloid-derived ARG1 and nitric oxide synthase that is HIF1α-dependent (38). Thus, on the basis of inverse correlation between TAMs and $CD8^+$ T cells in human breast cancer, and the fact that TAMs infiltrating mammary carcinomas directly suppress CTL activity in a HIF1α-dependent manner (38), we postulated that TAM depletion would foster antitumor immunity by relieving TAM-mediated CTL suppression and thereby enhance response to cytotoxic therapy. Accordingly, combined treatment of MMTV-PyMT mice with PTX, and either αCSF1 mAb or PLX3397, slowed primary tumor development, reduced development of high-grade carcinomas (Fig. 4), and decreased pulmonary metastasis by 85% (Fig. 6), features of mammary carcinogenesis accompanied by decreased vascular density (Fig. 4), and increased $CD4^+$ and $CD8^+$ T-cell infiltration in primary tumors (Fig. 5). Increased presence of $CD8^+$ T cells was significant in this regard, as when specifically depleted, the added benefit of combined PLX3397/PTX therapy was lost (Fig. 6).

Immunosuppressive myeloid cells encompass a diverse population of $CD11b^+Gr1^+Ly6G^+$ cells, including myeloid-derived suppressor cells, inflammatory monocytes, neutrophils, and iMCs. Human equivalents have been identified as $LIN^{-/low}$ human leukocyte antigen (HLA)–DR–$CD33^+CD11b^+$ and $CD14^+$HLA-$DR^{-/low}$ cells (40). CSF1R blockade by PLX3397 depleted $CD11b^+Ly6G^-Ly6C^{low}F4/80^+$ TAMs, but not $CD11b^+Ly6G^+$ cells (Fig. 3C), which are 12-fold less abundant in MMTV-PyMT carcinomas. In contrast, immunosuppressive $CD11b^+Ly6G^+$ cells are more abundant in other mammary tumor models, such as 4T1 (41). This may be an important distinction between tumor types considering the fact that monocyte mobilization from bone marrow is impaired by genetic loss of CSF1, but unaltered following pharmacologic or immunologic inhibition of CSF1R. $Gr1^+CCR2^+CX3CR1^{low}$ iMCs are highly responsive to CCL2 (42), and CCL2 (MCP1) is expressed at high levels in MMTV-PyMT mammary tumors (Fig. 2C). Therefore, in extrapolating to the clinical scenario, it will be important to stratify human breast cancers containing predominantly high levels of mature tissue TAMs, compared with those containing $LIN^{-/low}$HLA-$DR^-CD33^+CD11b^+$ or $CD14^+$HLA-$DR^{-/low}$ iMCs, because these breast cancers would likely be less responsive to combinatorial therapy involving CSF1R-targeted agents.

Tissue Specificity and Clinical Implications

Stromal infiltration of TAMs is a poor prognostic indicator for some solid tumor types (43); however, infiltration of TAMs inside tumor nests, particularly when $CD8^+$ CTLs are also present, can correlate with improved survival outcome (44). These differences might be explained in part by the fact that TAMs produce either protumor or antitumor bioactivities depending on the types of cytokines to which they are exposed (43). TAMs regulated by T_H1 cytokines including IFN-γ, TNF-α, and granulocyte monocyte colony stimulating factor enhance TAM cytotoxic activity, production of proinflammatory cytokines, and antigen presentation (45). In contrast, tissue macrophages exposed to T_H2 cytokines, immune complexes, or immunosuppressive cytokines instead block CTL activity and promote angiogenesis and tissue remodeling (43, 45). In non–small cell lung cancer, TAMs that localize to tumor nests and correlate with favorable clinical outcomes exhibit an $M1/T_H1$ cytokine profile and express high levels of HLA-DR (46, 47). In contrast, CD163 and CD204 expressing TAMs ($M2/T_H2$ markers) correlate with poor clinical outcomes in melanoma, non–small cell lung cancer, and pancreatic cancer (48, 49). We found that tumor tissue from PLX3397/PTX-treated mice had increased *IL12p35* and *IFNα1* mRNA expression, indicative of bolstered antitumor immunity, indicating that PLX3397/PTX therapy fostered a general reprogramming of the immune microenvironment, in addition to blocking TAM infiltration that together favored $CD8^+$ T-cell–mediated tumor suppression. Data presented herein do not reveal whether the improved outcome for tumor-bearing mice or the antitumor immune microenvironment fostered under these conditions resulted directly from reduced presence of alternatively activated TAMs, decreased vessel density, or a combination of the two. Given the fact that PLX3397 as monotherapy efficiently reduced TAM presence but had no effect on vessel density, primary carcinoma (Fig. 4), or pulmonary metastasis development (Fig. 6), it seems reasonable to speculate that TAM depletion resulted in loss of an important epithelial cell survival pathway (possibly mediated by EGF) that resists chemotherapy-induced cell death; certainly, however, effects on vascular pathways may also play a role, as has been recently reported by Rolny and colleagues (50). It will be interesting to determine whether directly reprogramming TAMs—for example, by neutralization of IL-4—to favor the presence of classically activated (M1) TAMs, as we have previously reported (11), also similarly enhances antitumor immune programs and chemosensitivity and, if so, whether those responses are also $CD8^+$ T-cell–dependent.

Microtubule inhibitors constitute one of the most effective classes of cytotoxic agents available for treating both early- and late-stage breast cancer, and are considered the standard of care for treatment of metastatic disease. Several agents that affect microtubule dynamics are active antitumor agents and induce polymerization or cause nonfunctional tubulin aggregates. These compounds block cell division by interfering with function of the mitotic spindle and consequently result in cell-cycle arrest and cell death. PTX is among the most widely used agents in this class. Despite the clinical activity of taxanes, median time to progression in patients treated with PTX is only 6 to 9 months in the first- and second-line setting, and 3 to 4 months in patients with previous exposure to taxanes (51). Although addition of the antiangiogenic agent bevacizumab to PTX improved response and time to progression, it was without impact on OS (52). Glucocorticoid premedication is required for PTX to prevent increased bone marrow and peripheral nerve toxicity as well as allergic reactions and anaphylaxis due to the Cremaphor solvent base. For other cytotoxic agents, glucocorticoids are also commonly used to prevent toxicities such as nausea, vomiting, and fluid retention. Although these agents are standard additions to many chemotherapies, they suppress production of proinflammatory cytokines and chemokines, severely impair differentiation of antigen presentation by DCs, suppress development of T_H1 cells, and bias immune responses toward T_H2 cell types (53). Our neoadjuvant studies in MMTV-PyMT and orthotopic tumor–bearing mice were performed without dexamethasone, an H_2 antagonist, or diphenhydramine. Thus, it is possible that the $CD8^+$ T-cell–dependent antitumor program fostered by combined PLX3397/PTX would have been dampened in the presence of dexamethasone. An understanding of the mechanisms that lead to inadequate or poor response to taxanes is urgently needed, as are prognostic biomarkers that predict which patients will respond favorably. That said, it seems reasonable that administration of cytotoxic agents not requiring steroids, in combination with novel strategies such as TAM ablation (or TAM reprogramming), which together bolster natural antitumor immunity, would improve outcomes and extend long-term survival for patients with breast cancer, as well as other cancer types. The clinical outcome of pharmacologically (or immunologically) targeting TAMs directly or the pathways that regulate their recruitment must be considered carefully because all cancer types may not respond in a similar fashion. This study provides a compelling rationale for clinical evaluation of combinatorial therapies inhibiting TAM recruitment, in combination with standard-of-care chemotherapy for treatment of breast cancer, and underscores the importance of identifying a population of patients who, by virtue of their immune profile and CSF1R status, may benefit most from such therapies.

METHODS

Patients and Tumor Samples

Tissue microarray studies were conducted on 2 separate patient cohorts. The screening cohort, Cohort I, described elsewhere in detail (54), was constructed from 179 cases of invasive breast cancer diagnosed at the Department of Pathology, Malmö University Hospital, Malmö, Sweden, between 2001 and 2002. The median age at diagnosis was 65 years of age, and the median follow-up time for OS was 52 months. Patients had not received neoadjuvant therapy and were treated with either modified radical mastectomy or wide local excision. The median tumor size was 2.2 cm; 62% of the tumors were PR-positive and 72% were ER-positive. Complete endocrine treatment data were available for 143 patients, 67 of whom received adjuvant tamoxifen, 3 an aromatase inhibitor, and 25 a combination of tamoxifen and an aromatase inhibitor. Information on adjuvant chemotherapy was available for 143 patients, of whom 30 received treatment. The second (validation) cohort, Cohort II, included 498 patients with primary invasive breast cancer diagnosed at the Malmö University Hospital between 1988 and 1992. These cases belonged to an original cohort of 512 patients, as previously described in detail (55). The median age at diagnosis was 65 years, and median follow-up time to first breast cancer event was 128 months. Information regarding the date of death was obtained from regional cause-of-death registries for all patients in both cohorts. Complete endocrine treatment data were available for 379 patients, 160 of whom received adjuvant tamoxifen. Information on adjuvant chemotherapy was available for 382 patients, of whom 23 received treatment. To assemble tissue microarrays, clearly defined areas of tumor tissue were indicated on a slide with a fresh tissue section from the paraffin block. Two biopsy samples, 1.0 mm in diameter, were taken from each donor paraffin block corresponding to the marked area. Recipient blocks were limited to ~200 cores each. In general, cores were taken from the peripheral aspect of the tumor. Necrotic tissue was avoided. For IHC analyses, 4.0-μm paraffin sections were used. The ethical committee at Lund University (Malmö, Sweden) approved this study.

Automated Image Acquisition, Management, and Analysis

Fully automated image acquisition was used for the results presented in this article. The Aperio ScanScope XT Slide Scanner (Aperio Technologies) was used to capture whole-slide digital images with a 20× objective. Slides were dearrayed to visualize individual cores, using Spectrum software (Aperio). A tumor-specific nuclear algorithm (IHC-MARK) developed in house was modified to quantify CD4, CD8, and CD68 expression. IHC-MARK was initially designed to identify tumor cells on the basis of nuclear morphologic features (56); however, this was modified for evaluating leukocyte infiltration based on specific nuclear morphologic features.

Image and Statistical Analysis

A decision tree–supervised algorithm was used to group patients based on immune cell IHC density. For decision tree analysis, all patients were randomly divided into 10 subsets. A decision tree model was selected using a 10-fold cross-validation approach (16). Ten consecutive decision tree models were independently constructed with the immune cell infiltration density continuous output from 9 subsets. Survival outcome predictive power of each decision tree model was tested on the remaining set of patients, and the model with the higher accuracy was selected as optimal for the dataset. Kaplan-Meier analysis and the log-rank test were used to illustrate differences between OS and RFS according to individual CD68, CD4, and CD8 expression. A Cox regression proportional hazards model was used to estimate the relationship to OS of the CD68/CD4/CD8 immune profile; lymph node status; tumor grade; and HER2, PR, and ER status in the patient cohorts. A P value of <0.05 was considered statistically significant, and calculations were assessed using Statistical Package for the Social Sciences (SPSS, Inc.).

Neoadjuvant Cohort

The neoadjuvant cohort consisted of 2 gene expression cohorts representing 311 patients treated with neoadjuvant chemotherapy (26, 27), with complete pathologic response in 60 (19%) patients. The majority of patients received PTX and fluorouracil-doxorubicin-cyclophosphamide. Both datasets were examined on the same array platform (Affymetrix U133A), using a standard operating procedure and normalization method (dCHIP) as previously reported (57, 58). Data were downloaded from the Gene Expression Omnibus (59) and an institutional website (60). Normalized expression values for both CD8 and CD68 were established as previously described (54).

Preclinical Mouse Models and Animal Husbandry

Mice harboring the PyMT transgene under the control of the MMTV promoter in the FVB/n strain were obtained from Dr. Zena Werb [University of California, San Francisco (UCSF), San Francisco, California] and have been previously described (14). Two murine models of mammary tumor development were used to analyze response to chemotherapy (Supplementary Fig. S3). The first model used MMTV-PyMT mice (Supplementary Fig. S3A). The 80-day-old MMTV-PyMT female littermates were randomized by initial tumor volume and fed either PLX3397 (20, 61, 62) formulated in mouse chow or control chow (provided by Plexxikon Inc). PLX3397 was formulated in mouse chow so that the average dose per animal per day was 40 mg/kg. When PLX3397-treated MMTV-PyMT mice reached 85 days of age, they were then administered PTX (Hospira) every 5 days by i.v. injection into the retroorbital plexus. PTX was given at 10 mg/kg of the animal per injection, diluted in PBS. Tumor burden was evaluated by caliper measurement every 5 days following the start of PLX3397 treatment. Prior to tissue collection, mice were cardiac-perfused with PBS to clear peripheral blood. Mammary tumor tissue from PBS-perfused MMTV-PyMT mice was analyzed by flow cytometry and qRT-PCR 2 days after the second dose of PTX, when metastatic burden and tumor grade were determined. Primary tumor burden was determined by caliper measurements on live sedated mice. Metastatic burden was assessed by serial sectioning of formalin-fixed paraffin-embedded lung tissue whereby the entire lung was sectioned and the number of metastatic foci (>5 cells) was determined on 6 sections taken every 100 μm following H&E staining. Lungs from >10 mice/group were analyzed.

To assess tumor grade, the stage characterization technique classified tumor tissue into 3 levels of histologic progression by quantifying the area of transformed glands occupied by each stage (15, 38). Progression follows from a "precancerous stage" characterized by premalignant hyperplasia and adenoma/mouse intestinal epithelium but with the retention of some normal ductal and acinar mammary gland morphology, to a more epithelial cell–dense "early carcinoma" with some stromal invasion, and finally to an invasive, high–mitotic index "late-stage carcinoma."

The IHC analysis was conducted on tissue sections following the end of studies on 100-day-old MMTV-PyMT mice (detailed in Supplementary Fig. S4A). Vehicle-treated mice received PBS-only injections. We also used a syngeneic orthotopic implantable tumor model (referred to as PyMT-implantable in all figures and detailed in Supplementary Fig. S4B). For this model, single-cell suspensions of tumor cell pools isolated from mammary tumors of 3 or 4 100-day-old MMTV-PyMT mice were generated following collagenase A digestion (see discussion of flow cytometry analysis earlier). A total of 1.0 million tumor cells from pools were diluted in medium and basement membrane extract (Matrigel, BD Pharmingen) and injected orthotopically into uncleared mammary fat pads (4th gland) of 10-week-old virgin FVB/n female mice. Following implantation, tumors were allowed to grow to a mean diameter of 1.0 cm before enrollment into studies. Mice were randomized into treatment groups based on tumor size and treated with PLX3397 and PTX, as described above. For some studies, CBDCA (Hospira) was used and administered at 10 mg/kg of mouse per injection, in a similar manner to administration of PTX (see above). For mice with implantable tumors, tumor burden was evaluated by caliper measurement every 2 to 3 days following the start of PLX3397 treatment, and mammary tissue was analyzed by flow cytometry, IHC, and qRT-PCR at the end of the study (Supplementary Fig. S3B). Immune-depleted mice were injected i.p. every 5 days with either 1.0 mg anti-CD8 immunoglobulin G (YTS169.4) or isotype control rat immunoglobulin on day 1 followed by 500 µg every 5 days. All mice were maintained within the UCSF Laboratory for Animal Care barrier facility, and the UCSF Institutional Animal Care and Use Committee approved all experiments involving animals.

Additional information on methods and cohorts is available in the Supplementary Data.

Disclosure of Potential Conflicts of Interest

E. Rexhepaj, D.J. Brennan, and W.M. Gallagher are inventors of a pending patent application in relation to the development of novel automated image analysis approaches in histopathology, and D.G. DeNardo, D.J. Brennan and L.M. Coussens are inventors of a pending patent application in relation to immune-based signatures for predicting breast cancer risk. B.L. West is an employee of Plexxikon Inc. but had no involvement in data collection, analysis, or interpretation.

Acknowledgments

The authors thank the UCSF Helen Diller Family Comprehensive Cancer Center Laboratory for Cell Analysis and Mouse Pathology shared resource core facilities; members of the Coussens lab for critical discussion; and Plexxikon Inc. for providing PLX3397.

Grant Support

This work was supported by the American Cancer Society and National Cancer Institute Postdoctoral Training Grants (D.G. DeNardo); Department of Defense Breast Cancer Research Program and a Dr. Susan Love Research Foundation Instructional Grant (B. Ruffell); Breast Cancer Research Foundation (H.S. Rugo); and The University College Dublin Conway Institute, which is funded by the Programme for Research in Third Level Institutions, as administered by the Higher Education Authority of Ireland. Funding is acknowledged from Enterprise Ireland (D.J. Brennan, E. Rexhepaj, and W.M. Gallagher); Science Foundation Ireland Strategic Research Cluster award to Molecular Therapeutics for Cancer Ireland (W.M. Gallagher and S.F. Madden); and NIH/National Cancer Institute Grants R01CA130980, R01CA132566, R01CA140943, and P50CA58207, and the Department of Defense Grants W81XWH-06-1-0416 and PR080717 (L.M. Coussens).

Received November 30, 2010; revised February 7, 2011; accepted February 8, 2011; published OnlineFirst April 3, 2011.

REFERENCES

1. Pollard JW. Trophic macrophages in development and disease. Nat Rev Immunol 2009;9:259–70.
2. Qian BZ, Pollard JW. Macrophage diversity enhances tumor progression and metastasis. Cell 2010;141:39–51.
3. Tang R, Beuvon F, Ojeda M, Mosseri V, Pouillart P, Scholl S. M-CSF (monocyte colony stimulating factor) and M-CSF receptor expression by breast tumour cells: M-CSF mediated recruitment of tumour infiltrating monocytes? J Cell Biochem 1992;50:350–6.
4. Wei S, Nandi S, Chitu V, Yeung YG, Yu W, Huang M, et al. Functional overlap but differential expression of CSF-1 and IL-34 in their CSF-1 receptor-mediated regulation of myeloid cells. J Leukoc Biol 2010;88:495–505.
5. Campbell MJ, Tonlaar NY, Garwood ER, Huo D, Moore DH, Khramtsov AI, et al. Proliferating macrophages associated with high grade, hormone receptor negative breast cancer and poor clinical outcome. Breast Cancer Res Treat 2010 [Epub ahead of print].
6. Steidl C, Lee T, Shah SP, Farinha P, Han G, Nayar T, et al. Tumor-associated macrophages and survival in classic Hodgkin's lymphoma. N Engl J Med 2010;362:875–85.
7. Sharma M, Beck AH, Webster JA, Espinosa I, Montgomery K, Varma S, et al. Analysis of stromal signatures in the tumor microenvironment of ductal carcinoma in situ. Breast Cancer Res Treat 2010;123:397–404.
8. Espinosa I, Beck AH, Lee CH, Zhu S, Montgomery KD, Marinelli RJ, et al. Coordinate expression of colony-stimulating factor-1 and colony-stimulating factor-1-related proteins is associated with poor prognosis in gynecological and nongynecological leiomyosarcoma. Am J Pathol 2009;174:2347–56.
9. Beck AH, Espinosa I, Edris B, Li R, Montgomery K, Zhu S, et al. The macrophage colony-stimulating factor 1 response signature in breast carcinoma. Clin Cancer Res 2009;15:778–87.
10. de Visser KE, Korets LV, Coussens LM. De novo carcinogenesis promoted by chronic inflammation is B lymphocyte dependent. Cancer Cell 2005;7:411–23.
11. DeNardo DG, Barreto JB, Andreu P, Vasquez L, Tawfik D, Kolhatkar N, et al. CD4(+) T cells regulate pulmonary metastasis of mammary carcinomas by enhancing protumor properties of macrophages. Cancer Cell 2009;16:91–102.
12. Andreu P, Johansson M, Affara NI, Pucci F, Tan T, Junankar S, et al. FcRgamma activation regulates inflammation-associated squamous carcinogenesis. Cancer Cell 2010;17:121–34.
13. Ammirante M, Luo JL, Grivennikov S, Dedospasov S, Karin M. B-cell-derived lymphotoxin promotes castration-resistant prostate cancer. Nature 2010;464:302–6.
14. Guy CT, Cardiff RD, Muller WJ. Induction of mammary tumors by expression of polyomavirus middle T oncogene: a transgenic mouse model for metastatic disease. Mol Cell Biol 1992;12:954–61.
15. Lin EY, Nguyen AV, Russell RG, Pollard JW. Colony-stimulating factor 1 promotes progression of mammary tumors to malignancy. J Exp Med 2001;193:727–40.
16. Breiman L, Friedman JH, Olshen R, Stone CJ. Classification and regression trees. Pacific Grove, (CA): Wadsworth and Brooks/Cole Advanced Books and Software; 1984.
17. DeNardo DG, Andreu P, Coussens LM. Interactions between lymphocytes and myeloid cells regulate pro- versus anti-tumor immunity. Cancer Metastasis Rev 2010;29:309–16.
18. Gabrilovich DI, Nagaraj S. Myeloid-derived suppressor cells as regulators of the immune system. Nat Rev Immunol 2009;9:162–74.
19. Haile LA, Gamrekelashvili J, Manns MP, Korangy F, Greten TF. CD49d is a new marker for distinct myeloid-derived suppressor cell subpopulations in mice. J Immunol 2010;185:203–10.
20. Artis DR, Bremer R, Gillette S, Hurt CR, Ibrahim PL, Zuckerman RL, Inventors; Plexxikon Inc., assignee. Molecular scaffolds for kinase ligand development. United States patent US-20050164300. July 28, 2005.

21. Lin EY, Jones JG, Li P, Zhu L, Whitney KD, Muller WJ, et al. Progression to malignancy in the polyoma middle T oncoprotein mouse breast cancer model provides a reliable model for human diseases. Am J Pathol 2003;163:2113–26.
22. Lin EY, Li JF, Gnatovskiy L, Deng Y, Zhu L, Grzesik DA, et al. Macrophages regulate the angiogenic switch in a mouse model of breast cancer. Cancer Res 2006;66:11238–46.
23. Lin EY, Pollard JW. Tumor-associated macrophages press the angiogenic switch in breast cancer. Cancer Res 2007;67:5064–6.
24. Lin EY, Li JF, Bricard G, Wang W, Deng Y, Sellers R, et al. VEGF testores delayed tumor progression in tumors depleted of macrophages. Mol Oncol 2007;1:288–302.
25. Stockmann C, Doedens A, Weidemann A, Zhang N, Takeda N, Greenberg JI, et al. Deletion of vascular endothelial growth factor in myeloid cells accelerates tumorigenesis. Nature 2008;456:814–8.
26. Hess KR, Anderson K, Symmans WF, Valero V, Ibrahim N, Mejia JA, et al. Pharmacogenomic predictor of sensitivity to preoperative chemotherapy with paclitaxel and fluorouracil, doxorubicin, and cyclophosphamide in breast cancer. J Clin Oncol 2006;24:4236–44.
27. Tabchy A, Valero V, Vidaurre T, Lluch A, Gomez H, Martin M, et al. Evaluation of a 30-gene paclitaxel, fluorouracil, doxorubicin, and cyclophosphamide chemotherapy response predictor in a multicenter randomized trial in breast cancer. Clin Cancer Res 2010;16:5351–61.
28. Perou CM, Sorlie T, Eisen MB, van de Rijn M, Jeffrey SS, Rees CA, et al. Molecular portraits of human breast tumours. Nature 2000;406:747–52.
29. Sorlie T, Perou CM, Tibshirani R, Aas T, Geisler S, Johnsen H, et al. Gene expression patterns of breast carcinomas distinguish tumor subclasses with clinical implications. Proc Natl Acad Sci U S A 2001;98:10869–74.
30. Sorlie T, Tibshirani R, Parker J, Hastie T, Marron JS, Nobel A, et al. Repeated observation of breast tumor subtypes in independent gene expression data sets. Proc Natl Acad Sci U S A 2003;100:8418–23.
31. Kohrt HE, Nouri N, Nowels K, Johnson D, Holmes S, Lee PP. Profile of immune cells in axillary lymph nodes predicts disease-free survival in breast cancer. PLoS Med 2005;2:e284.
32. Finak G, Bertos N, Pepin F, Sadekova S, Souleimanova M, Zhao H, et al. Stromal gene expression predicts clinical outcome in breast cancer. Nat Med 2008;14:518–27.
33. Leek RD, Lewis CE, Whitehouse R, Greenall M, Clarke J, Harris AL. Association of macrophage infiltration with angiogenesis and prognosis in invasive breast carcinoma. Cancer Res 1996;56: 4625–9.
34. Patsialou A, Wyckoff J, Wang Y, Goswami S, Stanley ER, Condeelis JS. Invasion of human breast cancer cells in vivo requires both paracrine and autocrine loops involving the colony-stimulating factor-1 receptor. Cancer Res 2009;69:9498–506.
35. Nowicki A, Szenajch J, Ostrowska G, Wojtowicz A, Wojtowicz K, Kruszewski AA, et al. Impaired tumor growth in colony-stimulating factor 1 (CSF-1)–deficient, macrophage-deficient op/op mouse: evidence for a role of CSF-1–dependent macrophages in formation of tumor stroma. Int J Cancer 1996;65:112–9.
36. Qian B, Deng Y, Im JH, Muschel RJ, Zou Y, Li J, et al. A distinct macrophage population mediates metastatic breast cancer cell extravasation, establishment and growth. PLoS One 2009;4:e6562.
37. Manthey CL, Johnson DL, Illig CR, Tuman RW, Zhou Z, Baker JF, et al. JNJ-28312141, a novel orally active colony-stimulating factor-1 receptor/FMS-related receptor tyrosine kinase-3 receptor tyrosine kinase inhibitor with potential utility in solid tumors, bone metastases, and acute myeloid leukemia. Mol Cancer Ther 2009;8:3151–61.
38. Doedens AL, Stockmann C, Rubinstein MP, Liao D, Zhang N, Denardo DG, et al. Macrophage expression of hypoxia-inducible factor-1α suppresses T-cell function and promotes tumor progression. Cancer Res 2010;70:7465–75.
39. Wyckoff J, Wang W, Lin EY, Wang Y, Pixley F, Stanley ER, et al. A paracrine loop between tumor cells and macrophages is required for tumor cell migration in mammary tumors. Cancer Res 2004;64:7022–9.
40. Serafini P, Borrello I, Bronte V. Myeloid suppressor cells in cancer: recruitment, phenotype, properties, and mechanisms of immune suppression. Semin Cancer Biol 2006;16:53–65.
41. Bunt SK, Yang L, Sinha P, Clements VK, Leips J, Ostrand-Rosenberg S. Reduced inflammation in the tumor microenvironment delays the accumulation of myeloid-derived suppressor cells and limits tumor progression. Cancer Res 2007;67:10019–26.
42. Zhang J, Patel L, Pienta KJ. CC chemokine ligand 2 (CCL2) promotes prostate cancer tumorigenesis and metastasis. Cytokine Growth Factor Rev 2010;21:41–8.
43. Ruffell B, Denardo DG, Affara NI, Coussens LM. Lymphocytes in cancer development: polarization towards pro-tumor immunity. Cytokine Growth Factor Rev 2010;21:3–10.
44. Kawai O, Ishii G, Kubota K, Murata Y, Naito Y, Mizuno T, et al. Predominant infiltration of macrophages and CD8(+) T cells in cancer nests is a significant predictor of survival in stage IV nonsmall cell lung cancer. Cancer 2008;113:1387–95.
45. Mantovani A, Locati M. Orchestration of macrophage polarization. Blood 2009;114:3135–6.
46. Ma J, Liu L, Che G, Yu N, Dai F, You Z. The M1 form of tumor-associated macrophages in non-small cell lung cancer is positively associated with survival time. BMC Cancer 2010;10:112.
47. Ohri CM, Shikotra A, Green RH, Waller DA, Bradding P. Macrophages within NSCLC tumour islets are predominantly of a cytotoxic M1 phenotype associated with extended survival. Eur Respir J 2009;33:118–26.
48. Bronkhorst IH, Ly LV, Jordanova ES, Vrolijk H, Versluis M, Luyten GP, et al. Detection of M2 macrophages in uveal melanoma and relation with survival. Invest Ophthalmol Vis Sci 2011;52:643–50.
49. Kurahara H, Shinchi H, Mataki Y, Maemura K, Noma H, Kubo F, et al. Significance of M2-polarized tumor-associated macrophage in pancreatic cancer. J Surg Res 2009 [Epub ahead of print].
50. Rolny C, Mazzone M, Tugues S, Laoui D, Johansson I, Coulon C, et al. HRG inhibits tumor growth and metastasis by inducing macrophage polarization and vessel normalization through downregulation of PlGF. Cancer Cell 2011;19:31–44.
51. Twelves C, Cortes J, Vahdat LT, Wanders J, Akerele C, Kaufman PA. Phase III trials of eribulin mesylate (E7389) in extensively pretreated patients with locally recurrent or metastatic breast cancer. Clin Breast Cancer 2010;10:160–3.
52. Miller K, Wang M, Gralow J, Dickler M, Cobleigh M, Perez EA, et al. Paclitaxel plus bevacizumab versus paclitaxel alone for metastatic breast cancer. N Engl J Med 2007;357:2666–76.
53. Zitvogel L, Kroemer G. The dilemma of anticancer therapy: tumor-specific versus immune effects. Blood 2008;112:4364–5.
54. Brennan DJ, Rexhepaj E, O'Brien SL, McSherry E, O'Connor DP, Fagan A, et al. Altered cytoplasmic-to-nuclear ratio of survivin is a prognostic indicator in breast cancer. Clin Cancer Res 2008;14:2681–9.
55. Paulsson J, Sjoblom T, Micke P, Ponten F, Landberg G, Heldin CH, et al. Prognostic significance of stromal platelet-derived growth factor beta-receptor expression in human breast cancer. Am J Pathol 2009;175:334–41.
56. Rexhepaj E, Brennan DJ, Holloway P, Kay EW, McCann AH, Landberg G, et al. Novel image analysis approach for quantifying expression of nuclear proteins assessed by immunohistochemistry: application to measurement of oestrogen and progesterone receptor levels in breast cancer. Breast Cancer Res 2008;10:R89.
57. Mazouni C, Peintinger F, Wan-Kau S, Andre F, Gonzalez-Angulo AM, Symmans WF, et al. Residual ductal carcinoma in situ in patients with complete eradication of invasive breast cancer after neoadjuvant chemotherapy does not adversely affect patient outcome. J Clin Oncol 2007;25:2650–5.
58. Moody SE, Perez D, Pan TC, Sarkisian CJ, Portocarrero CP, Sterner CJ, et al. The transcriptional repressor Snail promotes mammary tumor recurrence. Cancer Cell 2005;8:197–209.
59. Gene Expression Omnibus [database on the Internet]. Bethesda (MD): National Center for Biotechnology Information/National Library of Medicine/NIH. 2010 [cited 2011]. Available from http://www.ncbi.nlm.nih.gov/geo/query/acc.cgi?acc=GSE20271
60. Department of Bioinformatics and Computational Biology [database on the Internet]. Houston (TX): The University of Texas MD Anderson Cancer Center. 2003 [cited 2011]. Available from http://bioinformatics.mdanderson.org/pubdata.html
61. Tsai J, Lee JT, Wang W, Zhang J, Cho H, Mamo S, et al. Discovery of a selective inhibitor of oncogenic B-Raf kinase with potent antimelanoma activity. Proc Natl Acad Sci U S A 2008;105:3041–6.
62. Louvet C, Szot GL, Lang J, Lee MR, Martinier N, Bollag G, et al. Tyrosine kinase inhibitors reverse type 1 diabetes in nonobese diabetic mice. Proc Natl Acad Sci U S A 2008;105:18895–900.